UiT
THE ARCTIC
UNIVERSITY
OF NORWAY

Faculty of Science and Technology

Department of Geology

Sedimentation environment during deglaciation and Holocene in Southern Sentralbanken, Barents Sea

Monica Hultin

GEO-3900 Master thesis in Geology
May 2016

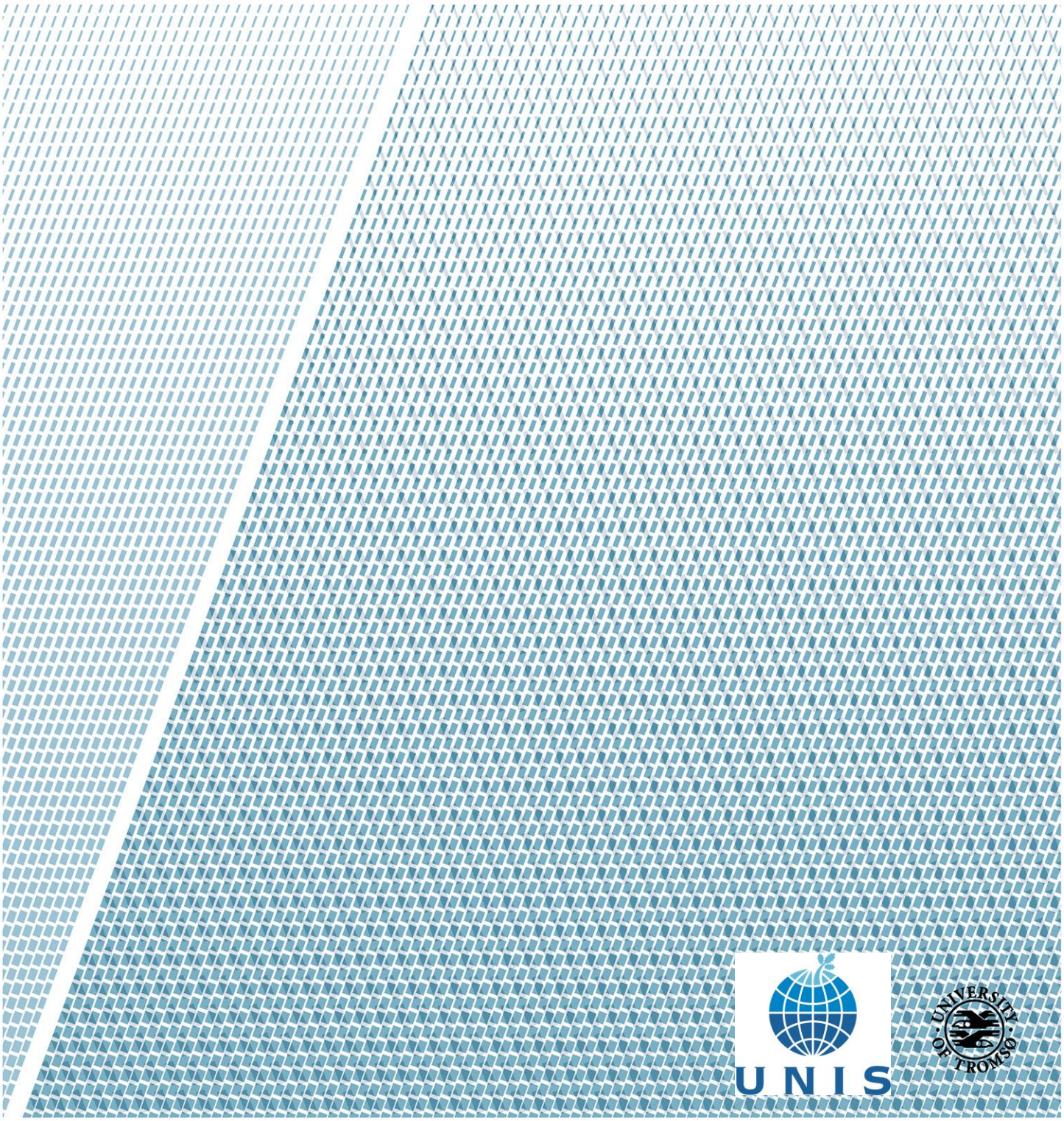

Abstract

Grounding zone wedges and ridges throughout the Barents Sea gives good spatial constraints of the Late Weichselian deglaciation of the Barents Sea, however, little is known about Late Weichselian ice dynamics in the Central Barents Sea, primarily due to a lack of data. The study is carried out south of Sentralbanken in Sentralbankrenna which was likely an important source area feeding the Bjørnøyrenna ice stream during the glaciation and throughout the deglaciation. Previous studies have documented a network of tunnel valleys (Bjarnadottir et al., 2012; 2014), and has for the first time provided evidence for abundant meltwater activity in this area. Understanding how ice retreated through this trough is important for reconstructing behaviour of the Bjørnøyrenna Ice stream and the Barents Sea Ice Sheet as a whole. Four sediments gravity cores were retrieved and investigated by lithological logs, physical properties, XRF scan, X-ray and particle size analyser to reveal the sedimentary processes dominating Sentralbankrenna from the deglaciation throughout Holocene. Close to 200 samples were collected throughout the cores allowing detailed investigation of grain size distribution. Sentralbankrenna serves as a funnel for sediments coming from North, Northeast, East and Southeast, and an analysis of the sediments deposited in this area will therefore help to understand the pattern of ice flow and sediment transport. The study reveals a deglacial environment dominated by IRD, meltwater plumes and suspensions settling. Foraminifera of different age and a belemnite found in the deeper part of the core suggest the lamination is a product of reworking and transport of sediments with origin in the northern Barents Sea. After the deglaciation a homogenous sediments pack reveals a change in deposition and transport mechanism, indicating a warmer climate and sedimentation dominated by bottom currents and reworking of sediments.

Acknowledgements

This master thesis is my final work as a part of my master of science in Geology, and represents my last period as a student. First I would like to thank my supervisors Juho Junttila, Monica Winsborrow and Lena Håkansson for all help and motivation throughout the whole year. A special thanks to my main supervisor Juho Junttila for help in the lab, for making it easier for me to live on Svalbard and write my thesis from here and for still making it possible to discuss via skype, and always being reachable on e-mail. I would also like to thank Noortje Dijkstra, for helping me in the lab with identifying foraminifera.

Big thanks to Kine and Rasmus for reading through my thesis, giving me feedbacks, and to Sarah for helping me with sentences and English grammar and words. Thanks to all the girls at the office for lunch breaks, coffee breaks, good talks and for in general making my days entertaining.

Further, I would like to give a thank you to my family and friends for help and support along the way, and a special thanks to my niece Alma for entering this world earlier than planned, so my last days of stress and writing didn't have to be overwhelmed by more feelings and excitement other than handing in this work.

Contents

1. Introduction 1
   1.1. Objectives 1
   1.2. Project 1
   1.3. Background 2
      1.3.1. Ice sheets and ice streams 2
      1.3.2. The Last Glacial Maximum and Early Deglaciation 2
      1.3.3. Late Deglaciation and Holocene 5
      1.3.4. Sedimentation of the Barents Sea 5
   1.4. Ocean Currents 8
   1.5. Sedimentation processes 10
      1.5.1. Mass waste 10
      1.5.2. Meltwater plumes 11
      1.5.3. Ice Rafted Debris 11
2. Setting 15
   2.1. Geomorphology 15
      2.1.1. Geomorphological features 17
      2.1.2. Geomorphological features in Sentralbanken 19
3. Methods 23
   3.1. Collecting data 23
      3.1.1. Multibeam echosounder 23
      3.1.2. Sub bottom Profiler (Chirp Sonar) 24
      3.1.3. Gravity Cores 24
   3.2. Data analysis 26
      3.2.1. X-ray 26
      3.2.2. Multi Sensor Core Logger (MSCL) 26
      3.2.3. Grain-size Analysis 29
      3.2.4. XRF 31
   3.3. Sortable silt 32
   3.4. Sedimentological description and logging 34
   3.5. Counting of IRD 34
   3.6. Radiocarbon dating And Calibration 34
4. Results: Acoustic Data 37
   4.1. Swath Bathymetry and mapping 37

4.1.1. Tunnel valleys 38
4.2. Swath bathymetry and core position 40
4.3. Sub bottom profiler; Chirp 43
4.3.1. Interpretation 48
5. Results: Litostratigraphy 49
Unit 1 51
Unit 2 51
Element chemistry 52
Grain size distribution 53
5.1. HH12-900 GC and HH12-901 GC 54
5.1.1. Unit 1 54
5.1.2. Unit 2 55
5.2. HH12-904 GC and HH12-905 GC 61
5.2.1. Unit 1 61
5.2.2. Unit 2 62
5.3. Interpretation of sediment cores 68
5.4. ^{14}C AMS Dating 68
6. Discussion 71
6.1. AMS ^{14}C dating and foraminifera 71
6.2. Acoustic Data 72
6.3. Correlation of acoustic and sedimentary data 73
6.4. Unit 2: Deglaciation 73
6.4.1. Mass waste 74
6.4.2. Meltwater plumes 74
6.4.3. Ice Rafted Debris 75
6.4.4. Sortable silt and relative current speed 77
6.5. Unit 1: Holocene 78
6.5.1. Bottom currents and sediment transportation 78
6.5.2. Sortable silt and relative current speed 78
6.5.3. Winnowing 79
6.6. Sediments Provenance 81
7. Conclusions 83
8. References 85

1. Introduction

1.1. Objectives

The objectives of the project are to study the sedimentary environment during the last deglaciation and Holocene in the South Western Barents Sea. The focus has been to describe the retreat of the Barents Sea ice sheet and to explain the sedimentary processes dominating during the deglaciation and throughout Holocene.

1.2. Project

The project is carried out by the UiT; The Arctic University of Norway, and is connected to the BARCUT project and to CAGE – Centre for Arctic Gas Hydrate, Environment and Climate.

The understanding of processes leading to a retreat of marine based ice sheets such as the West Antarctic Ice Sheet (WAIS) today is limited. The ice sheet is vulnerable to ongoing increases in ocean temperatures as its ice shelf is in direct contact with water (Patton et al., 2015; Rignot & Jacobs, 2002). By studying how former ice sheets responded to warmer periods or events, and by looking at the retreat of an ice sheet with similarities it can be possible to predict how threatened ice sheets today will respond to the ongoing climatic changes (bjarnadottir, 2012). Therefore it has been shown great interest in ice streams and their impact on ice sheets the last 20 years (Bennet, 2003) and their reaction to collapses and retreats due to a warming climate.

The Barents Sea ice sheet (BSIS) shows several similarities with the West Antarctic Ice Sheet (WAIS) today, such as size during the last glacial maximum, the location at high latitudes, they both are marine based and rest below sea level on sedimentary rock, and both were at or near the shelf break (Andreassen & Winsborrow, 2009; Bennet, 2003)

1.3. Background

1.3.1. Ice sheets and ice streams

"Ice sheets are thick sheet of ice which submerge the landscape and are not topography dependent" (Benn & Evans, 2010). An ice sheet consists of an ice dome of slower moving ice, as well as several outlet glaciers and ice streams which is parts where the ice flows much faster than the rest of the ice sheet (Swithinbank, 1954; Bennet, 2003). This is where most of the ice, meltwater and sediments are discharged (Winsborrow et al., 2010).

An ice sheet consists of moving ice and several ice streams have the important task of transporting the ice away from the ice sheet. About 90% of the ice in an ice sheet is transported away by ice streams (Bamber & Joughin, 2000) and the discharge of an ice sheet is therefore largely dependent on the ice streams operating. When draining the ice masses away the ice streams erodes and transport huge amounts of sediments over big distances, leaving troughs and sediment depocenters behind.

The Barents Sea Ice Sheet was a marine based ice sheet, meaning it was resting below sea level. These ice sheets are poorly understood (Winsborrow et al., 2010) and the retreat are very much dependent on changes in water temperature and ocean currents, as the ice shelf of the ice sheets are at all times in contact with water (Patton et al., 2015; Rignot & Jacobs, 2002).

1.3.2. The Last Glacial Maximum and Early Deglaciation

The Barents Sea has been covered by grounded ice sheets several times during the late Cenozoic (Vorren et al., 1988). 28 000 years ago the ice sheet which was resting on the Scandinavian inland started to grow. Rapidly it grew towards the shelf edges, and by 20 000 years ago, the ice sheet was at it largest, as shown in Figure 1.1. The ice sheet was covering the whole Barents Sea, the land areas around including the whole Fennoscandia, and in the South it was connected to the ice sheet occupying Great Britain today. This is now known as the peak of the late Weichselian ice age; the last glacial maximum (LGM). Figure 1.1 shows the extent of the Barents Sea Ice Sheet during LGM.

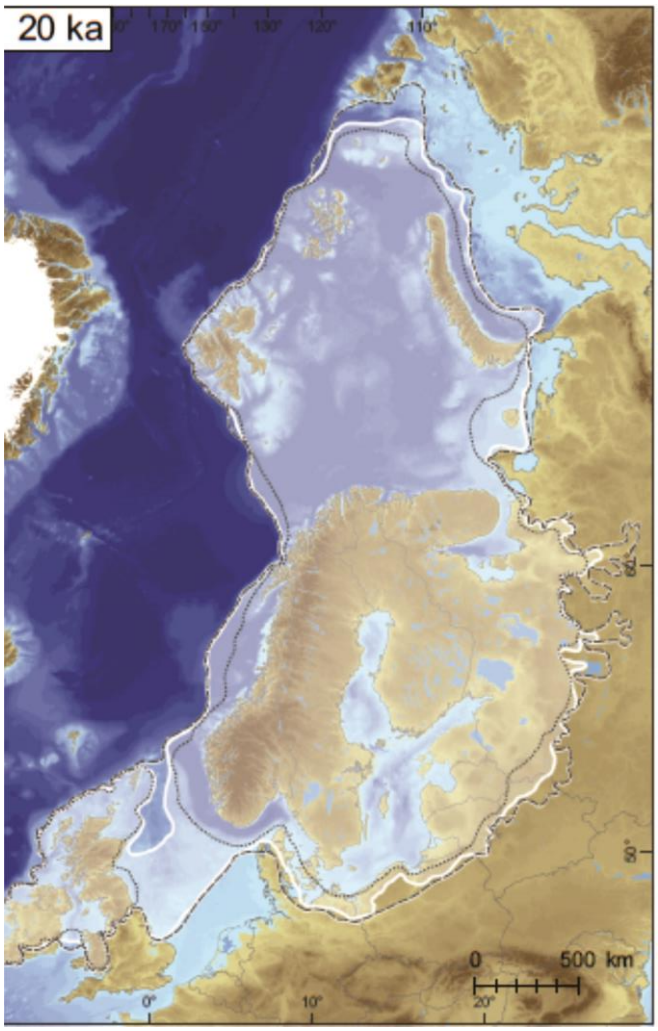

Figure 1.1: Figure showing the extent of the LGM 20 000 years ago. Ice thickness over the Northern Barents Sea was 1 km. Picture modified from Hughes et al. 2015.

At this time the entire Barents Sea was covered by grounded ice with a 1 km thick ice sheet resting over the northern Barents Sea. (Hughes et al., 2015; Siegert et al., 2001; Landvik et al., 1998).

In order to time the retreat of the ice sheet several authors have dated sediments found in ridges and depositional features. Datings from Ingøydjupet, north of Norway, shows ice free conditions already by 18.7 cal ka (Junttila et al., 2010) and at the mouth of Bjørnøyrenna the deglaciation is dated to ~17 ka (Rüther et al., 2011) due to warmer temperatures, a sea level rise and protrusion of the Atlantic Water (Dokken & Hald, 1996; Duplessy et al., 2001; Ivanova et al., 2002; Slubowski-Woldenengen et al., 2008). By ~15 ka the Barents Sea wasmostly ice free (Vorren & Kristoffersen, 1986; Laberg et al., 1998; Hughes et al., 2015).

Salvigsen (1981) found the deglaciation of Kong Karls Land to be 11.1-11.6 cal ka indicating that the ice remained on land for a longer time period.

Figure 1.2 shows an empirical reconstruction done by Hughes (2015) of the minimum and maximum extent of the glacier front during the deglaciation 14, 15 and 16 ka. The spatial evolution of the ice sheet every 1000 years from 25 ka to 10 ka is shown in her paper.

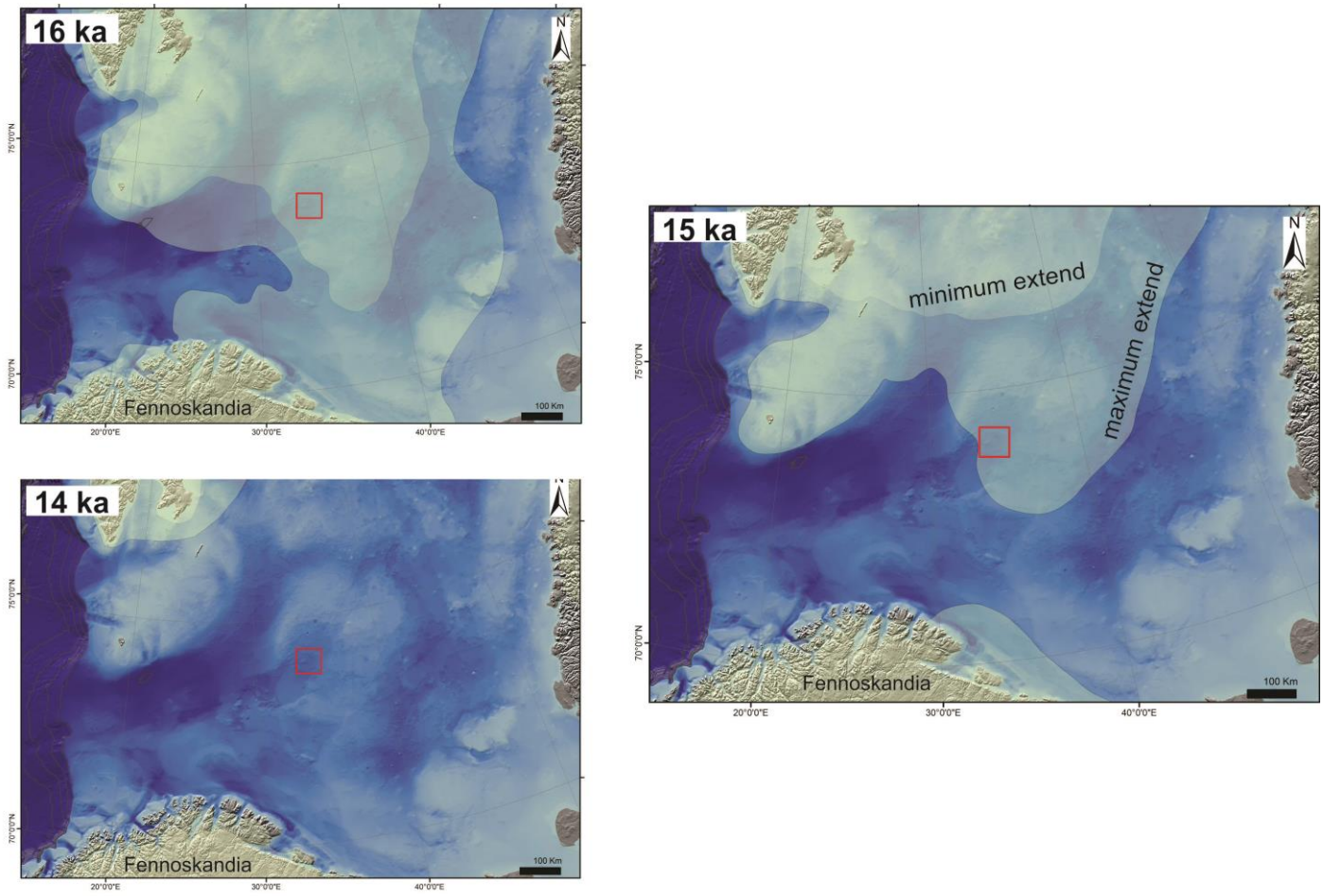

Figure 1.2: Imperical estimations done by Hughes (2015) show the minimum and maximum extend of the BSIS 16 ka, 15 ka and 14 ka. Study area is marked with a red square. Modified from Hughes 2015.

The figure shows how the ice sheet went from covering huge parts of the Barents sea 16 000 years ago, to a rapid retreat, to remaining mainly on land by 14 000 years ago. The area in this study is marked with a red square.

Dating of the sediments in the Barents Sea is difficult, giving a poor temporal constraint of the deglaciation. However, good spatial constraints are given from several lineations, moraines,

ridges and grounding zone wedges along the trough. These features show a retreat of the ice sheet consisting of streaming, slow down and stagnations. This as well as indications that the BSIS was a warmed based ice sheet reveals a dynamic ice sheet with an episodic retreat (Andreassen et al., 2014; Bjørnadottir et al., 2014; Winnsborrow, 2010).

1.3.3. Late Deglaciation and Holocene

The epoch Holocene started about 11 700 years ago and continues up to today. This is a warmer period marking the end of the previous ice age, the Weichselian. The warming of the late Weichselian and transition to the Holocene are linked to the North Atlantic surface water flowing into the Polar North Atlantic water (Dokken & Hald, 1996). Already by 16 ka higher amounts of IRD are recorded as a result from the decaying BSIS (Slubowska-Woldenengen et al., 2008).

The Bølling-Allerød interstadial was a milder period in the end of the Weichselian from 14.5-13.5 ka, where the Atlantic Water started entering the Barens Sea. This was followed by a stadial; a colder period, similar to the last glacial with polar conditions and a large sea ice cover reaching all the way to Iceland from 12.5 to 11.5 ka.

In the very beginning of the Holocene there was a strong protrusion of the Atlantic Water, and therefore the early Holocene was the warmest period, reflected in little IRD and no ice. 4000 years ago polar conditions were returning and a weakening of the Atlantic Water flow occurred; during this time sea ice was formed in winter time (Slubowska-Woldenengen et al., 2008; Duplessy et al., 2001).

1.3.4. Sedimentation of the Barents Sea

The Barents Sea consists of a thick layer of late Palaeozoic to Neogene sedimentary rocks (~300 ma) lays on top of a Precambrian crust. Many basins and heights in the Barents Sea are formed by these sedimentary rocks during the formation of the Atlantic Ocean (Dallmann et al., 2015). Figure 1.3 illustrates the sedimentary bedrocks found in the Barents Sea.

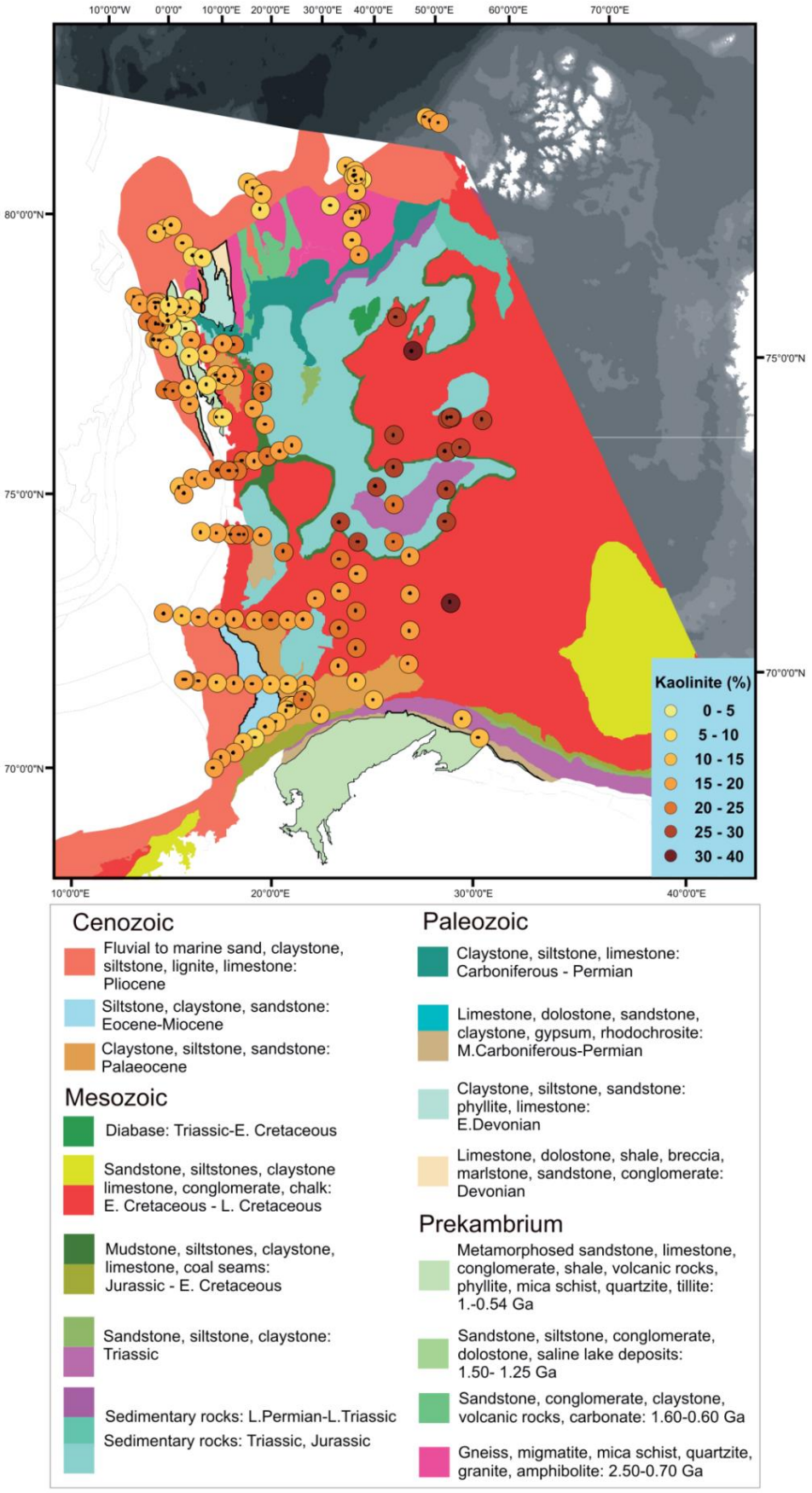

Figure 1.3: The distribution of kaolinite in the Barents Sea, show high values in the Central Parts, the background map is a simplified bedrock map of the Barents Sea. Modified from Vogt & Knies, 2009.

As figure 1.3 illustrate, are the bigger parts of the central Barents Sea of clastic sedimentary rock from the early Cretaceous. The banks in the northern parts consist of siltstone and claystone, including Sentralbanken. An increasing amount of Kaolinite can be observed towards the Central Barents Sea. Higher levels of kaolinite in sediment records indicate glacial erosion, while kaolinite usually comes from reworked sediments from the northern and central Barents Sea (Vogt & Knies, 2009).

During the Quaternary and the Tertiary the glacial erosion in the Barents Sea has been high. In the troughs about 1000-1100 m of sediments was eroded in this period. (Løseth et al., 1992; Richardsen et al., 1993; Laberg et al., 2012). The glacial sediments in the Barents Sea are separated from the bedrock by an upper regional unconformity. The sediment layer of the Barents Sea varies and is at its thickest in the western and outer part of Bjørnøyrenna where it exceeds 500 meters. It decreases towards the inner part of the trough and the Central Barents Sea. In general the sediment depths are ~10-20 metres of till and glacimarine deposits, depending on the water depths in the area, covered by a layer of Holocene mud usually around 1 – 1,5 meters (Vorren et al., 1989; Elverhøi & Solheim, 1983). Depending on the position of the sea ice margin and the polar front, the glacimarine sediments gradually show a more marine environment (Ivanova et al., 2002).

1.4. Ocean Currents

The Barents Sea is where the cold and low salinity Arctic Water (ArW) interacts with the warmer and high salinity Atlantic Water (AW) from the South.

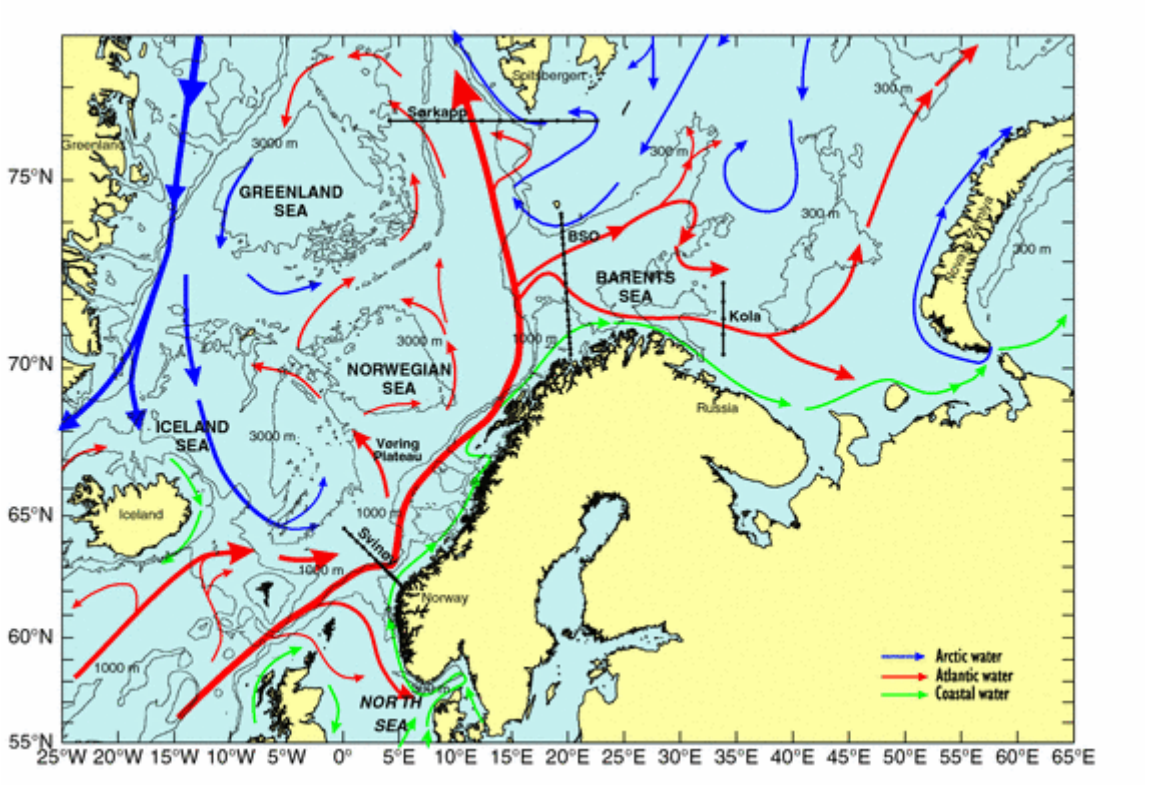

Figure 1.4: Figure illustrating the Atlantic water migrating along the Norwegian coast into the Barents Sea, where it meets and mixes with the Arctic water from the North. Picture from Skageset et al., 2008.

As illustrated in figure 1.4 the AW flows along the west coast of Norway and breach into two outside Bjørnøyrenna. Here one branch flows northwards along the west coast of Svalbard, while the other flow eastward, entering the Barents Sea through Bjørnøyrenna as the North Cape Current. The cold ArW enters the Barents Sea through the Archipelago's in the north (Murdmaa et al., 2006).

The zone where the two waters AW and ArW meet is called the polar front and are illustrated with a black line in figure 1.5, here the two water masses are mixed, and the warm, saline and dense Atlantic Water sinks underneath the cold Arctic Water.

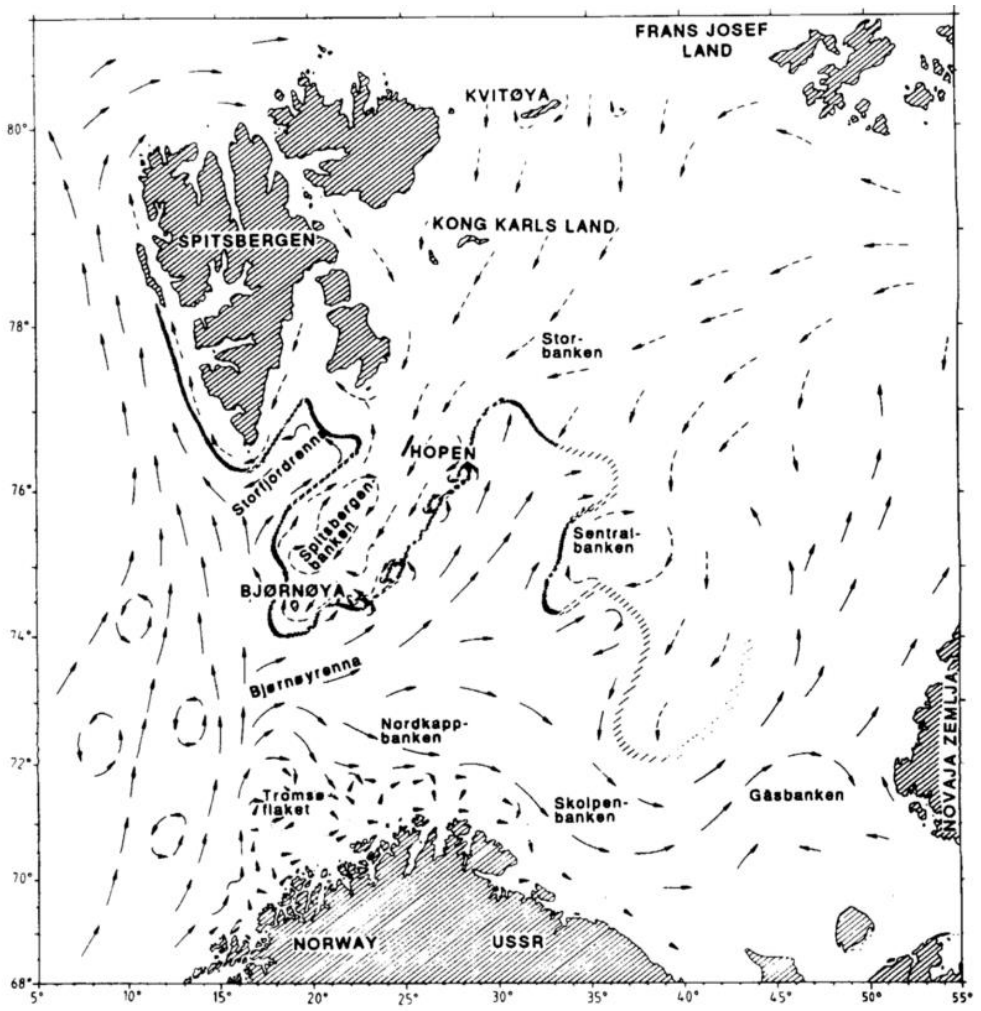

Figure 1.5: Figure showing the currents entering the Barents Sea, and the zone where the water masses meet and mix, called the polar front. Figure by Loeng, 1991.

Figure 1.5 shows the currents with arrows and the polar front with a black line, where intense downwelling of water masses occur. The Polar front is in general varying between 74˚ and 76˚N, from being rather stable close to Spitsbergenbanken, is it highly diffuse in the Sentralbanken area illustrated with a broken line In figure 1.5 (McClimans 1993; Murdmaa, 2006). In this area parts of the North Cape Current turns eastwards between Storbanken and Sentralbanken and continues as a subsurface flow.

In the southern Barents Sea the currents mainly move towards the East, while in the North the currents move westwards (Loeng, 1991) following a counter clockwise pattern. A high variation in bathymetry dominates the Barents Sea, with its deep troughs and shallow banks, which has a strong influence on the currents. Around Sentralbaken a large anti-cyclonic eddy is created from the bottom topography, also shown in figure 1.5 (Loeng, 1991).

1.5. Sedimentation processes

The distribution of sediments from an ice front is largely influenced by meltwater discharge and ice berg calving. They are so dispersed by ice contact processes, fluvial processes, rafting by ice bergs or sea ice and deep water currents. The sediments may be redistributed after deposition; these are processes such as slides and mass wasting (Syvitski, 1989).

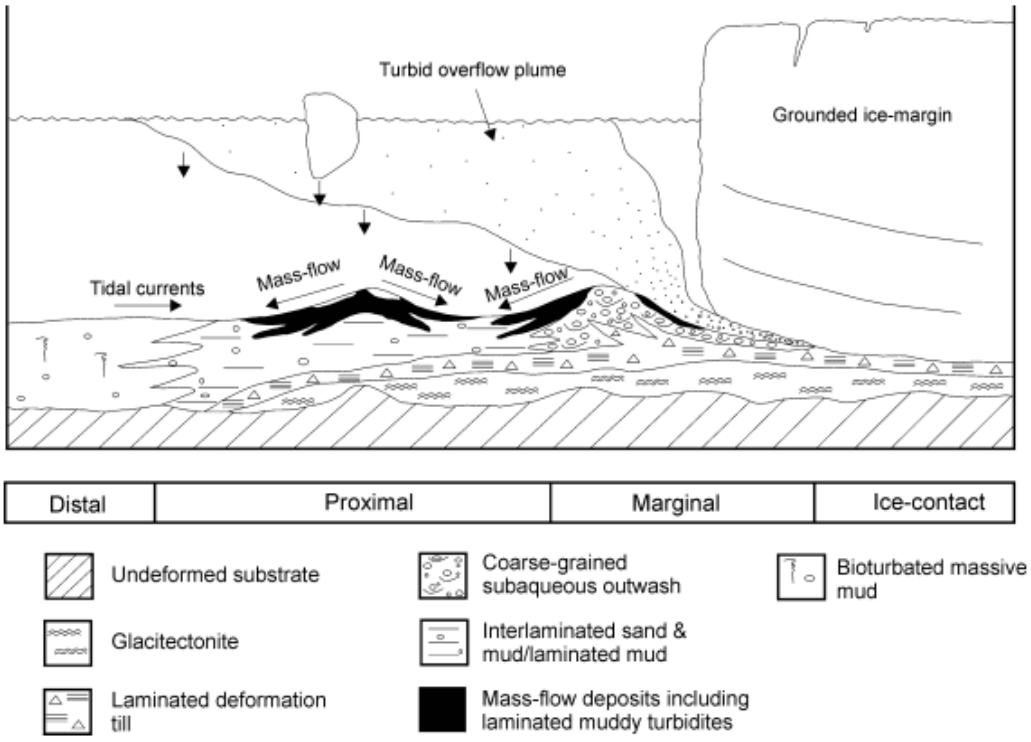

Figure 1.6: Showing the sediment deposition in front of a glacier front, from ice contact subglacial till to distal deposition of finer sediments. Illustration from O Cofraigh & Dowdeswell, 2001.

Figure 1.6 illustrate the sediment transport dominating in front of a glacier front, Ice contact processes, marginal and proximal to distal processes show different characteristics, making it possible to recognize and reconstruct the paleoenvironment. Sediments usually have a distal fining from the glacial front, as well as the sedimentation rate decrease from the ice margin (O Cofaigh & Dowdeswell, 2001; Syvitsky, 1989)

1.5.1. Mass waste

Mass flow is an important process redistributing sediments and occur where the sedimentation rated are high. Away from the ice margin the sediments are fine grained, except when slides or turbidity flows has occurred (Dowdeswell et al., 1998; Syvitski, 1990).

Turbidity current deposits are laminated mud alternating gravely sand usually, and they can be massive, graded or irregular. Usually they have a scoured base and inner structures as loading cast features or ripples are common (O Cofaigh & Dowdeswell, 2001).

1.5.2. Meltwater plumes

Sand and coarse silt are heavy particles and therefore deposited rapidly from suspension. Finer sediments as clay and fine silt can be held in suspension for a longer period and will be transported by plumes for further distances, making the sediments have a distal fining from the glacier front as showed in figure 1.6.

Meltwater discharge changes with temperature, as higher temperatures causes more melting. Meltwater plumes can transport material up to fine sand in suspension. The distances of transportation will vary with the strength of the meltwater plume as well as the strength of the currents and eddies in the water column (O Cofaigh & Dowdeswell, 2001).

When meltwater enters a water column, buoyancy and density differences will cause the plume to float upwards. Depending on the strength of the meltwater discharge the plumes can carry material up to fine sand horizontally in the water column. Suspension settling from meltwater plumes produces planar, parallel lamina grading upwards from fine sand and silt to poorly sorted mud lamina (O Cofaigh & Dowdeswell, 2001). Ice proximal deposition of sediments by meltwater result in a pulsated sedimentation where meltwater flows as nepheloid layers towards the deeper depths, contributing to laminated or stratified sediments (Ivanova et al., 2002; Murdmaa et al., 2006).

1.5.3. Ice Rafted Debris

A huge part of the sediments deposited in a glacimarine environment is rafted debris, which can reveal information about both the oceanic and the terrestrial environment in the surrounding area. The loading of the sediments to the ice occur when the ice freeze to the bottom of the glacier, while they usually melt out one at a time producing dropstones, but they can also be deposited by dumps of sediments. Ice bergs are the main mechanism responsible for transporting coarser sediments to the seafloor (Dowdeswell et al., 1998; Gilbert, 1990).

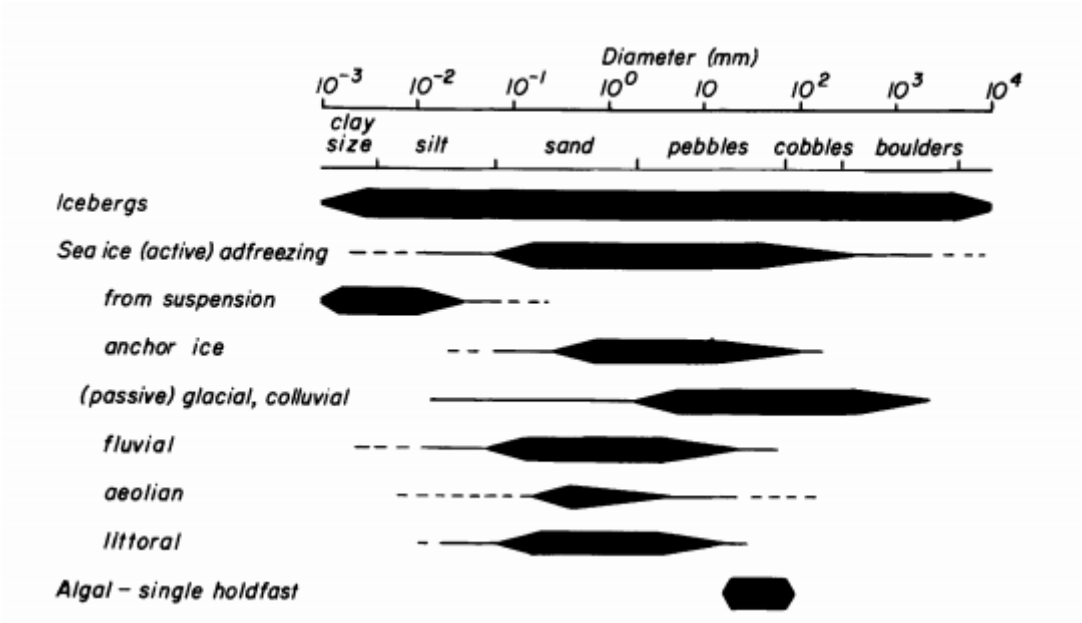

Figure 1.7: transport mechanisms for different grain sizes. Illustrating that icebergs can transport all sort of sediments to the seafloor, indicating a bad sorting of the sediments deposited. Figure from Gilbert, 1990.

Figure 1.7 illustrates what particle size different transport mechanisms are able to transport. The uppermost black line indicates that icebergs can carry all sorts of sediments from clay to boulders, ice rafted debris are therefore poorly sorted deposits.

IRD can be randomly dispersed in sediments in front of a glacier, but ice rafted deposits can also show a laminated nature. Figure 1.8 explains one way of how multiyear shore ice can suppress ice berg migration, resulting in IRD rich layers alternating IRD poor layers

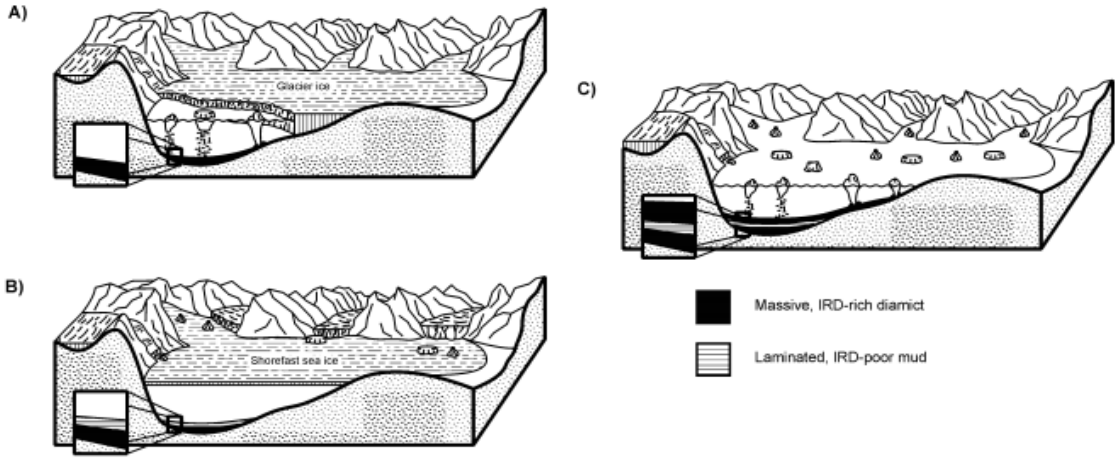

Figure 1.8: Laminated sediments produce during multiyear shore ice. Modified from O Cfaigh & Dowdeswell, 2001.

Figure 1.8 is a model showing in A) how ice can suppress drift of sea ice and icebergs, resulting in few to none IRD further away from the glacial front, since the icebergs are concentrated in the very front of the glacier. B) Illustrates a colder period, where the water is covered by sea ice. This leads to calmer sea and deposition of finer sediments, resulting in laminas of mud and clay. C) is a warmer period of no sea ice, the icebergs are now free to migrate and IRD are ramdomly dispersed aournd. (O Cofaigh & Dowdeswell, 2001).

2. Setting

The Barents Sea is one of the most extensive continental shelf seas in the world with a mean depth of ca 240 metres. It covers an area of about 1,2 x 10^6 km^2 . Figure 2.1 shows the position of the Barents Sea and how it connects to the Arctic Ocean in the north, the Kara Sea in the east, and to Fennoscandia in the South.

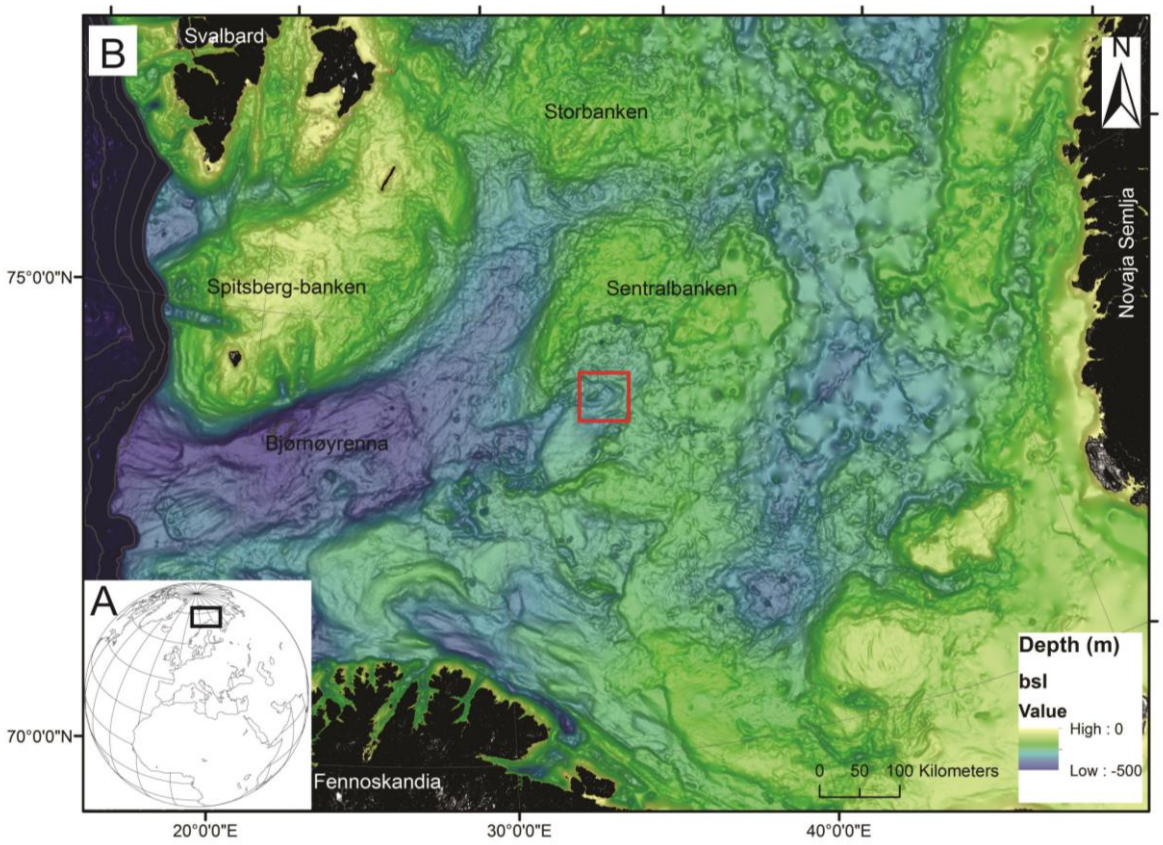

Figure 2.1: A) Barents Sea positioned on the world map B) Bathymetrical map showing the Barents Sea. The study area is in the Southern part of Sentralbanken, marked with a red square.

The morphology of the seafloor shows that the Barents Sea is strongly influenced by past glaciations, including troughs and banks. Deep troughs are from 300 to more than 500 meters deep, while the shallow banks are at water depths between less than 50 to more than 300 metres (Laberg, 2012). The study area is in the central part of the Barents Sea, in Sentralbankrenna south of Sentralbanken, marked with a red square in figure 2.1.

2.1. Geomorphology

The biggest and most prominent feature of the Barents Sea is the Bjørnøyrenna as marked in figure 2.1. This is the biggest trough in the Barents Sea, where most of the ice drained through during the last glacial maximum and the deglaciation, eroding a channel crossing the continental shelf. Bjørnøyrenna is 750 km long and 150-200 km wide. Grounding zone

wedges, moraines and ridges along Bjørnøyrenna shows the retreat of the ice sheet (Figure 2.2). In the mouth of Bjørnøyrenna there is a fan called a trough mouth fan which are made from the sediments transported through the trough and finally deposited on the shelf edge at the ice margin.

The dome and ice divide of BSIS during LGM was located over the northern Barents Sea (Landvik, 1998), Shown in figure 2.2. Giving Bjørnøyrenna ice stream a huge source area, reaching from the north east around Kong Karls Land, Storbanken and Sentralbanken ice masses came from East over Murmaskbanken, as well as the mainland of Fennoskandia (Bjarnadottir et al., 2014; Winsborrow, 2010).

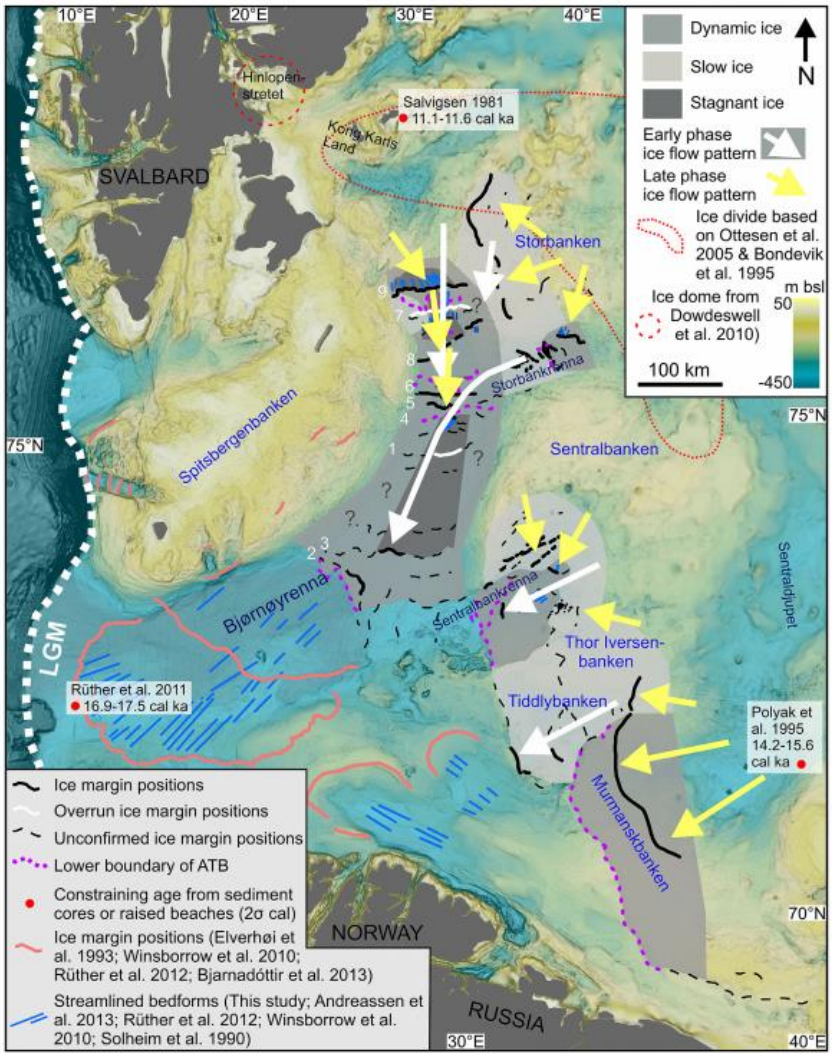

Figure 2.2: Large scale morphology of the Barents Sea, The ice dome, datings and ice flow directions. Figure by Bjarnadottir (2014).

As illustrated in figure 2.2 Bjørnøyrenna was again fed by several small troughs, leading ice masses down from the shallow bank areas.

The study area is in the central Barents Sea, in the southern part of Sentralbanken. Sentralbanken is one of several banks in the Barents Sea, situated at 74˚ North, with a small trough (Sentralbankrenna) on the Southern side entering the major Bjørnøyrenna. This was likely an important source area, feeding ice into the Bjørnøyrenna ice stream under maximum glaciation, and also an area onto which ice retreated during the deglaciation. Little is known about Late Weichselian ice dynamics in this part of the Central Barents Sea, primarily due to a lack of data.

2.1.1. Geomorphological features

Landforms are shapes from previous environments. A fast flowing glacier will leave several characteristic landforms behind. And particularly when an ice sheet has a fast retreat, these landforms are better preserved (Benn & Evans, 2010). Figure 2.3 illustrates geomorphological features characteristic for a fast flowing ice stream.

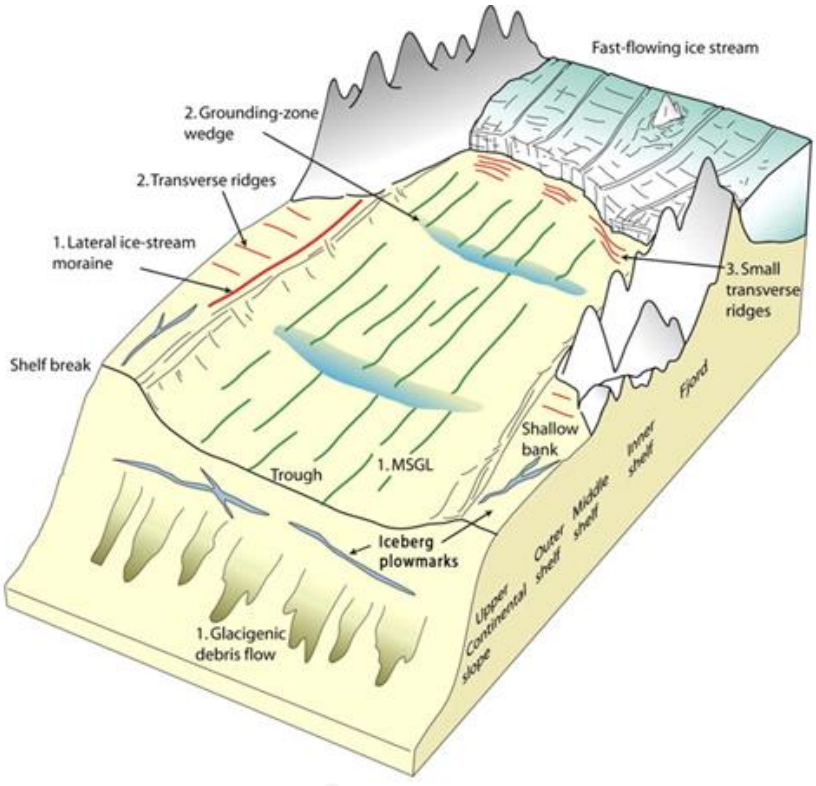

Figure 2.3: Morphological features produced by a fast flowing ice stream. Modified by Ottesen & Dowdeswell, 2009.

Grounding zone wedges are huge sediment depocentres deposited by glacial meltwater during a standstill in an ice sheet retreat. They are asymmetrical and steeper in the ice distal side; they are formed by rapid sedimentation and can therefore be several kilometres long. A grounding zone wedge has a high sedimentation rate; they can be kilometres in length and usually has a flat top (Batchelor et al., 2015).

Furrows are produced when a glacier ploughs the ground as it moves. When the ice has a fast retreat these lineations are well preserved, as well as their direction shows the palaeo ice-flow of the former ice stream (Clark et al., 2003).

Moraine ridges are small compared to the grounding zone wedges, indicating that the glacier has had a relatively short hiatus at that position during the retreat (Batchelor et al., 2015).

A trough mouth fan consists of sediments pushed and deposited by the glacier and several stacked units of debris flows. West of the Bjørnøyrenna there is a huge fan deposited, this is produced by sediments eroded by the glacier ice stream and deposited at the shelf edge (Vorren and Laberg 1997).

2.1.2. Geomorphological features in Sentralbanken

The first extensive geomorphological mapping of this area was carried out by Bjørnadottir et al. (2014), based on low resolution OLEX bathymetry data. This showed for the first time the retreat patterns of the Bjørnøyrenna ice stream in this area and also documented evidence of abundant meltwater activity. In the early stages of the deglaciation the ice masses drained from the ice divide in the Eastern Barents Sea, through the Sentralbanken area to feed the Bjørnøyrenna ice stream. Figure 2.4 shows the morphological features of Sentralbankrenna.

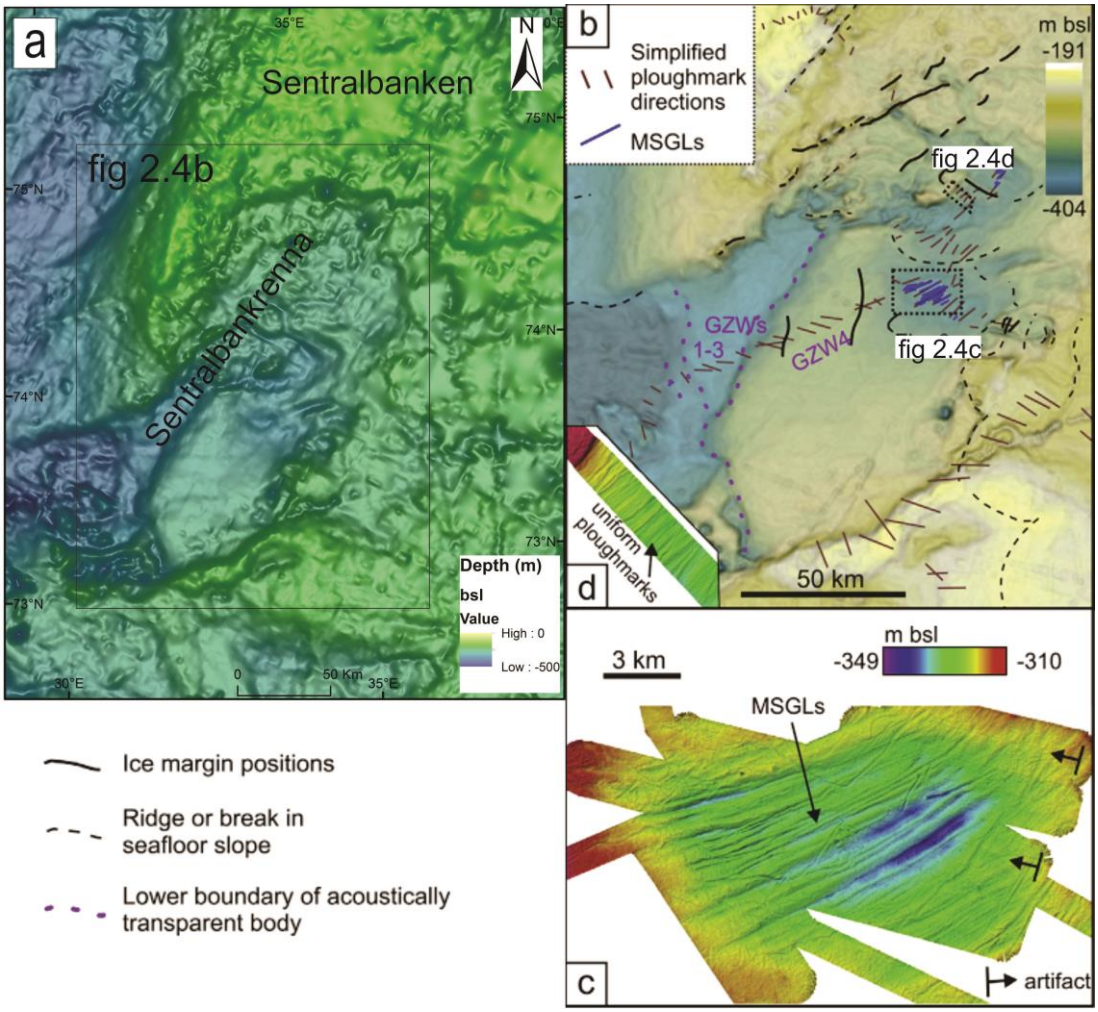

Figure 2.4: Bathymetry map showing the morphological features found and identified in Sentralbanken by bjarnadottir (2014). Four grounding zone wedges, MSGL's revealing the direction of ice flow and former ice margin positions. Modified from Bjarnadottir et al., 2014.

Four features interpreted to be grounding zone wedges are found in the lower area of Sentralbankrenna and marked in figure 2.4, these are suggested to be deposited by meltwater from the margin of an ice stream. The ridges found above the grounding zone wedges are suggested to be recessional moraines, which are much smaller, and indicates stillstands; a slow and episodic retreat of the ice. These features together illustrate a dynamic ice sheet with

rapid melting between the stagnations, including basal meltwater pressures indicating a warm based glacier (Bjørnadottir et al., 2014).

On grounding zone wedge 4 MSGL are found with a NE - SW orientation, formed beneath a fast flowing ice stream. In the early stages of the deglaciation the ice flow direction was from ENE towards WSW. While later in the deglaciation, the ice masses became more topographically dependent, draining ice masses from North, East and Southeast into Bjørnøyrenna. The bathymetry in the area is also dominated by tunnel valleys indicating that the drainage of meltwater during the later deglaciation was channelized (bjarnadottir et al., 2014). In Sentralbankrenna there is a network of these valleys, including basins which can contain up to 70 meters of sediments. These basins may have acted like traps for meltwater. Recessional moraines are breached by these tunnel valleys, indicating that the tunnel valleys were active at the same time as the moraines were deposited. On the other hand the unbreached moraines indicated that no meltwater was running through during the deposition. The channel the cores are collected from is breaching one of these moraines (Bjarnadottir, 2012).

The cores in this study are collected from one of the tunnel valleys mapped by Bjarnadottir et al., 2014. Figure 2.5 shows the location of the four cores on a bathymetrical map over Sentralbanken area.

.

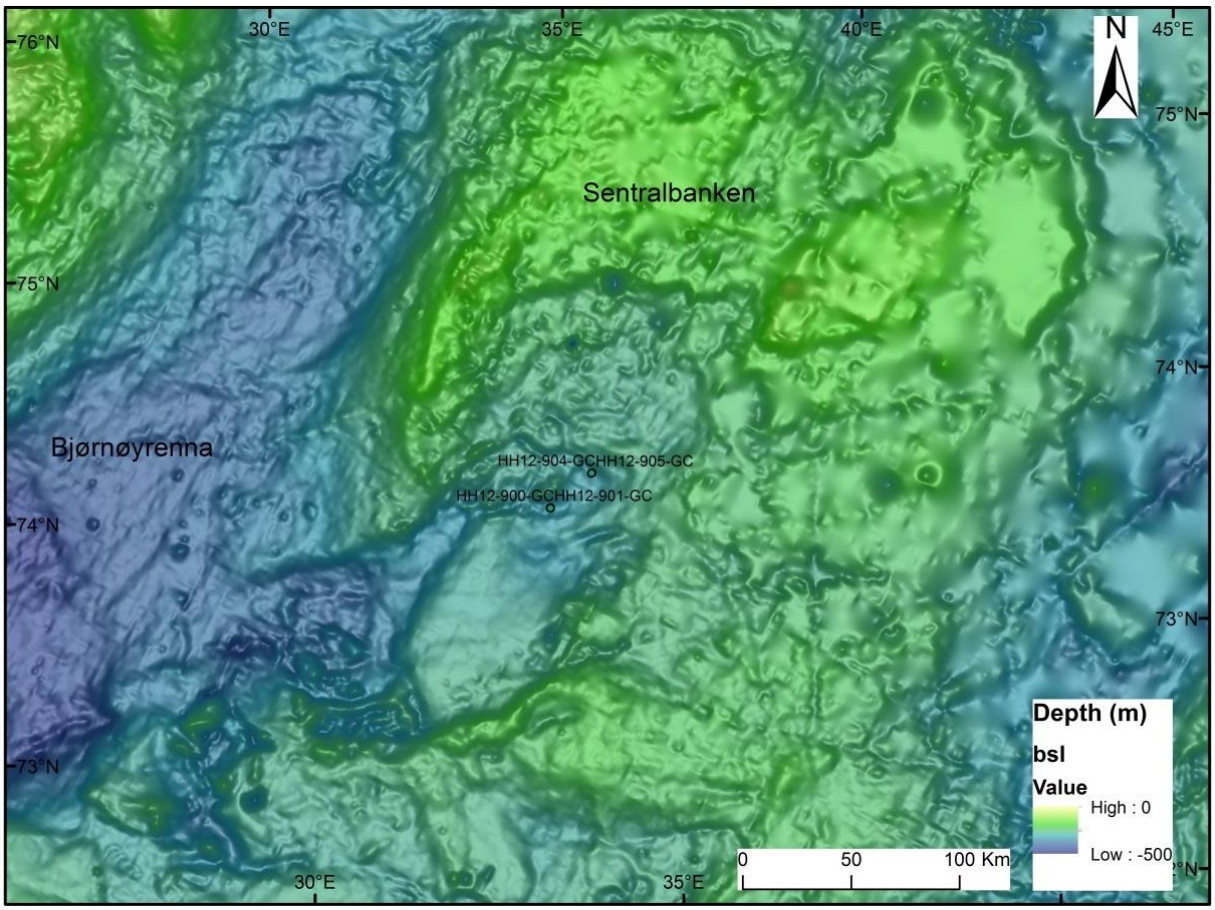

Figure 2.5: Bathymetry of Sentralbanken showing the location of the cores

As illustrated in figure 2.5 are the cores in this study collected within one of the tunnel valleys mapped by Bjarnadottir et al (2014), four cores are collected from two different basins. The amount of ridges and grounding zone wedges in this area indicates a very much dynamic ice stream. Sentralbankrenna is an area which has undergone ice streams and melting from several directions (bjarnadottir et al., 2014). From figure 2.4 b the glacier has been retreating in a Northwestern direction, cores in these position will therefore likely always been exposed for meltwater and sediment depositions from the glacier.

3. Methods

3.1. Collecting data

All data is collected on R/V Helmer Hanssen in 2012, a vessel operated by UiT (The Arctic University of Norway). The data consist of seismic data, chirp lines and four sediment cores from different locations within the study area.

3.1.1. Multibeam echosounder

A multi beam emits a fan of sound beams to the seafloor where the backscatter (echo) is used to reveal information about the sea floor. Helmer Hanssen is equipped with a Kongsberg Simrad EM300. The fan (perpendicular to the ships track) produced underneath the vessel is made of 135 beams, where each beam covers 1˚. When operating with a frequency of 30 kHz it has an angular coverage of up to 150 degrees. At the water depths of 150-400 m found in the study area, swath width would have been 1-2 km.

A multi beam echo sounder measures depth, seabed shape and slopes by analysing the strength and time of the back scattered signal. The acoustic waves provide information about the sub sea surface and can penetrate up to a few tenth of cm in soft sediments. By recording the strength of the back scattered signal, the type and distribution of sediments can also be detected (Carter, 2012). The bathymetric dataset was gridded to a horizontal resolution of 15 m and has a vertical resolution of ~10 cm.

Figure 3.1: Multi beam fan produced by a multi beam echo sounder. Figure retrieved from Kongsberg, 2010

3.1.2. Sub bottom Profiler (Chirp Sonar)

The chirp profiler used for these profiles is an Edgetech Chirp 3300-HM which is a hull mounted, high resolution frequency modulated sub-bottom profiler.

A chirp profiler is a high frequency measurement revealing quantitative information about the sub-sea floor stratigraphy. Signals are reflected at different densities, giving the transition between layers as well as the colour changes with density where less dense sediments will appear darker. With frequencies ranging from 1, 5 – 12 kHz it can penetrate the sediments with a vertical resolution up to 30 meters of unconsolidated sediments, depending on sediment type and thickness. The Central Barents Sea has a thin sediments cover, where till and glacialmarine sediments reduces the penetration depth. The chirp sonar gives real time, artifact-free, high resolution estimates of different sediment layers of the seafloor (schock, 1989; Quinn et al., 1998; Elverhøi & Solheim, 1983).

Pulses of 1,5 -9 kHz were applied for 40 ms, where high frequency signal give a high resolution, but also a low penetration. The vessel travelled at a speed between 7 and 11 knots and the shot rate was 1.

Multiples are delayed signals from the emitter, and therefore a mirror image from another layer.

3.1.3. Gravity Cores

Four cores were collected south of Storbanken area July 2012, information is shown in table 1.

Table 3.1: Core log

Station	Date	Time (UTC)	Location	Position Latitude [N] Longitude [E]	Water depth (m)	Penetration (GC)	Recovery (GC)	Comments
HH12-900 GC	13.07.2012	21:50:59	Sentralbanken South	73˚57.912N 033˚51.640E	333	Full	3,8 m	Core catcher sampled
HH12-901 GC	13.07.2012	22:20:35	Sentralbanken South	73˚57.884N 033˚48.876E	333	5 m	3,19 m	Both core cutter and catcher sampled
HH12-904 GC	14.07.2012	01:38:12	Sentralbanken South	74˚05.312342N 034˚29.759924E	325.21	full	4,05 m	Both core cutter and catcher sampled
HH12-905 GC	14.07.1012	02:19:02	Sentralbanken South	74˚05.242813N 034˚29.553478E	324.3	full	3,65 m	Both core cutter and catcher sampled

The sediment cores were collected from the sea floor using a **gravity corer**, a six-meter long steel barrel, with an additional weight of 1900 kg. The corer is lowered vertically from the vessel, and dropped about 20 meters above the seafloor, penetrating the sediments using gravity. An 11 cm wide plastic tube is on the inside of the steel barrel, collecting the sediments. A *core cutter* and a *core catcher* are mounted to the end of the tube to penetrate the sediments easier and to prevent sediments from falling back out when the corer is pulled back into the vessel. On board the samples are cut into sections of 1 meter, sealed, numbered and stored in a cooling room.

3.2. Data analysis

At the University of Tromsø the cores has been stored in a cool room.

3.2.1. X-ray

Before splitting the cores for visual analysis **X-ray** images were taken, using The X-ray machine operated by UiT, a Geotek MSCL-XCT. X-ray images can provide information about the internal structures, lithological variations fragments as clasts and shells as well as organic material and bioturbation of sediment cores.

X rays are light, only they have shorter wave length than visible light (and they have a smooth and continuous spectrum). Short wave length has better penetration power (Fujifilm, 2014). When a x-ray is taken the object is placed in between a source of accelerating electrons emitted, and a detector. The darkness of the image varies with the amount of radiation that hits the detector, making denser parts of the material appear light on the image, and less dense material will appear darker.

3.2.2. Multi Sensor Core Logger (MSCL)

Multi Sensor Core Logger (MSCL) shown in figure 3.2 can be used either on whole or on half cores. The MSCL-S in Tromsø is from Geotek. When logging cores using the multi sensor core logger the core is pushed through the instrument using a core pusher. For every cm of the core measurements are taken to reveal information such as density, p-wave velocity and amplitude, magnetic susceptibility (loop and point sensors) acoustic impedance, CT, fraction porosity. The instrument is also equipped with a colour spectrophotometer. A

thermometer is used to measure the room temperature to make sure all measurements are done under same conditions.

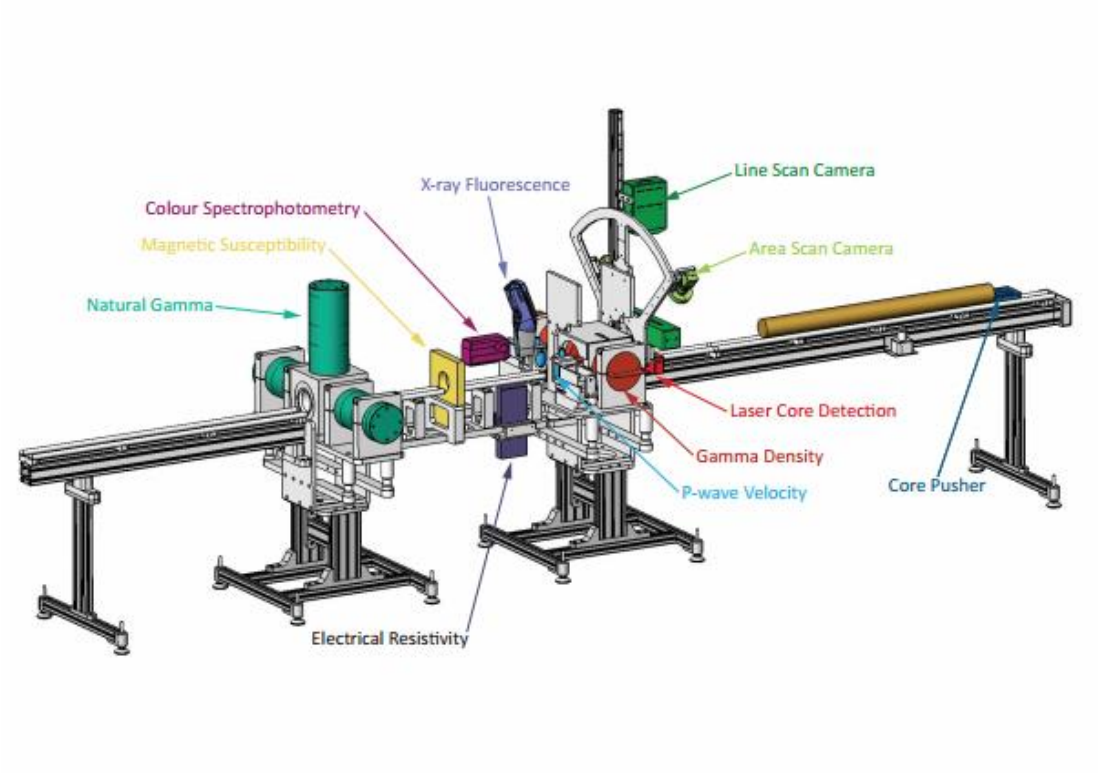

Figure 3.2: Geotek Multi Sensor Core Logger. Figure retrieved from Geotek, 2014b.

Wet bulk density

The density of a material is a measure of how tightly the matter within it is packed together and is given by the ratio of mass to its volume **(**Geotek, 2014**).**

Collimated gamma rays are emitted from a source. Photons passes through the core before detected on the other side. Within the core the photons are scattered by electrons leading to a slight energy loss for the photon. By measuring the amount of emitted gamma photons that has passed the core unattenuated the density of the material can be determined **(**Geotek, 2014**).**

Processes that affect the sediment porosity are the gravitational compaction, and bulk density therefore indicates the accumulation rate (Dadey, 1992).

P-Wave velocity

Primary waves (P-waves) are compressional waves of pressure, moving through all types of material solids, liquids and gases. P-waves travel through the earth at speeds between 1 and 14m/s, depending on material. (Gelius, 2007).

P-wave velocity graphs provide detailed cross correlation of offset holes at the same site. It helps us identify sedimentary features rapidly (eg slumps and turbidites) and together with gamma attenuation and porosity evaluator the detailed density and velocity profiles required to generate accurate synthetic seismograms that can be correlated with seismic profiles (Schultheiss et al., 1986).

A short P-wave pulse is produced; it propagates through the core and is detected on the other side. Travel time is measured, along with the distance which is measured as the core diameter (Geotek, 2014).

Magnetic Susceptibility

The magnetic susceptibility of a material can tell us about changes in source area, and therefore it can help explaining sediment transportation and depositional processes.

Magnetic susceptibility is measured on the whole core using a loop sensor. This loop has a wide measuring field, and is not as sensitive to small anomalies in the core. The overlapping measurements will give a smooth graph.

Magnetic susceptibility is the degree of magnetization of a material in response to an applied magnetic field. Positive values means the magnetic field is strengthened by the presence of the material, while negative values means the magnetic field is weakened by the magnetic field (Geotek, 2014).

Acoustic Impedance and Fraction Porosity

The Acoustic Impedance is the product of P-wave velocity and density, $Z = V * \rho$.

The acoustic impedance can be related to layer interfaces that cause reflections of incident seismic waves (Breitzke, M. 1993)

If the sediments are fully saturated and we know both mineral grain density and fluid density fraction porosity can be calculated (Geotek, 2014).

Colour Spectrophotometer

The multi sensor core logger is equipped with a portable Konica Minolta CM-700d spectrophotometer that measures the surface reflectance on half cores. After cutting the cores, using Marinetechnik Kawohol sediment liner saw, the MSCL spectrophotometer was used. The machine gives the Munsell colour code for every measurement done (Geotek, 2014).

3.2.3. Grain-size Analysis

In order to analyse grain size distribution, one cm of sediments was collected every tenth cm of all cores. Within a part of all cores lamination was found from the x-ray photos and samples were collected every fifth cm in these areas. In total 196 samples was analyzed.

A type C Beckman Coulter LS 13320 is used for the grain size analysis. The particle size analyzer uses a laser beam to calculate the distribution of fine grained material under 2000 µm within a sample, so that clasts are counted individually.

Preparation

Before using the grain size analyser, all carboniferous and organic material has to be removed. Carbonate is removed by leaving the sample in HCl for 24 hours. The tube is filled half way up with HCl. After putting the sample in the sentrifuge the liquid is easily poured out. The samples were washed twice with destilled water to make sure all HCl was gone. After this treatment, H_2O_2 was used to remove organic matter. To enhance the reaction the samples were put into a water pool of 85 degrees for two hours. This procedure was done twice to make sure most organic matter was gone. The samples were again washed with destilled water to make sure all H_2O_2 was gone, before left for drying in room temperature to prevent the sediments from harden while drying. 0,5 grams of sediments were taken out for analysis, 20 cl water was applied before they were shaken for 24 hours; a few drops calgon was added as well as the sample had an ultrasonic bath, all to prevent the clay from sticking together.

Measurements

The analysis is done using a laser particle size analyser of the type c Beckman Coulter LS 13320. 0,5g from each sample was applied for the analyser to determine the distribution of fine-grained particles. The particle size is measured using a light source whereas the pattern of the light scattered is measures. Because each particle scattering pattern is characteristic of its size, the angularity of scattered light can be transformed into a function (Beckman Coulter, 2011).

A sensor is measuring the density of the particles in the water which was between 95 – 99%. If the sampled reached 100% the water tank is filled with sediments meaning it is harder for the machine to detect individual particles, the sample therefore has to be diluted.

The measurement is done three times and the mean are calculated. Figure 3.3 shows the classifying used when sorting the sediments.

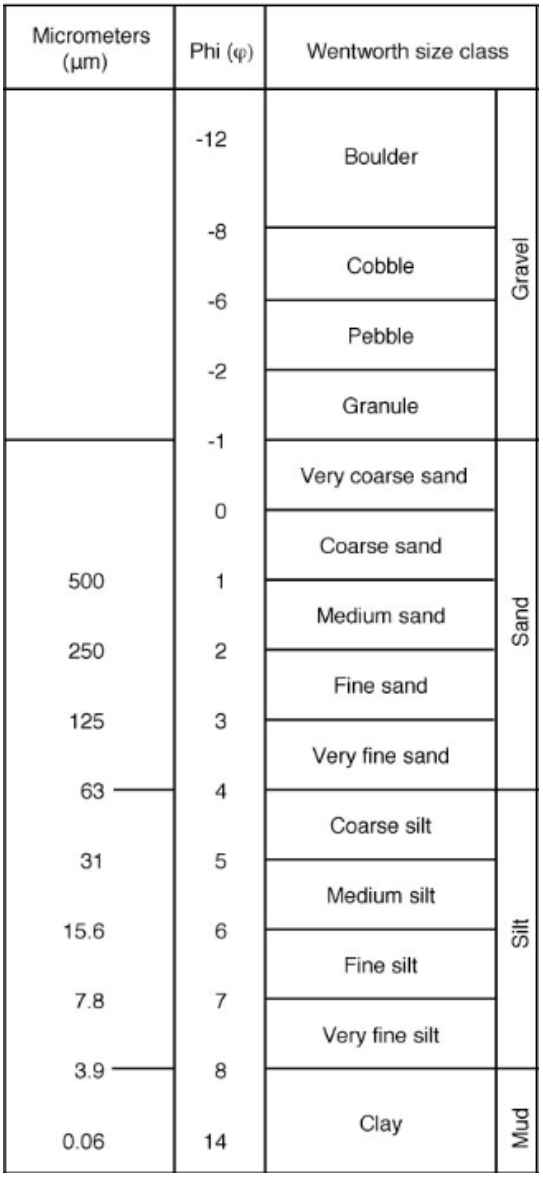

Figure 3.3: Classification of the different grain sizes measured in diameter. Figure modified from Wentworth, 1922

3.2.4. XRF

The XRF machine at UiT was of the type Avaateck core scanner. An X-ray fluorescence scan (XRF) is used for high resolution colour pictures and for elemental mapping of the sediment core.

High resolution colour photos were first taken on newly smoothened cores that were not covered.

To prepare the core for the XRF scan the cores were first adjusted to room temperature. The surfaces were then flattened and smoothened, before a 4 µm thick Ultralene film was applied to the core surface to avoid contamination. Trapped air between the film and sediment surface must be removed.

Measurements were done with 10 and 30 kV, every 10 mm.

A measuring prism is lowered to the sediment surface, radiation is generated in an X-ray tube and primary X-rays hit the surface with an angle of 45˚ as shown in figure 3.4. An element specific fluorescence radiation is emitted and is received by the detector on the other side which is also installed at a 45˚ angle.

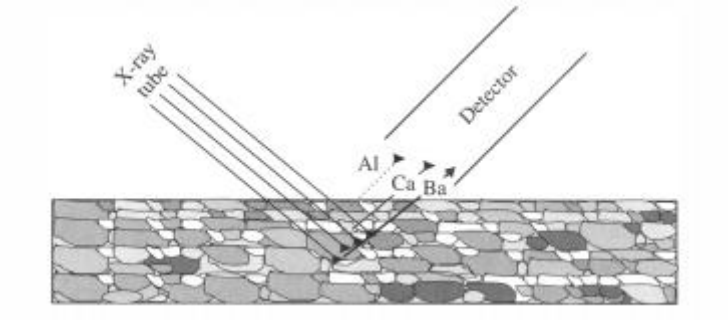

Figure 3.4: XRF scan. From Richter et al., 2006

The heavier the element is the stronger the fluorescence radiation it emits which again results in a larger penetration depth of the primary X-rays (Δx) (Tjallingii et al., 2007; Richter et al., 2006).

The elements analysed with the Avaateck XRF are from magnesium to uranium, which covers an atomic weight range from 13 to 92. Different currents (I) and voltages (V) are used because the energy required to excite the various elements is too large, so that measurements of the different elements has to be done in different runs (Forwick, 2013). 10 kV are used for

measurements from Mg to Co, 30 kV is used on semi-heavy elements from Ni to Mo and 50 kV are used on the heavy elements ranging from Mo to U. The system is filled with helium because it has a lower friction than air on the emitted radiation (Forwick, 2013).

To get the best results the samples needs to be homogenous, dry and have a flat and smooth surface. Marine cores are usually wet; they can contain shell fragments, foraminifera and IRD, leading to an inhomogeneous, rough surface (Richter, 2006). The presence of water in the cores has an effect on the lighter elements measured with 10 kV meaning the intensity of the lighter elements is reduced. This is not affecting the heavier elements (Kido et al., 2006; Tjallingii, 2007).

From the measurements relative numbers are given for each measurement done. There are a limit in which these numbers are valid or not (Forwick, 2013), if the values are above this limit they are valid to use, and are said to have "sufficient counts".

The use of element ratios is used to avoid misinterpretations. Ratios can help solving the problems of water improving the element concentration for the smaller atoms. It also helps alleviating the noise from elements that cannot be detected by the XRF (Weltje & Tjallingii, 2008)

3.3. Sortable silt

For a grain to be transported by a current a specific current energy is needed for that grain size to move. Figure 3.5 is a Hjulstrøm diagram illustrating erosion, transportation and deposition by grains of different size in a river of 1 meter depth.

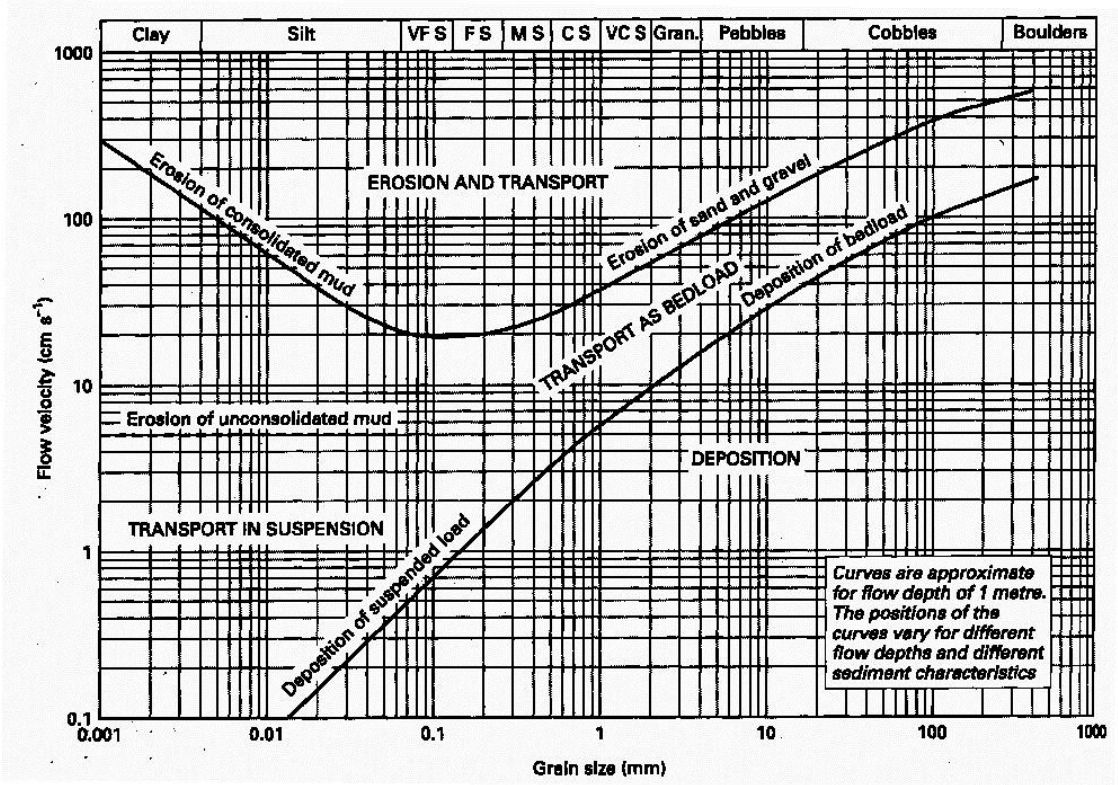

Figure 3.5: Hjulstrøm diagram made for eroding and transporting of sediment particles at 1 meter depth in a river. The illustration indicates current velocities needed to erode and transport different particle sizes.

The upper line in the plot shows the amount of energy required to erode and transport sediments, while the lower line show the current energy needed for a particle to settle from suspension (Nichols, 2009).

Sortable Silt is the coarsest silt fractions and the grain sizes between 10-63µm. Grain sizes smaller than 10µm like clay and fine silt are cohesive and forms aggregates, while sand particles, which are grains larger than 63µm are usually too heavy to be transported in suspension over longer distances, therefore sand is suggested to be mainly ice transported. Silt can also be transported by ice, therefore it can be more helpful to look at the stability of the SS plot, where current transport will chow a more stable SS plot than IRD influenced material would do (McCave et al., 1995; Hass, 2002)

If sand is ice transported and silt is current transported, there should be no correlation between the two (Hass, 2002). The stability of the sortable silt plot will also give an indication whether the sediments are current or ice transported, as currents will give smoother changes than random ice rafted deposits.

The correlation between the two parameters sortable silt and sand content are done by plotting them together. A regression line will show the correlation between the two parameters, and a

positive correlation line means than an increasing sand content leads to an increase in sortable silt size. An additional R^2-value is a measurement of the correlation, showing a value of 1 if all points were on the regression line. The R^2-value also shows if the calculations are statistically relevant (McCave et al., 1995; Hass, 2002).

The potential sortable silt (SS_{pot}) is found by using the regression equation, and describes the changes in sortable silt if there were no changes from the framed current speed conditions ($R^2 = 1$).

The equation $\Delta SS = SS - SS_{pot}$ will give the actual deviation from the framed current speed conditions. If SS are finer than the SS_{pot}, the currents must then have been weaker. In this way will a plot of ΔSS show the relative current speed.

3.4. Sedimentological description and logging

After the cores were cut in half on the long side, they were further studied and described. Visible clasts, changes in grain size and structures were noted as well as changes in colour and consistent. Colour was decided using the Munsell colour chart (Munsell, 1973). The lithological logs were made using the description, but clasts and lamination was done using X-ray Photography to get it more accurately.

3.5. Counting of IRD

By using the method by Grobe, (1987); the IRD in the cores was counted by X-ray photographs. Digital X-ray photos with a scale and the opportunity to change brightness to see contrasts better makes it easy to count all clasts > 1 mm. This is done for every 1 cm.

3.6. Radiocarbon dating And Calibration

Foraminifera were collected from a fraction between 100 µm to 1 mm in 1 cm sections where the sediments closest to the core edges was removed to avoid mixing with younger foraminifera from above. Between 2 and 3 mg foraminifera was collected from each section from each core, and sent to Poznan, Poland for dating. Poznan Radiocarbon Laboratory only needs 20-50 mg of pure carbon for dating, using the accelerating mass spectrometry method (AMS).

^{14}C is a radioactive isotope that is continuously produced in the upper atmosphere, absorbed by oceans and living organisms to become stored in various global reservoirs. Eventually it decays to form the stable element ^{14}N. After death the carbon uptake of the plant or animal

ceases and by knowing the rate of decay, the length of time since the organism died can be calculated from the residual ^{14}C activity (Lowe & Walker, 1997).

The activity of ^{14}C is halved every 5730±40 years. Which is why the method only can be used for organisms younger than 50 000 years BP.

Acceleration mass spectrometry (AMS) is an analytical method that uses the fact that each atom has a unique mass (Elmore & Philips, 1987). In the AMS method the actual number of ^{14}C are counted to predict the age of the organism. When particles are accelerated at high speed through a magnetic field, the angle of deflection of the moving particle is unique for its mass (Bowman, 1990).

Sea waters have an apparent age, because the transfer of radiocarbon only occurs through the ocean surface. The main control on the ^{14}C activity is in the water circulation, where the mixing rate of surface and deep waters is slow. The replenishment of carbon is lower; the decay will give a lower ^{14}C activity and a higher age depending on how long the water has been on this depth (Mangerud, 1972; Lowe & Walker, 1997). The reservoir effect of the Barents Sea is estimated to be 437 ± 14 (Mangerud et al., 2006) and therefore it has to be subtracted from the apparent age.

To calibrate the radiocarbon ages the CALIB 7.1.0 sofware was used. The Marine13 calibration curve was used and has a mean global reservoir correction of 405 years. The regional difference (ΔR) also has to be accounted for, where the reservoir age of 437 ± 14 was used (Stuiver & Reimer, 1993; http://calib.qub.ac.uk/calib).

In this study the dates are referred to as “cal yrs BP” meaning calibrated years before present, whereas before present is before 1950. 1950 is the zero point in the radiocarbon time scale due to fossil fuel burning and nuclear weapons activity, leading to lower $_{14}C$ content in the atmosphere (Bowman, 1990). The shortening ka is used as thousand years meaning “kilo-age”.

4. Results: Acoustic Data

Figure 4.1 shows the bathymetry of Sentralbankrenna. The line of different colours is the swath bathymetry, with data consisting of better resolution.

4.1. Swath Bathymetry and mapping

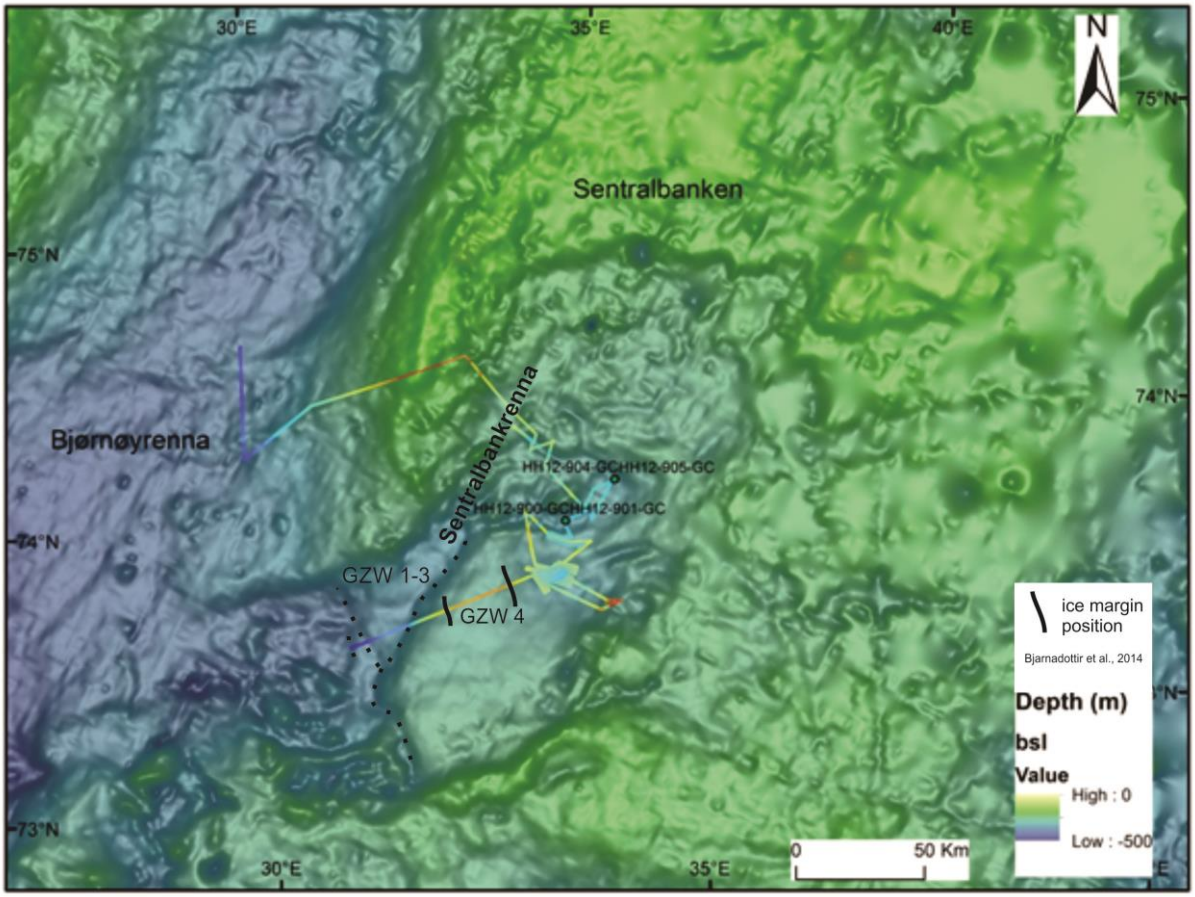

Figure 4.1: Map of Sentralbankrenna, south of Sentralbanken with the swath bathymetry collected from the area, and the position of the four cores. The figure also shows the grounding zone wedges interpreted by Bjarnadottir et al (2014)

Figure 4.1 shows the large scale seafloor morphology in the study area. In the North Sentralbanken is located, covering an area of about 30 000 km^2, with a depth of around 120 m bsl. Immediately SW of Sentralbanken is Sentralbankrenna, a trough ~ 80 km wide by ~270 km long. This trough is orientated approximate NE-SW feeding into Bjørnøyrenna. The trough has a depth of 120 m going down to 440 m bsl at its deepest. The seafloor in Sentralbankrenna is dominated by a large fan shaped sedimentary deposit ~100 km long and ~50 km wide. This area been interpreted by Bjarnadottir (2014) to consist of four grounding zone wedges (GZW1-3, GZW 4) also marked in figure 4.1, indicating that there has been several standstills during the retreat of the ice sheet. Based on the swath bathymetry data these grounding zone wedges are detected in the SW part of the trough as fan shaped elevations on the seafloor (Fig. 4.1).

4.1.1. Tunnel valleys

Figure 4.2 shows the small scale bathymetry of Sentralbankrenna and southwestern-most Sentralbanken. Ice margins and breached ice margins are illustrated with black lines and red crosses respectively in Figure 4.2a, while tunnel valleys are illustrated in 4.2b. Based on the shape of Bjarnadottir's tunnel valleys in the bathymetry map which are marked in red in Figure 4.2b we identify 5 additional channels in the upper Sentralbankrenna which are marked in black in Figure 4.2b.

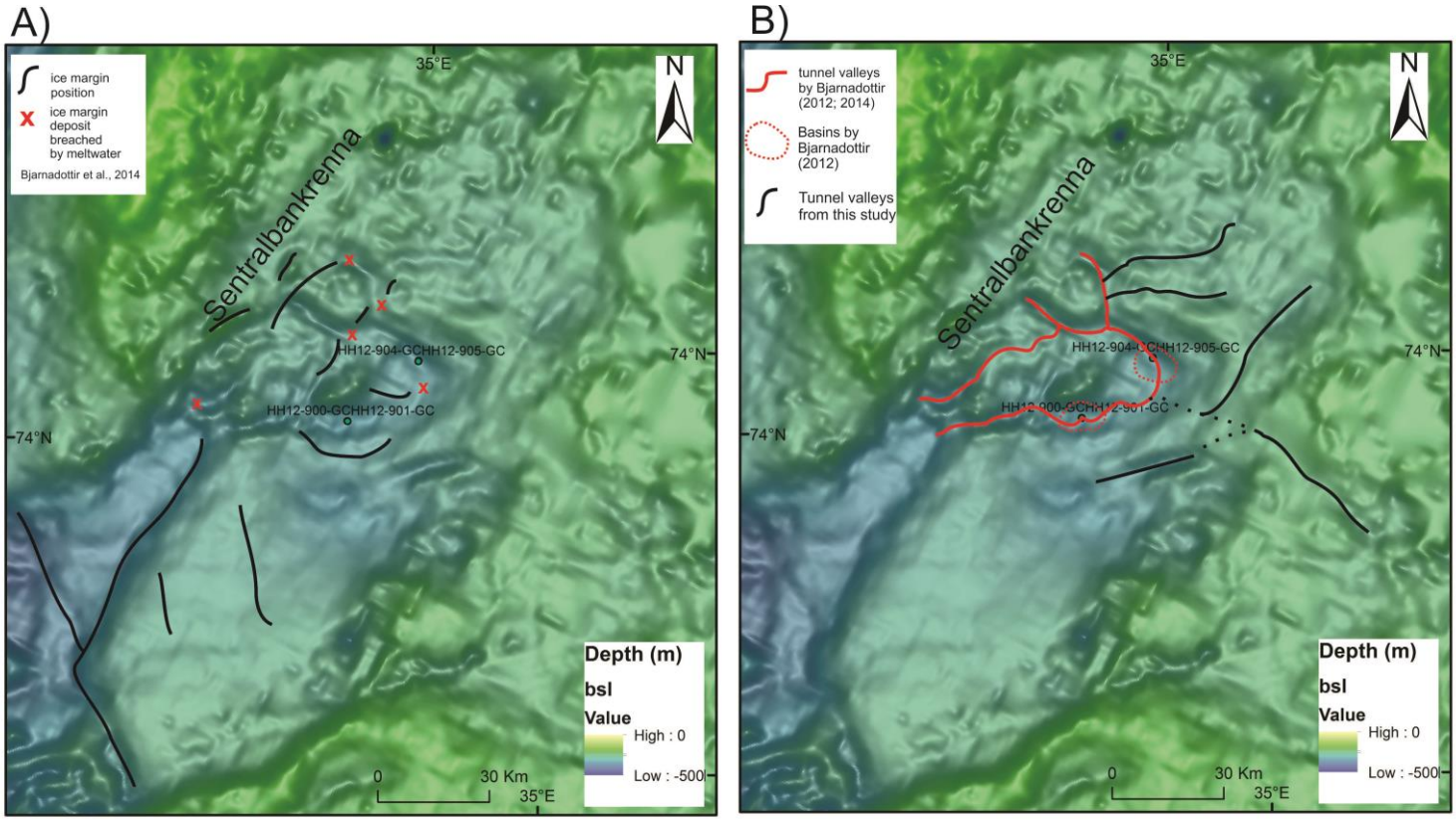

Figure 4.2: A) showing former ice margin positions and areas in sediments deposition where melt water channels has breached through (Bjarnadottir et al., 2014) B) Shows valleys and basins formed from channelized meltwater, where the main channel is interpreted by Bjarnadottir (red), and the blakc tributary channels are interpreted based on Bjarnadottir interpretations.

Figure 4.3 on the next page shows cross sectional profiles of the tunnel valleys interpreted by Bjarnadottir (2012; 2014), and the features found with a similar shape in Figure 4.2.

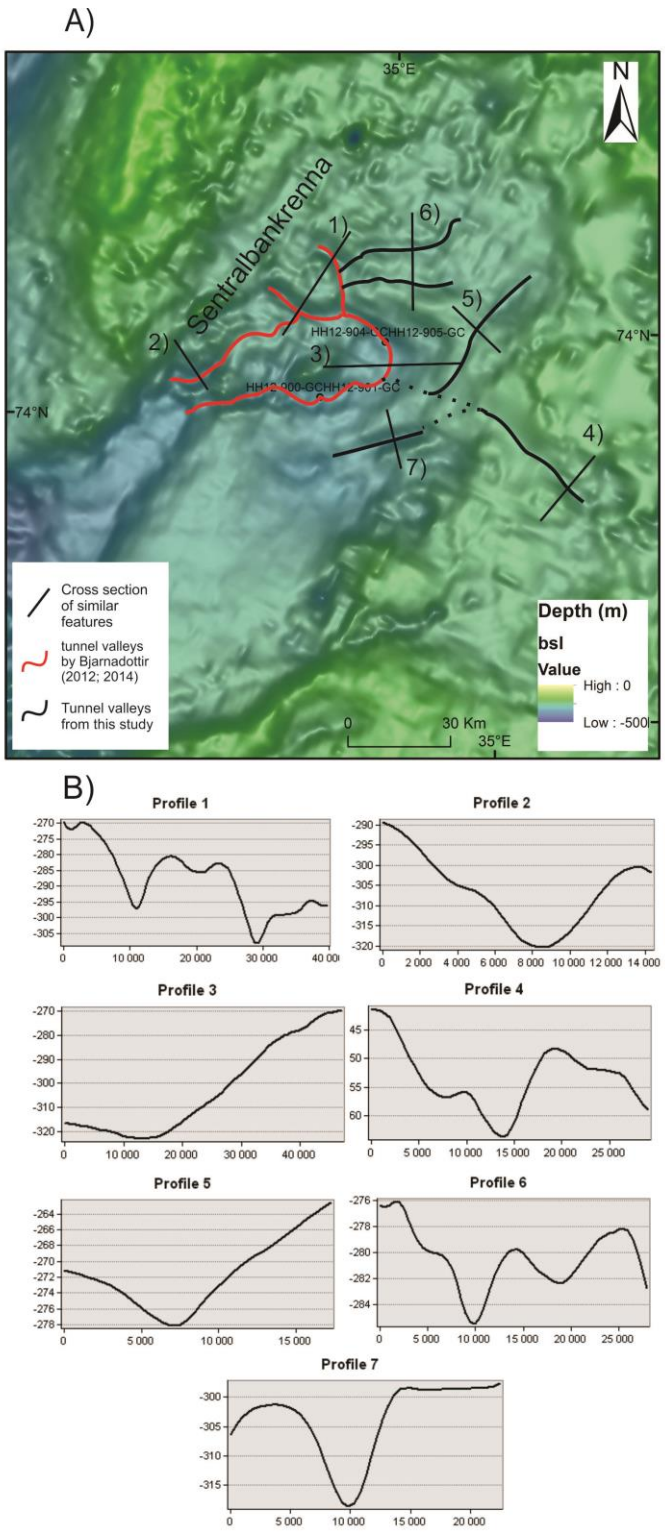

Figure 4.3: A) Cross sectional profiles taken across the former interpreted channels (red) and the potential channels (black) in Sentralbankrenna B) Shows the additional profiles from A) with depth bsl and length in metres

The valleys mapped have depths ranging from 7 to 20 meters, and thousand to several thousand meters wide. The additional cross sectional profiles are shown in figure 4.3 b, and the depths and widths are consistent with the measures of tunnel valleys identified by Bjarnadottir (2014; 2012).

Figure 4.4 shows profiles taken along the channels, to see the path and direction of flow.

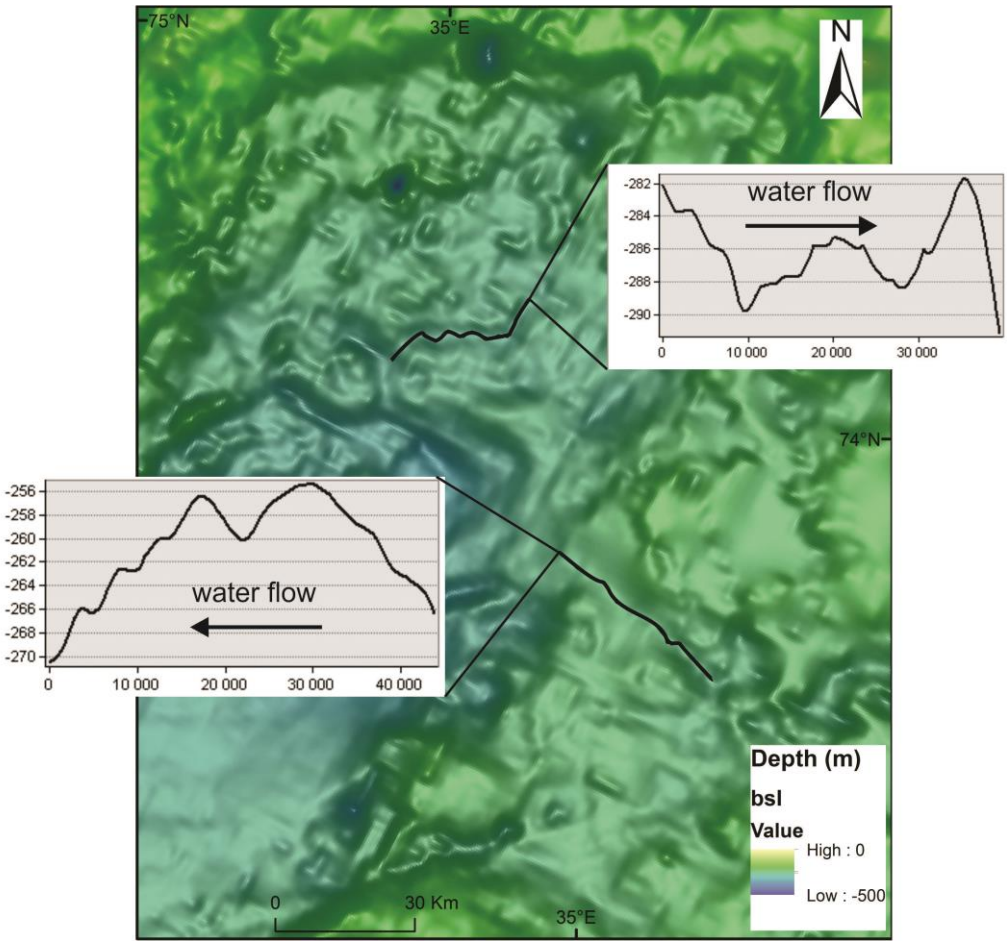

Figure 4.4: Profiles taken along the channel show bathymetry requiring an uphill flow of the water masses, which is a key characteristic of subglacial meltwater under pressure.

The figure proposes that the channels have areas requiring an upslope flow of water.

4.2. Swath bathymetry and core position

All four cores are collected from the same tunnel valley mapped by Bjarnadottir et al (2014). This channel curves from North West and ending in South west of a curved channel formed as a mirror image of the letter C, and is marked in red in figure 4.2b. In the channel two basins are mapped by Bjarnadottir et al (2014; 2012) and marked with a red broken line in figure 4.2b, measuring almost 10 km in length and a few hundred meters in width. Core HH12-900 GC and HH12-901 GC are collected from the same basin and in the southern part of the valley ~50 metres apart as shown in figure 4.5a. HH12-904 GC and HH12-905 GC are placed further north from another basin a little ~170 metres apart as illustrated in figure 4.5b.

HH12-900 GC and HH12-901 GC are collected from the middle and a deeper part of the basin. They are collected from the same depth, and a small depression is located SW from the two cores (fig 4.5a). Core HH12-904 GC and HH12-905 GC are collected from the northern

part of the channel in another basin. Here core 904 is placed further north than core 905. From 904 to 905 there is a slight uphill, so that 904 are collected from a slight deeper part of the basin than 905 (Fig 4.5b).

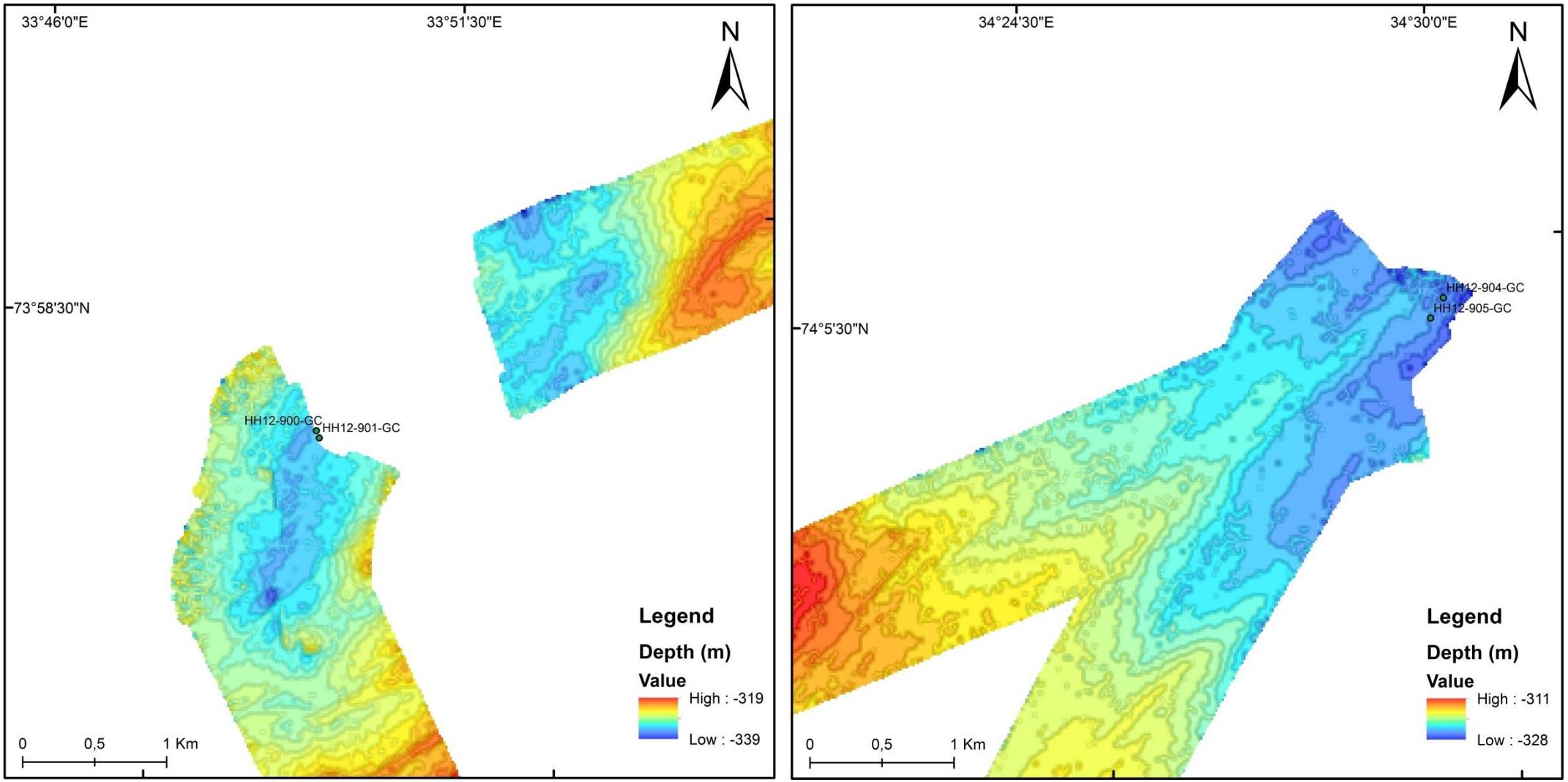

Figure 4.5: Swath bathymetry zoomed in to the two core locations. Figure A showing core HH12-900 GC and HH12-901 GC, placed the furthest south, while B; shows core HH12-904 GC and HH12-905 GC, placed the furthest north and in the inner part of Sentralbankrenna.

4.3. Sub bottom profiler; Chirp

Three chirp profiles are collected with the cores; HH12KA-035, HH12KA-037 and HH12KA-038 (referred to as 035, 036 and 037). Figure 4.6 show the locations of the chirp lines.

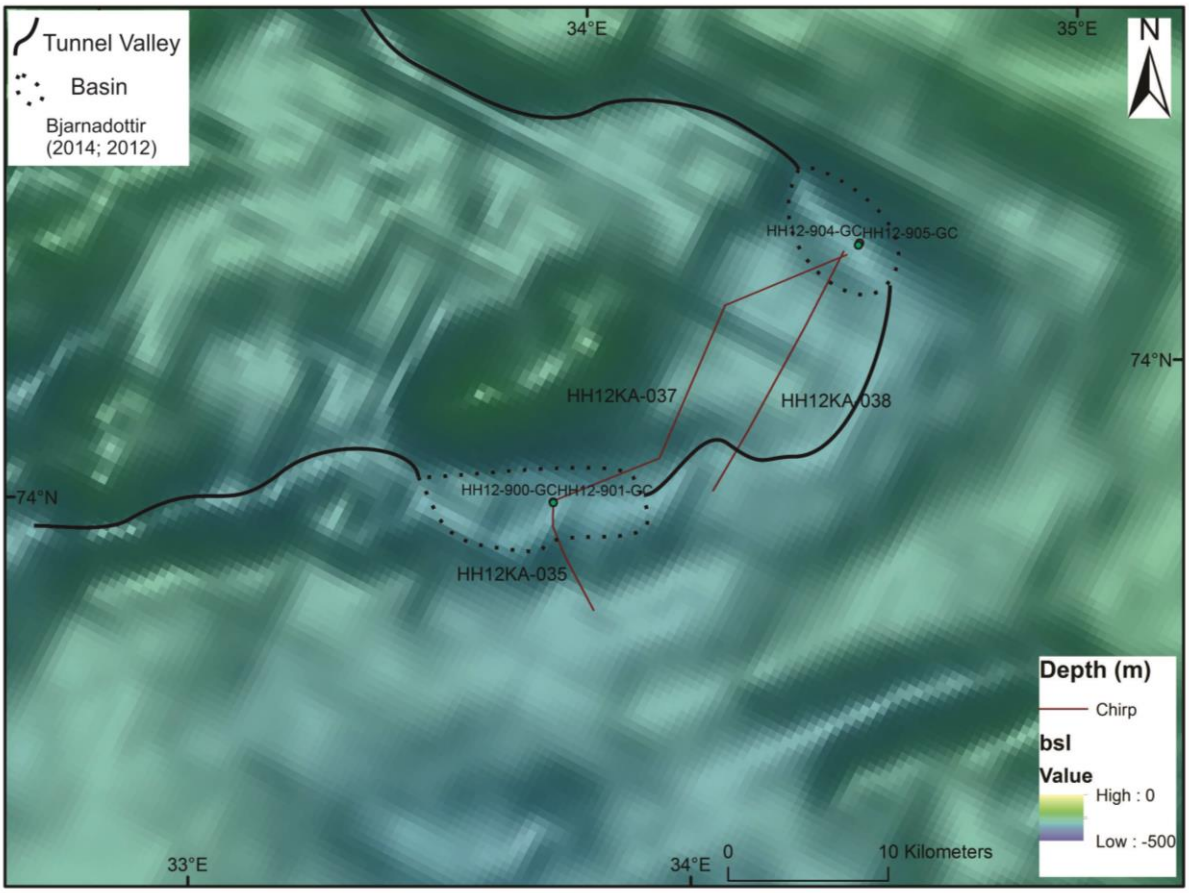

Figure 4.6: Map showing the chirp profiles; HH12KA-035, HH12KA-037 and HH12KA-038. The two cores 900 and 901 are collected from between HH12KA-035 and HH12KA-037 while cores 904 and 905 are collected at the very end of HH12KA-037, and in the very beginning of HH12KA-038. Bjarnadottir (2014; 2014) tunnel valleys and basins are also marked.

As figure 4.6 illustrates, the chirp lines are collected between the core sites.

Three layers are seen in all chirp profiles, all three are shown in figure 4.7.

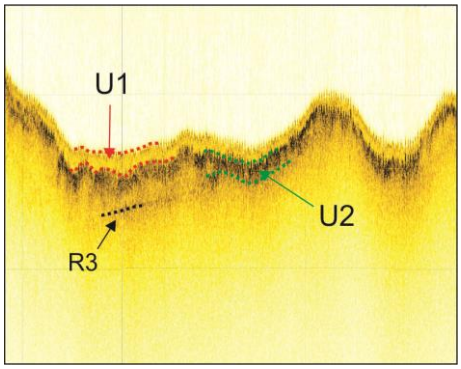

Figure 4.7: Illustration showing how the sediments and reflections are divided into layers

Figure 4.7 illustrate how the sediment pack is divided into layers or reflections. A top layer of transparent material, a darker layer of semi-transparent material and beneath these a third reflection is visible at some places.

The uppermost reflection, R1 is a strong transparent signal covering a sediment pack showing a bright appearance, U1. U1 is varying in thickness from less than 1 meter on slopes and ridges to 3-4 meters on flat ground and in depressions. The second reflection, R2, is semi-transparent. The reflection is dark, revealing a darker coloured layer underneath, U2, and show the same pattern as R1, but is harder to track in some places. The sediment pack also varies in thickness. The lowermost reflection, R3, is an impenetrable reflection, only visible in some places; this reflection shows the same pattern as the two other layers with hills and depressions, but not as detailed.

Figure 4.8, 4.9 and 4.10 shows the chirp profiles and their interpretation. Cores 900 and 901 are collected ~150 metres SW of chirp line 37. 904 and 905 are collected ~1 km NE of chirp profile 37 and ~1 km ENE of chirp line 38. All cores are collected from basin floors which are flat areas and not likely to change much over these distances. The cores are therefore still drawn into the profiles to give an indication of what sediments they cover and their depth of penetration. It appears that cores 900 and 901 penetrate U2, as the bottom of the cores reaches this layer in both 035 and 037. Cores 904 and 905 only penetrate the uppermost layer, U1.

HH12KA-035 is shown in figure 4.8. It starts on the elevated side of the channel in Southeast, and stops in the middle of the basin where cores 900 are collected. Core 901 was collected ~20 metres east from where it is placed on the chirp line. On the altitudes SSE from the channel the ground is rough with small hills and depressions only a couple of meters deep/high. The sediment packs both thickens towards NNW, from 1 meter to no sediment layer of U1 in some slopes and ridges and up to 4 meters in the basin where the cores are collected.

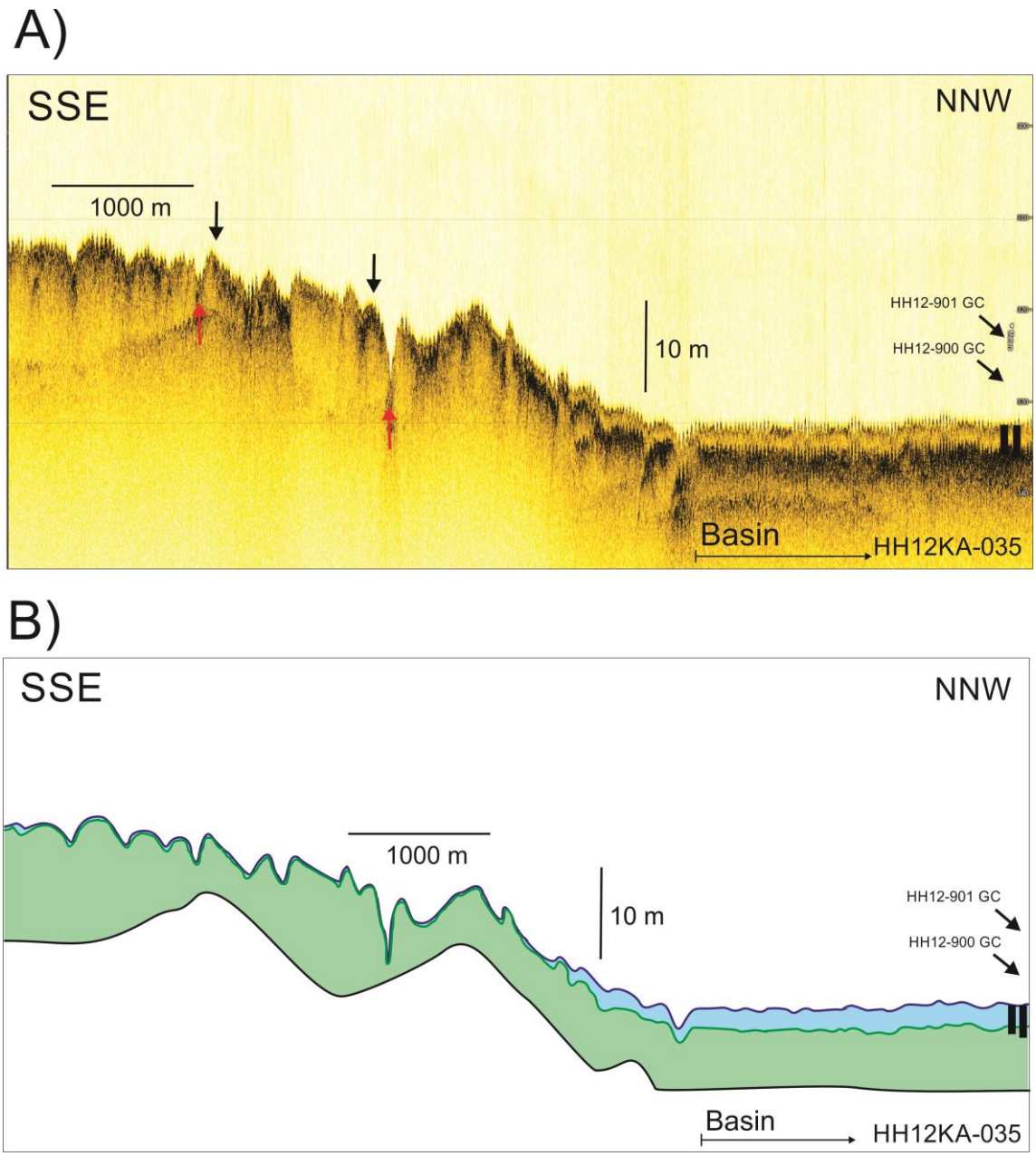

Figure 4.8: HH12KA-035 A) Chirp line showing the seafloor and the sediment cores illustrating the penetration depth B) Interpretation of chirp line and sediment layers, as well as sediment cores to see the penetration depth. See legend in figure 4.10

HH12KA-038 is shown in figure 4.9. It stretches from where cores 904 and 905 are collected in NW towards SW. The profile is collected directly across the curve in the meltwater channel, showing the topography from the channel basin, over the inside of the bank where the river meanders and down in the basin again. The highest altitudes in the profile are interpreted by Bjarnadottir to be an ice margin position, which can be seen in Figure 4.2a, and the sediment thickening towards the SW is the deposition of sediments as the glacier retreats. On this ridge several hill and depression marked in figure 4.8a with heights and depths measuring from 2 to 10 metres. In this profile there is a thickening of sediment layer U2 towards SW, where it goes from a thickness of ~4 metres in the NE to 15 metres depth in SW. The upper sediment layer, U1 also increase in thickness, but in the opposite direction. It is approximately 2 metres in SW reaching ~4 metres in NE.

HH12KA-037 is shown in figure 4.10. It stretches from where 900 and 901 are collected in south west to north east where cores 904 and 905 are collected. The line is not fully straight, and stretches from the channel bottom over the channel bank, only further west than HH12KA-038, where the altitude of the bank is higher (fig. 4.10) which is the same ice margin ridge seen in profile 038 as Bjarnadottir (2014) interpreted. The seafloor along this profile is more irregular than the 038, with higher ridges and deeper depressions (fig 4.9), with ridges up to 10 meters high, 10while the depressions are up to 3 meters deep. The sediment pack for both U1 and U2 are more equally distributed in this profile. U2 varies from below one meter in slopes to up to 12 metres thickness in depressions, while U1 range from less than 1 meter in slopes to 3-4 meters in basins and depressions.

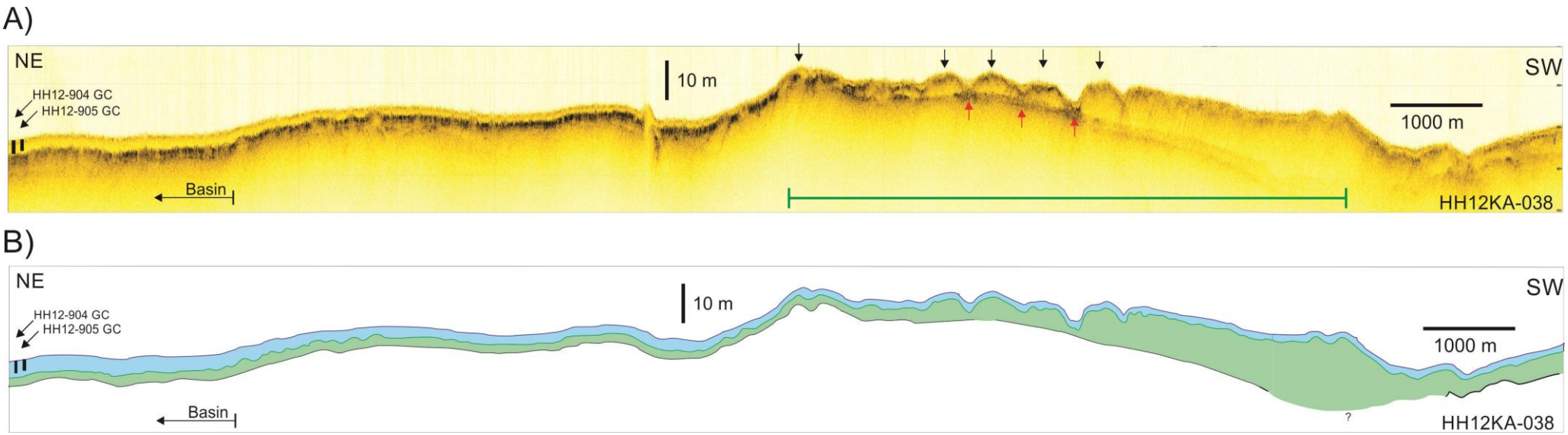

Figure 4.9: HH12KA-038 A) Chirp line showing the seafloor and the sediment cores illustrating the penetration depth B) Interpretation of chirp line and sediment layers as well as sediment cores to see the penetration depth. See legend in figure 4.10

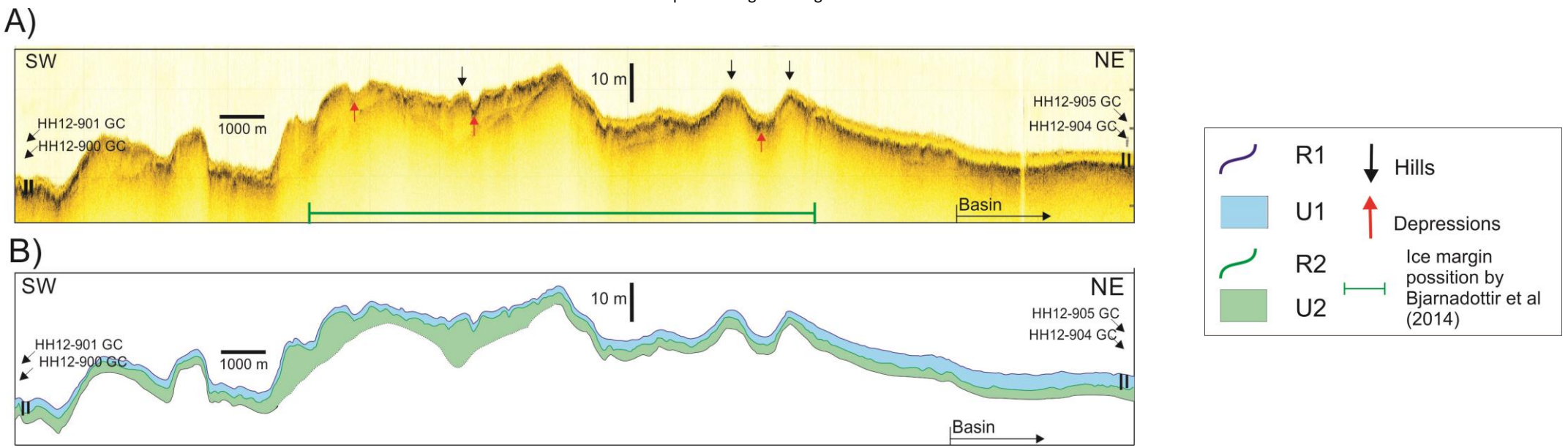

Figure 4.10: HH12KA -037 A) Chirp line showing the seafloor and the sediment cores to illustrate the penetration depth B) Interpretation of chirp line and sediment layers as well as sediment cores to see the penetration depth.

4.3.1. Interpretation

The sediment pack U1 is a layer which appears transparent, under the reflection R1, this reveals a sediment pack of finer unconsolidated sediments. U1 has no internal reflectors and most likely the sediment pack is soft and homogeneous, interpreted to be glacimarine and Holocene sediments (Murdmaa et al., 2006; Elverhøi & Solheim, 1983). The second reflection R2 is chaotic and the beginning of a sediment layer U2, consisting of coarser material, this layer is semitransparent and are interpreted to be the beginning of the deglaciation and glacial diamicton; a nonstratified unit of all grain sizes deposited by grounded ice (Murdmaa et al., 2006; Bjarnadottir et al., 2014). The fact that the third reflection R3 is impenetrable and non-structural is consistent with the lowermost unit being bedrock. (Bjarnadottir et al., 2014; Batchelor et al., 2011; Hjelstuen et al., 2009; Elverhøi & Solheim, 1983).

5. Results: Litostratigraphy

In this chapter the results are presented from the methods used in chapter 3.

The lithostratigraphy of the cores is based on visual observations and x-ray photos, where clasts larger than 1mm are considered as IRD, and marked in the lithological logs in figure 5.1 as individual features. All cores are divided into two main lithostratigraphic units, mainly distinguished from visual inspection, but also from changes in grain sizes, IRD content and density.

Since the cores HH12-900 GC and HH12-901 GC are collected from the same site, as HH12-904 GC and HH12-905 GC also are, they are expected to show more similar depositional environments, and are therefore presented together in this chapter.

First a general description of the different units is given to clarify the main differences between the two units. The next section is divided into sites, and the two cores from the same sites are described together. Eventually small similarities between all cores will be presented in the end.

In core 905 at 300 cm depth a part of a belemnite was found. This specific specie was extinct during Cretaceous. The belemnite was found in an interval of increasing sand content and IRD

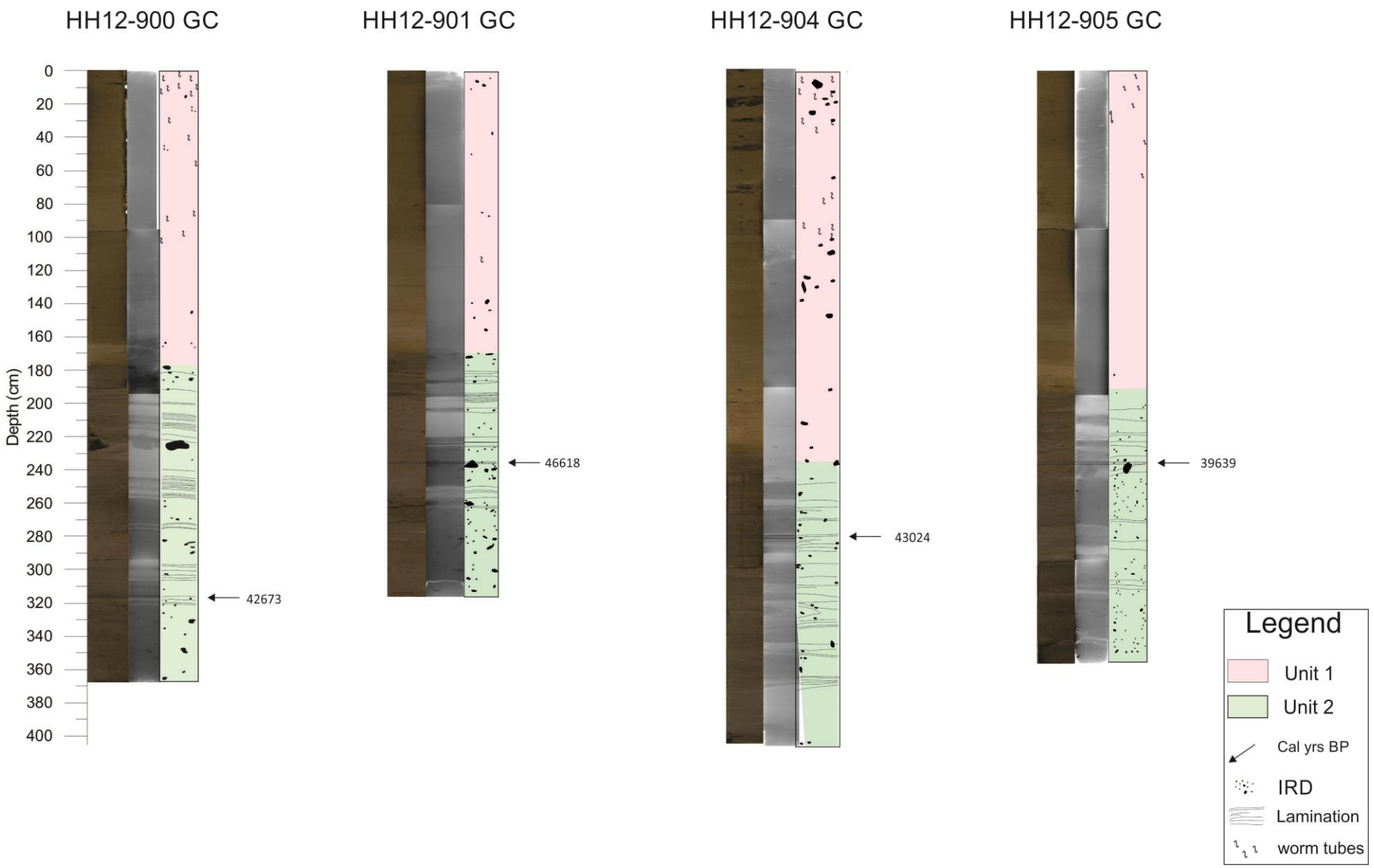

Figure 5.1: Figure showing colour photograpgy, X-ray images and the litological log of all cores relative to each other. Colourcodes are used for units. Dates are marked with black arrow.

Unit 1

The top part of all cores the color remains more or less the same. The unit is dominated by homogenous sediments with only small changes in grain size distribution, few IRD and an increasing amount of worm tubes are observed towards the top of the core.

This unit is divided into subunits to explain and compare the smaller differences in more detail.

Unit 2

The bottom part of the cores starts from 160 to 230 cm and stops at the very end. This unit contains high amounts of IRD and shows huge variations in sand content and in colour. All parameters in all cores show frequent fluctuations. From X-ray photos showed in figure 5.2 it is clear that this part of the cores is dominated by laminated sediments of different layer thicknesses.

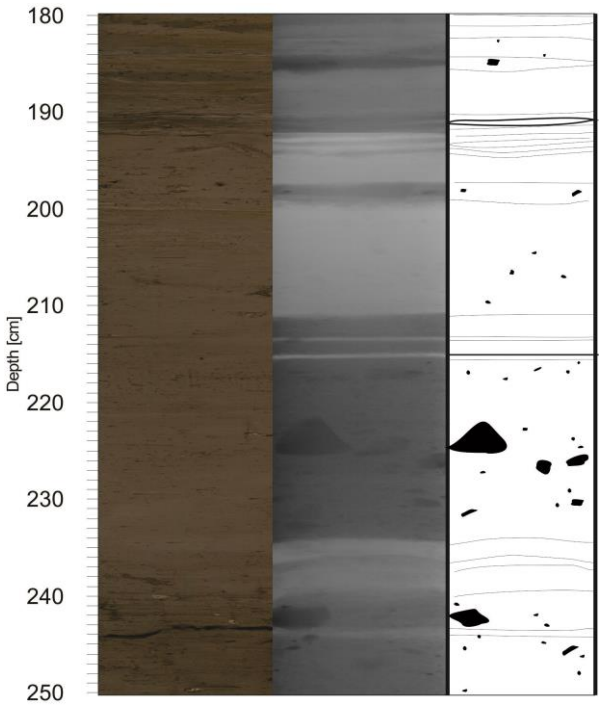

Figure 5.2: Figure showing the lamination which is characteristic for unit 2. From right; colour photograph, X-Ray photo and lithological log for a sequence of core HH12-901 GC

The layers are planar and parallel, and vary about 1 cm to mm scale in thickness. These layers show similar texture in all cores, where they change between dense and dry material to soupier, glossy sediments. Each soupy layer gradually turns in to a denser layer, which has an increasing density downwards before an abrupt change to another soupy layer.

Element chemistry

The XRF measure showed sufficient counts (Forwick, 2013) for only three elements in core 900; Si,K, and Fe. While core 901 showed good results for Si, K, Ca, Ti, Fe, Sr and Zr. 904 and 905 showed good results for Si, K, Ca, Fe and Ti. Five ratios were chosen to use when evaluating changes in the element geochemistry which are presented in table 5.1. These are the elements that showed the biggest differences throughout all cores. Core 900 did not have sufficient counts for only three elements as well as core 905 showed changing values for Ti which none of the other cores did, and was therefore taken into account.

Table 5.1: minimum, maximum and mean values of magnetic susceptibility and element ratios. The numbers are relative.

	HH12-900 GC	HH12-901 GC	HH12-904 GC	HH12-905 GC
Magnetic susceptibility				
min	11.4	12.6	8.5	8.5
Max	47.7	32.5	42.2	30.8
Mean	21.9	23.4	22.4	21.6
Unit 1				
min	11.4	12.6	8.5	8.5
Max	32.1	27.2	42.2	26.4
Mean	18.8	21.7	21	18.2
Unit 2				
min	17.1	16.5	19.5	18.1
Max	47.7	32.5	30	30.8
Mean	24.7	25.2	24.3	25.7
Fe/K				
min	3.3	3.8	3.6	3.6
Max	7.8	4.7	6.1	10.2
Mean	4.5	4.5	4.6	4.6
K/Ca	no data			
Min		2.1	0.7	0.8
Max		2.2	5.8	4.9
Mean		2.6	2.8	2.7
Fe/Ca	no data			
Min		8	2.7	3.6
Max		10.7	32.8	29
Mean		11.9	13.1	12.8
K/Si				
Min	0.5	0.5	0.5	0.5
Max	0.8	0.8	1.1	1.6
Mean	0.6	0.7	0.7	0.7
Fe/Si				
Min	2.1	2.1	2.2	2.1
Max	6.1	5.5	5.9	7.8
Mean	2.9	2.9	3.2	3.2

Grain size distribution

From the particle size analyser minimum maximum and mean content of the different grain sizes are calculated for unit 1 an unit 2 in all cores. Table 5.2 show the grain size distribution in all cores. The values are given in weight %.

Table 5.2: The minimum, maximum and mean values of all grain sizes of unit 1 and unit 2 of all cores. Values are given in weight %

	HH12-900 GC	HH12-901 GC	HH12-904 GC	HH12-905 GC
Sand				
Unit 1				
min	8.55	6.03	6.51	6.40
Max	18.01	17.84	15.03	21.42
Mean	14.65	12.35	10.04	11.49
Unit 2				
min	2.18	2.39	1.12	2.64
Max	20.51	20.86	18.29	19.44
Mean	10.88	11.95	9.99	12.04
silt				
Unit 1				
min	47.97	42.39	43.37	26.96
Max	52.99	55.12	58.30	47.55
Mean	47.56	49.98	53.09	34.56
Unit 2				
min	36.27	38.56	41.65	28.90
Max	55.24	54.86	57.34	55.15
Mean	50.93	50.05	50.95	51.42
clay				
Unit 1				
min	28.96	30.10	30.36	45.91
Max	39.77	49.51	46.49	57.15
Mean	33.83	37.46	37.33	53.69
Unit 2				
min	27.46	28.86	33.26	37.86
Max	60.39	55.75	51.18	56.58
Mean	43.89	38.22	41.97	40.23

5.1. HH12-900 GC and HH12-901 GC

Core HH12-900 GC and HH12- 901 GC are collected from the same depression at 333 meters depth and between the ice margin and the deepest depth.

The cores are clay and silt dominated and has a variation in sand content. The wet bulk density has increasing values towards the bottom of the core, while fraction porosity show decreasing values towards the bottom of the cores.

The additional figures to the descriptions are found under the text.

5.1.1. Unit 1

For Core HH12-900 GC unit 1 is from 0 – 176 cm depth, unit 1 in core HH12-901 GC is from 0 to 169 cm depth.

Core 900 and 901, unit 1 the general colour is dark greyish brown (Munsell code 2,5Y 4/2) where 900 has a band of dark grey (2,5Y 4/1) from 165 to 179 cm depth and 901 two olive brown (2,5Y 4/3) layers from 130 to 155 and from 164 to 169 cm depth. In both cores an interval of yellow-rusty coloured sediments are observed. In core 900 a yellow rusty layer is present at 166 cm depth, where the sediments turn more yellow until it changes back to dark greyish brown (2,5Y4/2) at 178 cm depth. Core 901 has an uneven “leopard pattern” from 152 to 169 cm, before a rusty layer appear from 169 to 170 cm.

Grain size

In these two cores this unit has a mean sand content of 15,5 % in core 900 and 12.7% in core 901. The sand content and the ratio between sand clay and silt show a uniform pattern, except a slight fining in grain size right before the change into unit 2 in both cores. This is from 165 cm to 176 cm in core 900 and from 120 cm to 170 cm in core 901. The rusty layer explained in the previous paragraph is corresponding with this interval in core 900, while for core 901 the rusty layer only cover the lower part of the increase in clay content. Silt is the most dominant grain size with mean content of 47, 6 and 50 percent for core 900 and 901 respectively. Clay has a mean content of 33.8% for core 900 and 37.5% for core 901. The sortable silt curve is shown in red on the grain size plot in figure 5.3 and 5.4, and shows the same pattern as the grain size distribution. The curve is inverted in this plot, to easier see the deflections from the grain size distribution.

The amount of IRD of unit 1 are rather small, but has a higher content in the top of both cores. Maximum 2-3 IRD are found per cm, except one interval in both cores where there are fewer clasts than in the rest of the unit, this is between ~85-170cm in 900 and ~60-140 cm in 901.

Physical properties

The magnetic susceptibility tends to follow the pattern of sand and IRD content. It has a mean value of 18.8 for 900 and 21.7 for 901. For 900 it has several peaks in the very beginning which seems to correspond to the high amount of sand and IRD, as well as one peak at around 120 cm depth, which seems to correlate with an IRD. For core 901 it has the highest values in the very top of the core, as well as an increase at 40 cm depth.

Element chemistry

The two cores show a relative increase in iron concentration which are marked in blue in figures 5.3 and 5.4. This interval starts at 130 cm in 900 and at 150 cm in core 901, they both continue into unit 2. Within this interval a single peak of increasing relative iron is also noted in both cores right before the change into unit 2, these increasing intervals correspond to where the rusty layers are observed. In core 900 the peak corresponds to a peak in clay content, while in core 901 the clay content seems to correspond to the Fe/Ca and K/Ca.

Sortable silt and relative current speed

The sortable silt plot in figure 5.3 and 5.4 shows that the sortable silt size is increasing as the grain size is increasing. Figure 5.5 show that sand content and sortable silt has a high correlation with r-values of 0.9 and 0.8 for core 900 and 901 respectively.

Figure 5.6 shows the correlation between sortable silt, clay content sand content and relative current speed (ΔSS), where the relative current speed decrease towards the bottom of the unit in both cores. It has the highest relative speed in the top and the lowest towards the bottom of the unit. In the very bottom of unit 1, in both cores there seems to be a correlation between the clay content and the relative speed, where the relative speed decreases with increasing sand content. In core 900 this is only true for the very end, from 160 cm towards the end of unit, while for core 901 the correlation seems to start at ~70 cm depth, continuing until the end of unit 1.

5.1.2. Unit 2

For core 900 unit 2 starts at 176 cm depth, while for 901 it starts at 169 cm depth and continues to the core ends.

Unit 2 has for 900 and 901 has the general colour of dark olive grey (5Y 3/2), for core 901 it is dark grey (2,5Y 4/1) at the top of unit 2, and black (5Y 2,5/2) at the very bottom.

Grain size

For both cores the unit has a mean sand content of 11.4% in core 900 and 11.7% in core 901. In core 900 the clay content has a mean of 43.9% while the silt content is 51 % For 901 clay has a percentage of 48.2% while silt is 50.1%.

Sand content and IRD content correlate and are fluctuating throughout the whole unit 2. The IRD content is highest in the very bottom, and seems to increase in pulses, showing a scalloped pattern in both cores. For 900 the first scallop ends at 200 cm depth, the next at 300 cm depth, while for 901 they end at 210 and a slight unclear end at 260 cm. Even though the sand and IRD correlates in the individual peaks, they do not correlate in this scalloping pattern.

Physical properties

The magnetic susceptibility is fluctuating, and follows the same pattern as the sand and IRD content in both cores. For 900 it has a mean value of 24.7 whereas for core 901 it has a mean value of 25.2.

Element chemistry

One interval of a relative increase in iron and potassium is found in each core. These are marked with blue and are found from 305-325 cm in core 900 and 265-285cm in core 901. In the same interval there is also an increase in clay content.

Sortable silt and relative current speed

The sortable silt coarsens with an increasing content of sand.

Figure 5.6 shows how the relative current speed fluctuates and seems to follow the grain size distribution, decreasing when the smaller grain sizes dominates, such as clay. The relative current speed rapidly switches between high and low velocities.

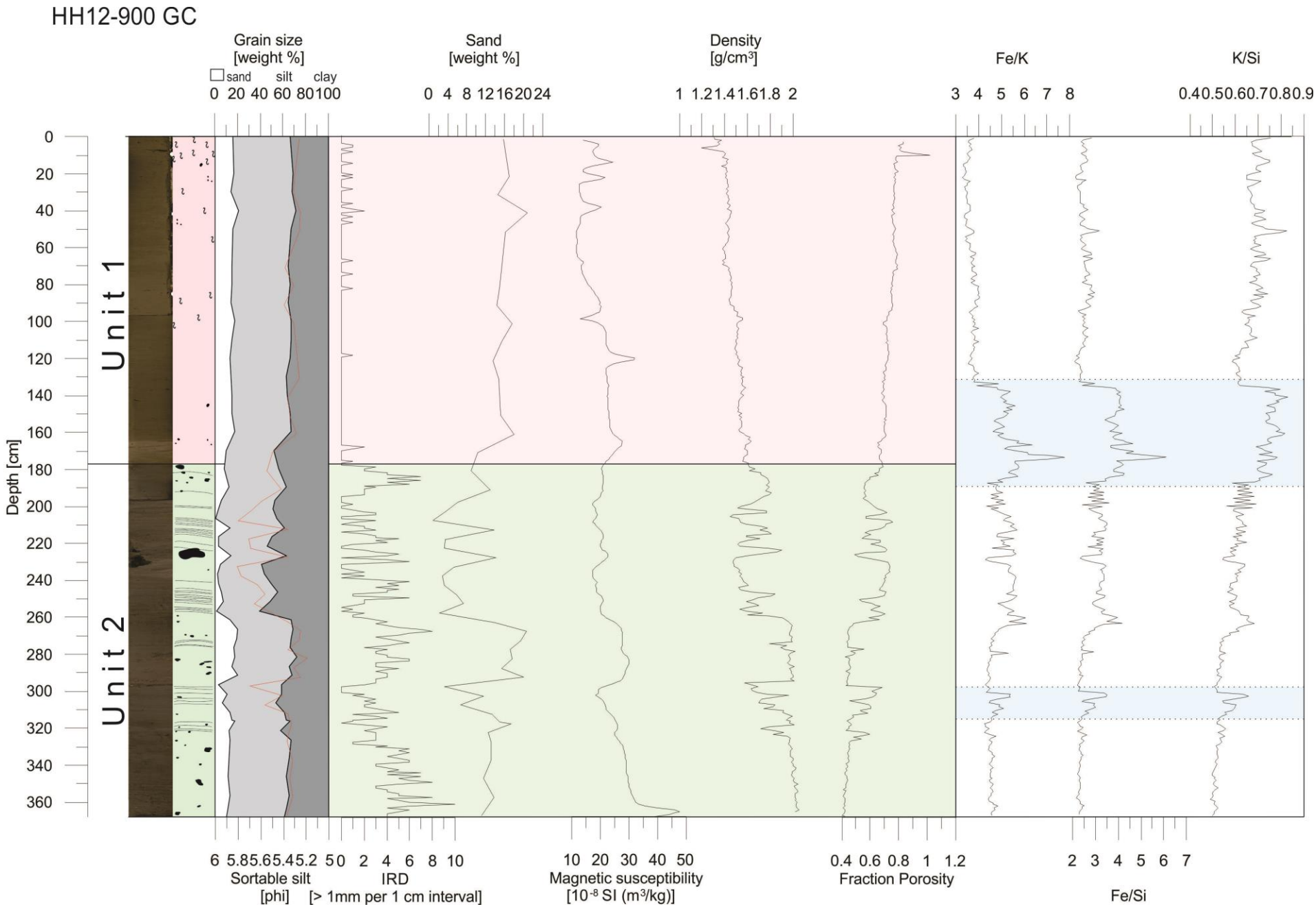

Figure 5.3: Colour picture, litostratigraphy (fig 5.1 for legend), grain size and sortable silt, IRD content, sand content, Magnetic susceptibility, density, fraction porosity, element ratios; Fe/K, Fe/Si, K/Si for core HH12-900 GC. Blue areas in the element ratio plots illustrate changes commented in the text.

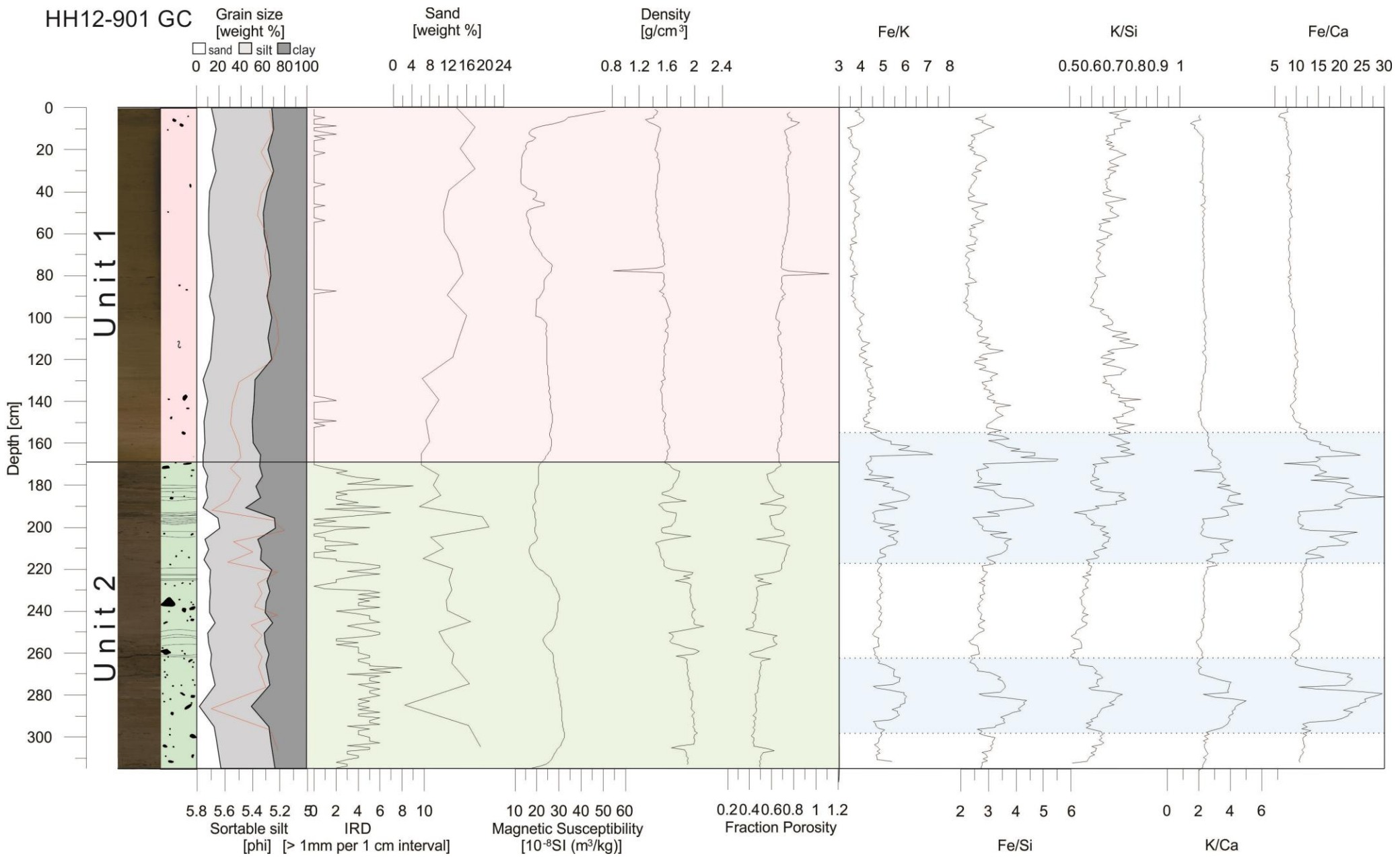

Figure 5.4: Colour picture, litostratigraphy (fig 5.1 for legend), grain size and sortable silt, IRD content, sand content, Magnetic susceptibility, density, fraction porosity, element ratios; Fe/K, Fe/Si, K/Si, K/Ca and Fe/Ca for core HH12-901 GC. Blue areas in the element ratio plots illustrate changes commented in the text.

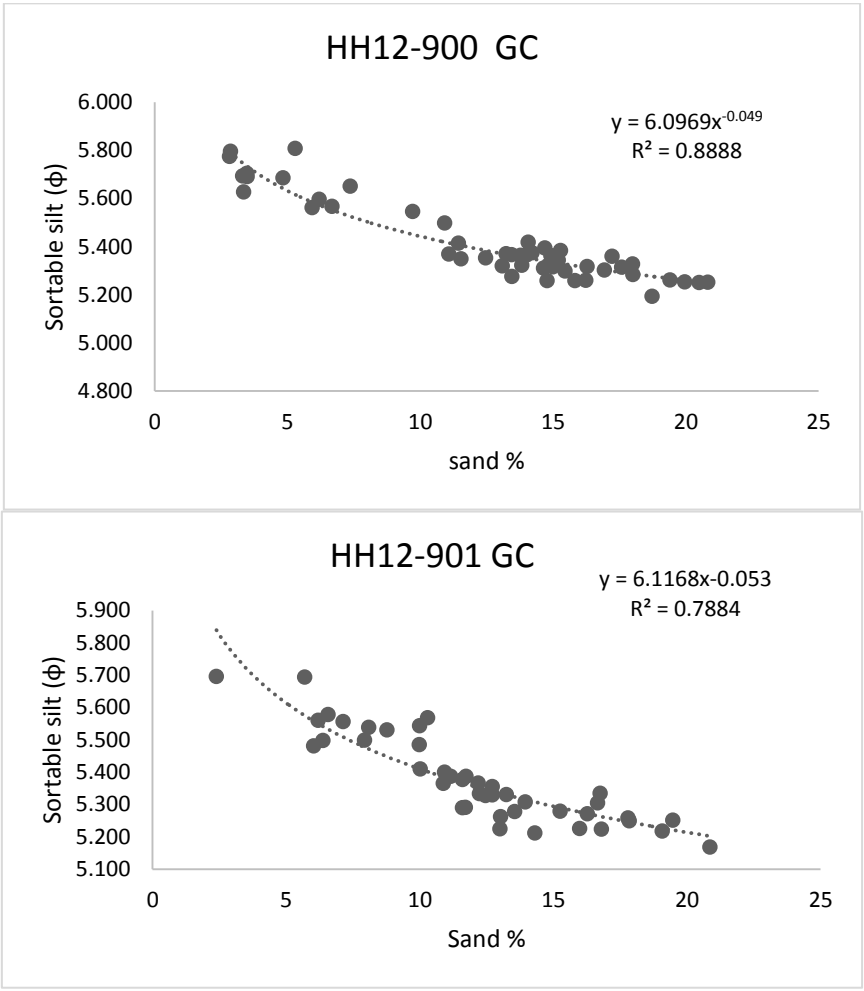

Figure 5.5: Sortable silt and sand show the correlation between them with aditional R-value and the regression formula giving SSpot

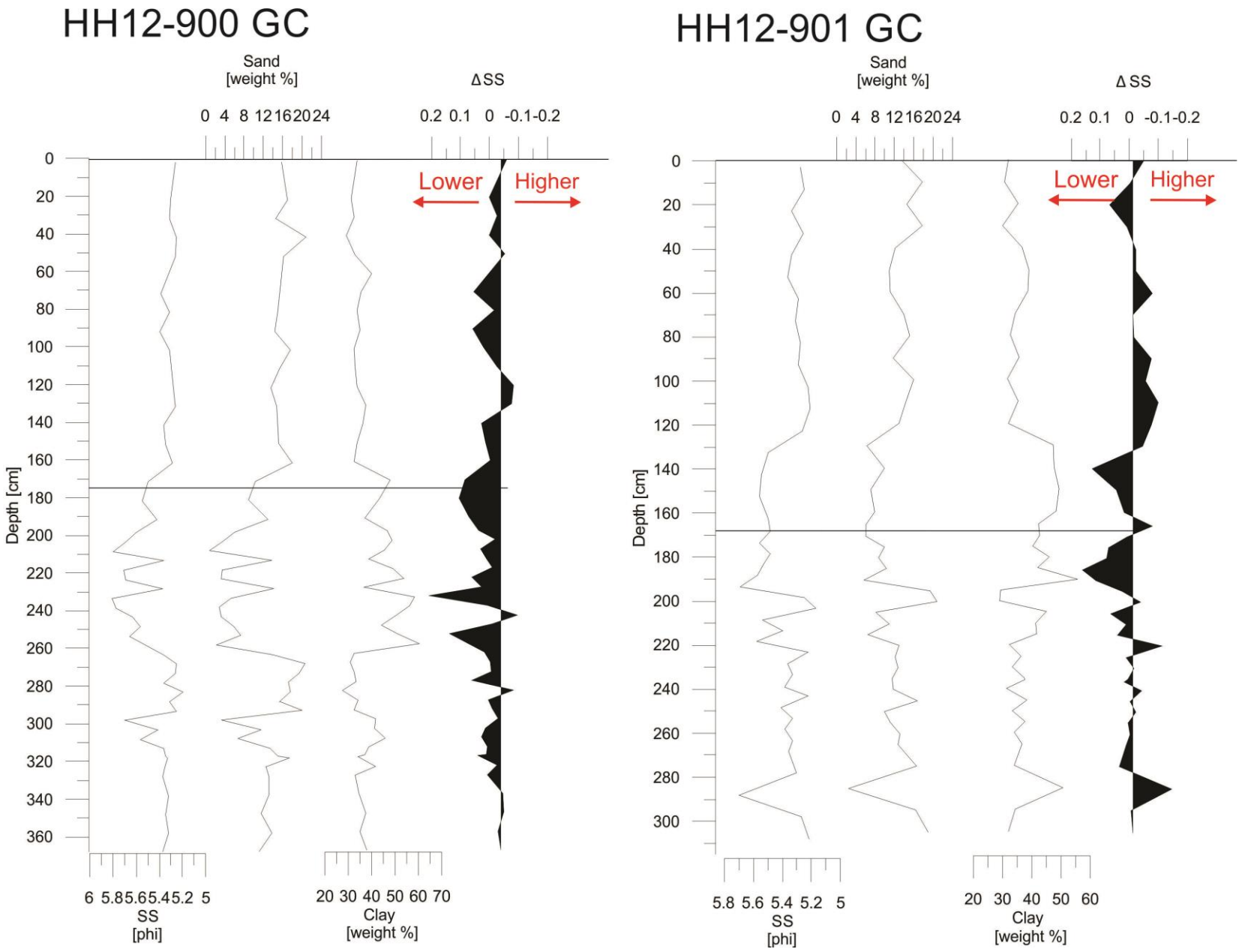

Figure 5.6: Sortable silt size (SS),Sand content, clay content and relative speed of the bottom currents for the two cores HH12-900 GC and HH12-901 GC

)

5.2. HH12-904 GC and HH12-905 GC

Core HH12- 904 GC and HH12-905 GC are collected about 30 km north east from the other two cores. These are collected from the same valley depression and are taken at depths of 325,2 and 324,3 respectively, just shallower than cores 900 and 901.

In both cores wet bulk density increases towards the bottom of the core, while fraction porosity decreases. Both cores are silt and clay dominated.

Figures described in the text are presented under the descriptions.

5.2.1. Unit 1

For Core HH12-904 GC unit 1 is from 0 – 234 cm depth, unit 1 in core HH12-905 GC is from 0 to 191 cm depth.

The general colour of 904 and 905, unit 1 is olive grey (5Y 4/2), where core 905 has a band of dark grey from 175 to 193 cm which changes to dark olive grey (5Y 3/2) right after. Core 904 changes straight to dark olive grey at 230 cm. In both cores an interval of yellow-rusty coloured sediments are observed. In core 904 the whole area between 230 and 253 cm is an area of unclear yellow rusty lenses or layers. Core 905 has brown rusty sediment aggregate from 187 to 192 cm.

Grain size

In unit 1, core 904 has a mean sand content of 9.7%, while for core 905 it is 11.7%. In core 904 the mean silt content is 53.1%, while the mean clay content is 37.3%. For core 905 mean silt content is 53.7% and the mean clay content is 34.6%. In figure 5.7 and 5.8 it can be seen that both cores have an increase in sand content, for 904 this interval is between 90 and 150 cm, while fore core 905 it is from 50 to 90 cm. The increase in core 904 is also supported by an increase in IRD and magnetic susceptibility. Both cores have a higher content of clay towards the change into unit 2, for core 904 the clay content starts increase at ~185 cm while in 905 it starts increasing at ~160 cm. For core 904 the high amount of clay does not start decreasing until 255 cm depth, which is approximately where the rusty layers also stops.

In core 904 there are two peaks in IRD, from 10 to 30 cm where magnetic susceptibility also increases, and the one form 90 to 150 cm, in both intervals the magnetic susceptibility also increases. The content of IRD also shows a slight increase towards unit 2 in core 904. In core 905 some IRD are observed ~10 cm before the change into unit 2.

Physical properties

The magnetic susceptibility has a mean value of 21.0 in core 904 and in core 905 it has a mean value of 18.2. In core 904 the magnetic susceptibility increases with the IRD in the two peaks, and show no changes apart from that.

Element chemistry

In core 904 at 200 cm depth there is a clear change in the element ratios K/Si, K/Ca and Fe/Ca, where iron and potassium dominates through the top of the core and calcium starts dominating at ~210 cm depth. In core 905 at 185 cm K/Ca, Fe/Ca and K/Ti also show a change dominating element, which is 5 cm above the unit change where Ca increases.

Sortable silt

The sortable silt plot in figure 5.7 and 5.8 shows that the sortable silt size is increasing as the grain size is increasing and figure 5.9 show that sand content and sortable silt has a r-value of 0.5 and 0.4, for 904 and 905 respectively.

In figure 5.10 relative current speed are plotted with grain sizes, shows a decrease in current speed towards the end of the unit. These two cores show a much higher relative speed than core 900 and 901 throughout the whole unit. The sand content decrease while the clay content increase toward the bottom. In the very bottom the relative decrease in speed in both cores corresponds to an increase in clay content.

5.2.2. Unit 2

For core 904 unit 2 starts at 134 cm depth, while for 905 it starts at 188 cm depth and continues to the core ends.

904 and 905 has a general colour of black olive (5Y 2,5/2) in unit 2, where core 905 fades into a black colour (5Y 2,5/1) in the bottom of the core.

Grain size

Core 904, unit 2 has a mean sand content of 10.6%, while for core 905 it is 11.5%. The silt content for core 904 is 50.9% while the silt content for 905 is 51.4%, and clay content are 42% and 40.2% respectively. Sand content, IRD and magnetic susceptibility tend to follow each other and fluctuate throughout the whole unit where the IRD content show pulses or a scalloped pattern. For core 904 there is a decrease in IRD and between scallops at 250 and 380 cm. Where the decrease at 380 is very pronounced, covering a few cm. For core 905 these breaks are at 240 and 290 cm depth. Core 905 has one distinct wave between 290 and 250 cm.

Physical peroperties

Mean magnetic susceptibility in core 904, unit 2 is 24.3, while for core 905 it is 25.7. The magnetic susceptibility and density shows the same trend as the peaks of IRD and sand in this unit, but not as the scalloped pattern of IRD explained above.

Element chemistry

Core 905 has a peak of increasing iron from 190 to 200 cm depth. From 240 to 280 all the fluctuation in the plots seems to stablelize for this interval.

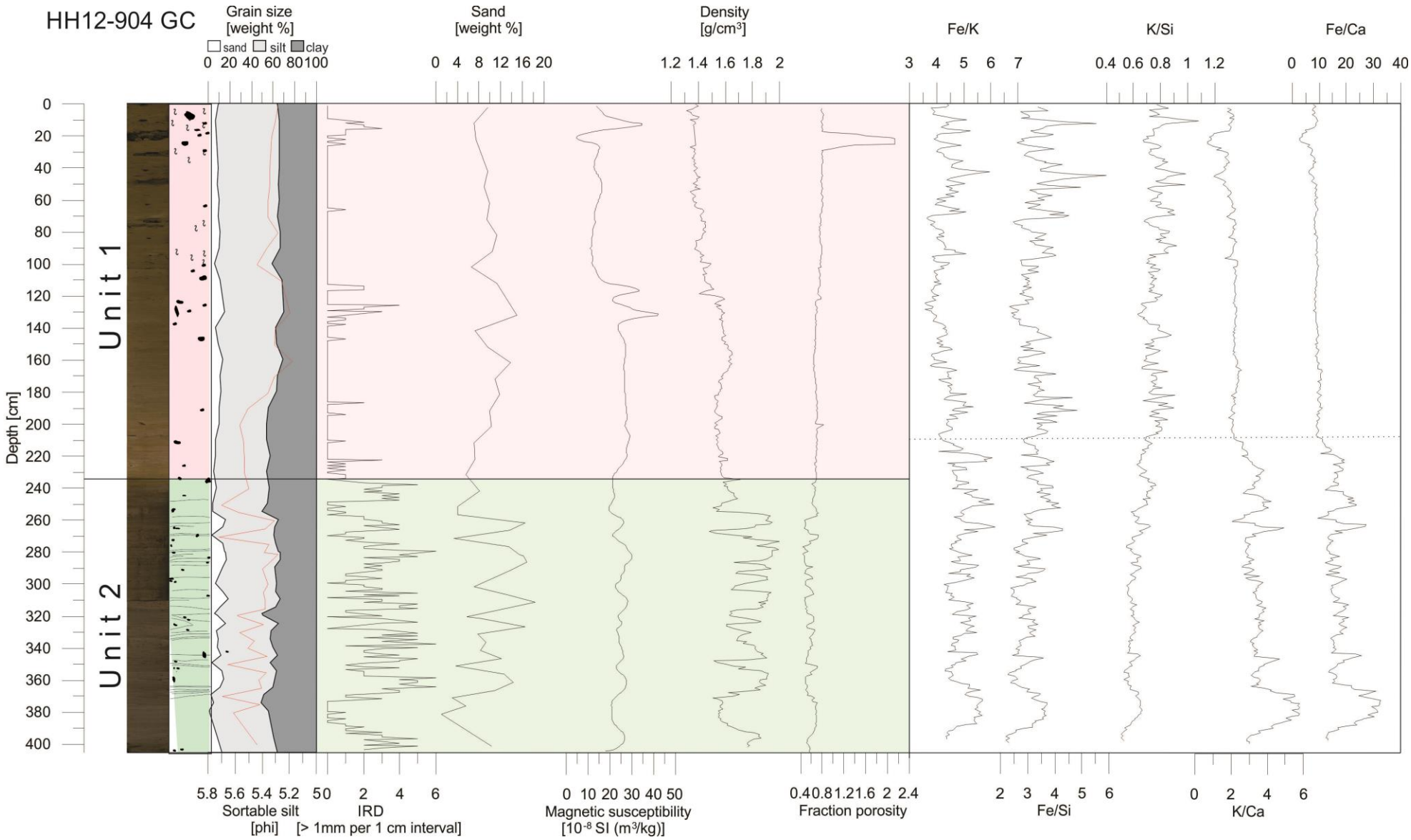

Figure 5.7: Colour picture, litostratigraphy (see fig 5.1 for legend), grain size and sortable silt (inverted), IRD content, sand content, Magnetic susceptibility, density, fraction porosity, element ratios; Fe/K, Fe/Si, K/Si, K/Ca and Fe/Ca for core HH12-904 GC. Stippled line in the element ratio plots illustrate changes commented in the text.

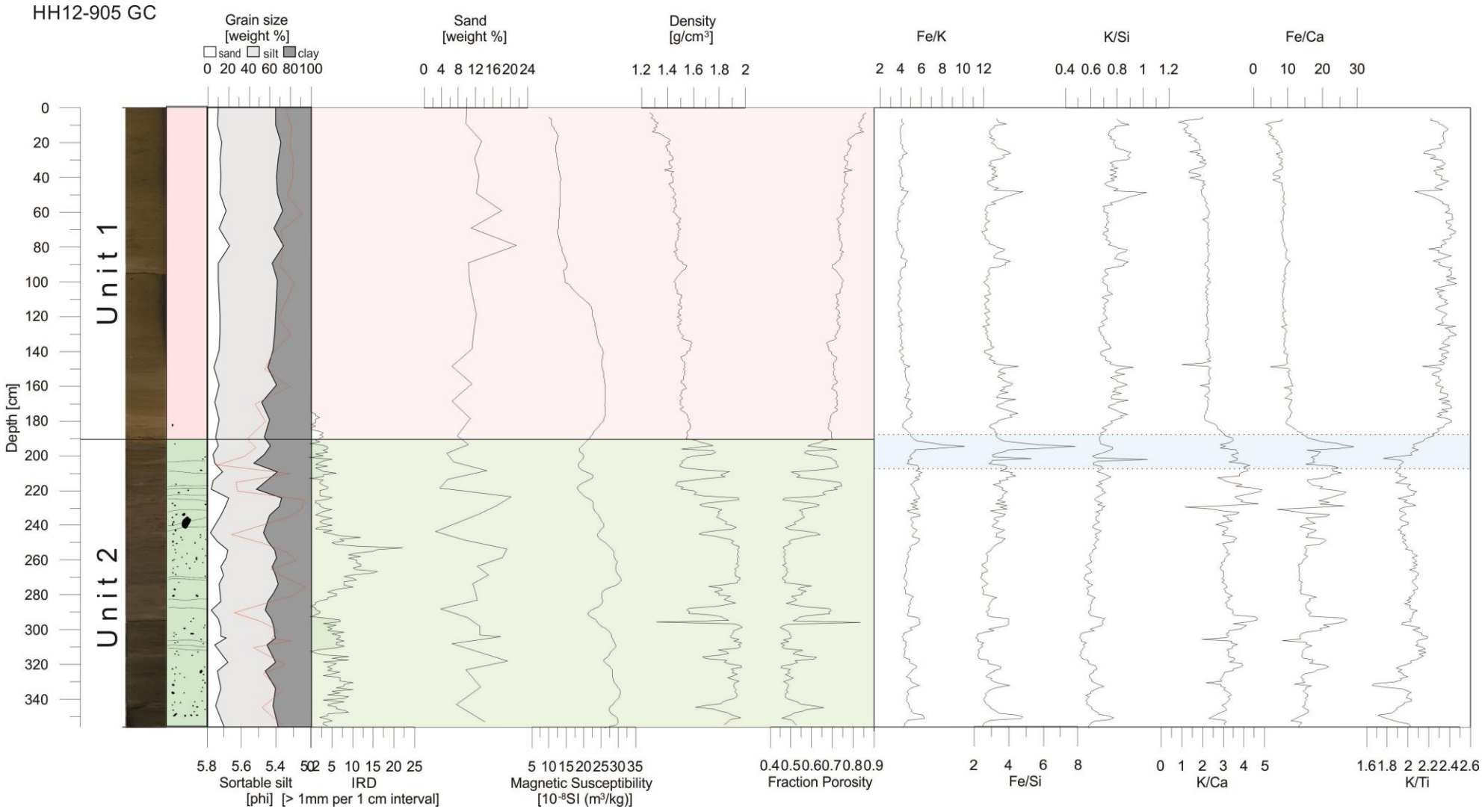

Figure 5.8: Colour picture, litostratigraphy (see fig 5.1 for legend), grain size and sortable silt (inverted), IRD content, sand content, Magnetic susceptibility, density, fraction porosity, element ratios; Fe/K, Fe/Si, K/Si, K/Ca, Fe/Ca and K/Ti for core HH12-905 GC. Blue areas in the element ratio plots illustrate changes commented in the text.

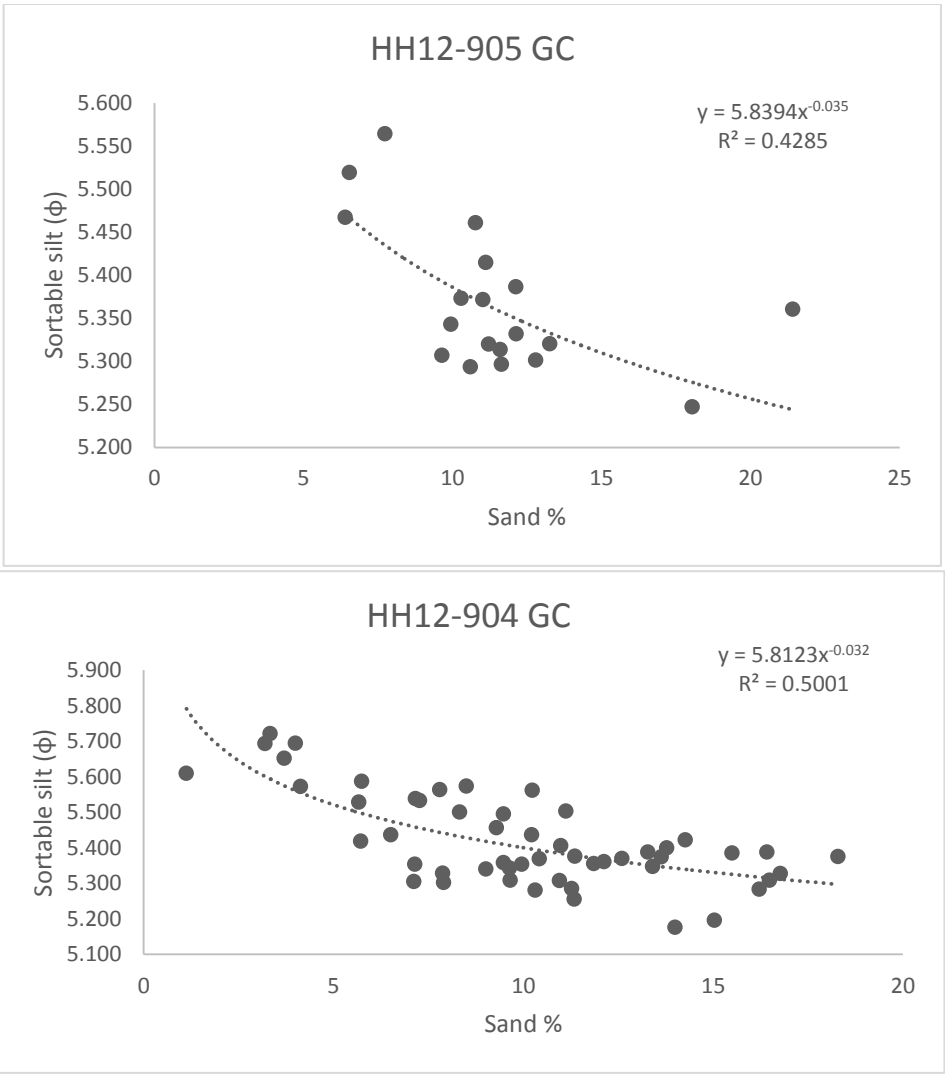

Figure 5.9: plots showing positive correlation between the sand and the silt content. Additional r-value shows whether the plot is statistically relevant. The regression line and regression equation used to calculate the potential sortable silt.

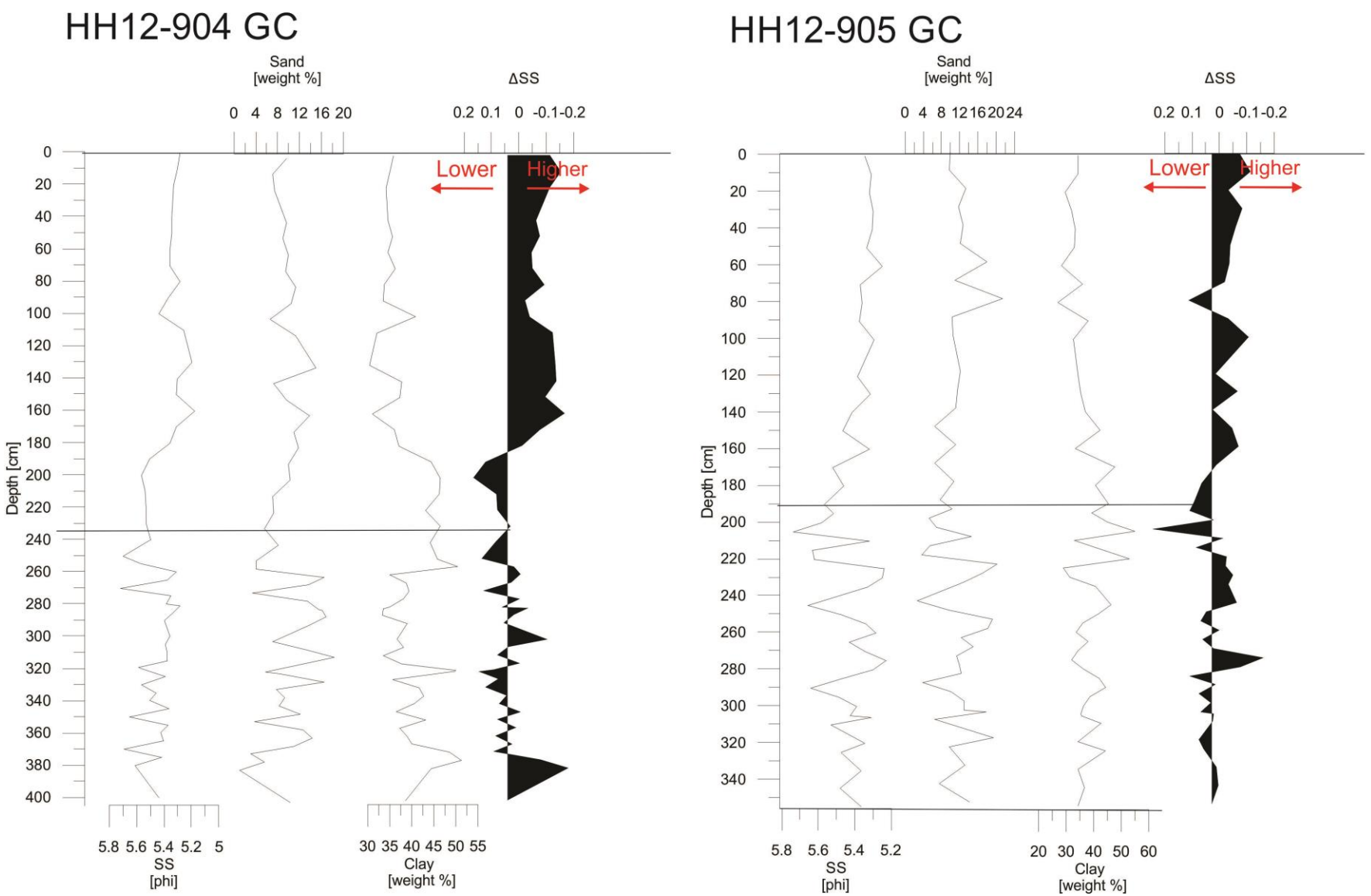

Figure 5.10: Sortable silt, sand content, clay content and relative current speed for the two cores HH12-904 GC and HH12-905 GC

5.3. Interpretation of sediment cores

All clasts > 1mm and sand content correlate and are suggested to be IRD deposited by ice bergs or sea ice (Grobe, 1987).

The density show increasing values towards the bottom of the core due to compression from the overlying sediments. From the same reasons the fraction porosity shows decreasing values towards the bottom. The Magnetic susceptibility generally shows the same trend as IRD and sand content, and can help indicate a source area. Peaks of increased magnetic susceptibility are most likely due to the presence of more magnetic clasts, while individual decreasing points may indicate wholes, cracks or areas of less sediment.

A classic sediment sequence in the Barents Sea usually consists of a unit of subglacial till; deposited underneath the glacier. One unit of proximal glacimarine sediments marking an early deglaciation consisting of coarse grained material, IRD and mass flow deposits. One unit of distal glacimarine sediments, indicating the retreat of the glacial front. In this layer finer sediments consist of gravity flows and less IRD. The last unit is a homogenous mud layer reflecting a marine environment throughout Holocene (e.g Benn & Evans, 2010; Murdmaa et al., 2006; Ivanova et al., 2002).

Unit 2 is dominated by laminated sediments, the lamination shows alternating sand and IRD with fine grained silt to mud dominated intervals. Due to its rather fine grained lamination and the high IRD content, this unit is interpreted to be deposited in the later stages of the deglaciation (O Cofaigh & Dowdeswell, 2001; Murdmaa et al., 2006).

Unit 1 is in general described as homogeneous fine grained material with no structures found. The main sedimentation process in unit 1 is most likely rain-out from meltwater from a distal source, or reworked sediments. Fine sediments like clay and fine silt can be held in suspension and transported for great distances (Hass, 2002; O Cofaigh & Dowdeswell, 2001).

5.4. ^{14}C AMS Dating

The AMS dating is shown in table 1 below. Only one depth from the lamination in each core had enough foraminifera for dating, and these were well preserved. Table 5.3 shows all dates with the additional information of depth and $_{14}$C years.

Table 5.3: Radiocarbon dating and calibration

Core	Sampling depth (cm)	14C age BP	Cal. Yr BP 1σ range	Cal. Yr BP 1σ mean	Cal. Yr BP 2σ range
HH12-900 GC	317-318	39500 ± 1800	41292-44289	42673	39378-45717
HH12-901 GC	236-238	44500 ± 3000	44934-49373	46618	42684-(5000)
HH12-904 GC	280-282	39900 ± 1600	41819-44356	43024	40279-45689
HH12-905 GC	235-236	36000 ± 1100	38573-40923	39639	36996-41784

6. Discussion

In this chapter the results from the two previous chapters will be discussed in order to reveal the sedimentary processes dominating in Sentralbankrenna during the deglaciation and throughout Holocene. The dates and acoustic data are discussed, before they are correlated with the sediment cores.

Concerning the sediment cores, they are discussed in units in this section, as they showed few major differences but what seems to be the same sedimentary environment. In the very end the sedimentary provenance will be tried to address.

6.1. AMS ^{14}C dating and foraminifera

During the deglaciation of the BSIS the Barents Sea was covered by sea ice which hindered biological production. I suggest that this, as well as turbulent meltwater and pulsated sedimentation, contributed to the lack of preserved microfossils (Murdmaa et al., 2006). Foraminifera previously found in the central deep and in the Percey trough are interpreted to be present because of increasing biological activity due to longer periods of ice free conditions in these parts of the southern and central Barents Sea (Iovanova et al., 2002; Murdmaa et al., 2001). The dating of the foraminifera found in unit 2 shows an improbably old age. The microfossils were of mixed ages, where the product is one total date. Datings from the Barents Sea indicates a much younger age for the deglaciation of the BSIS (Rüther et al., 2011; Salvigsen, 1981). Imperical estimations by Hughes (2015) suggest a deglaciation of the Sentralbanken area ~15 cal ka. As well as dates retrieved from laminated sediments in outer Sentralbankrenna show an age of 14650 cal yrs (Kaparulina et al., 2015). The fact that the foraminifera were well preserved indicates that they are reworked. Older microfossils can be transported into the sediment pack along with either meltwater flows or with ice bergs containing “products” of glacial erosion (Murdmaa et al., 2006).

The foraminifera found in the sample were mostly benthic species, only few to no planctic were found. The specie dominating the samples was of the type *Elphidium Excavatum* which is found near glacier environments, as well as a high amount of *Cassidulina reniforme* was found which are linked to glacimarine settings. Today these are found together in polar areas with cold fresh water (S´lubowska-Woldengen et al., 2008; Poliak, 1996), Indicating that fresh and cold bottom water, most likely form ice melting was present in the area where these were transported from.

Test samples were taken every tenth cm throughout the lamination in all cores. All samples showed no to only a few foraminifera during the intervals, except this one depth in all cores which makes it natural to think they are deposited during the same event. However, for cores 900 and 901 this depth is towards the bottom of the lamination, whereas in core 904 and 905 the foraminifera are found towards the top of the lamination. Since 900 and 901 are located further away from the estimated ice margin (Bjarnadottir et al., 2014) than 904 and 905, the location of the foraminifera within the lamination should have been the opposite, if any changes in this short distance.

6.2. Acoustic Data

The most prominent features in both swath bathymetry data and chirp are the tunnel valleys, where the cores are collected. These appears as depressions in the terrain and the chirp lines reveal a smoother surface and a thicker layer of sediments in these areas than on the adjacent areas of seafloor outside the channels.

A typical characteristic subglacial meltwater channel is that water can flow upslope due to pressure differences (Benn & Evans, 2010), the profiles along the channels are shown in figure 4.4, and indicates areas in the channels requiring an upslope flow of water, confirming there subglacial origin.

The curved valley where all four cores are collected is the most prominent in this study area and also the deepest, where the depth is ~40 m and the width is approximately 1 km at its narrowest (Bjarnadottir et al., 2012). I suggest that as such it was the main channel of the valley network, acting as an efficient pathway for subglacial evacuation of water. Age of these channels is unknown; however their association with ice marginal landforms of deglaciation age is consistent with their contemporaneous formation. Even if they formed earlier, they would certainly be occupied and used during the final deglaciation. We therefore infer that deglaciation of the Sentralbanken area was associated with abundant, efficient meltwater systems. During the deglaciation, as ice thinned, it became increasingly topographically constrained. At this time Sentralbankrenna is proposed to have drained ice from the North, East and Southeast (Bjarnadottir et al., 2014). I therefore suggest that at this time the meltwater flow was focused into the mapped channel, and most of the meltwater at some points passed the core locations or one of them.

6.3. Correlation of acoustic and sedimentary data

In all four cores one unit dominated by laminated sediments is found, as well as one unit of homogeneous mud. Laminated facies are usually found ice proximal in fjord settings where extensive ice masses have been present (O Cofaigh & Dowdeswell, 2001).

The cores were collected from two different basins within the same tunnel valley. Based on the bathymetry data and the chirp lines, the sediments in the cores are interpreted to be sediments deposited in the channel. The chirp line reveals a sediment pack in the channels of ~8 metres, where the uppermost ~4 metres is penetrated by the cores.

The chirp profile shows a layer of fine grained sediments uppermost, interpreted to represent homogeneous Holocene mud (unit 1),and a lower coarser layer (unit 2) interpreted to represent sediments deposited during an earlier phase of the deglaciation (Murdmaa et al., 2016; Bjarnadottir et al., 2014). The cores mostly penetrate the uppermost layer, and the lamination in the cores is clearly a part of the upper layer interpreted to be fine grained, homogenous sediments. This indicates that the laminated sediments observed in the cores are the end of the deglaciation, where a coarser layer of glacial deposits from an earlier time of the deglaciation most likely is found at deeper depths.

From the chirp profiles all the topographical heights have a series of depressions and hills on them. The largest ones are ~10 meters deep and ~1 km wide, and they are suggested to be produced by ploughing icebergs. MSGL are observed in the area from previous studies (Bjarnadottir et al., 2014), as well as these features show the same dimensions. Such features are found in sediments which have been overrun by a fast flowing ice stream (Alley et al., 1986). These features are not found in the basins, indicating a rather undisturbed mass of sediments. This proposes that sediments from suspension settling from meltwater plumes also can deposit in these valleys and stay undisturbed.

6.4. Unit 2: Deglaciation

Unit 2 is identified by its lamination. There is an abrupt change from mud to sand, before the sand gradually turns into a muddy layer again. Peaks of increased sand content and IRD correspond to each other, but the IRD has a scalloped pattern which the sand does not correspond to. This lamination is suggested to be from the later phase of the deglaciation as the sediments are relatively fine grained. Unit 2 has the same characteristics in all cores, and

is described as one unit consisting of more or less a pattern of the same transport mechanisms and depositions.

6.4.1. Mass waste

The coarser layers in the lamination normally contain around 20% sand and an increase of IRD, while the alternating layers are mostly is silt and mud and only ~10% sand, which is nicely illustrated in figure 5.7. The coarser layers of sand are graded upwards, while the pulses of IRD are more randomly distributed within the sand sections. However, due to a lack of the inner structures associated with turbidity currents, and lack of coarser particles (O Cofaigh & Dowdeswell, 2001) the laminations in the cores are most likely not deposited by such process.

Mass waste are common ice marginal and ice proximal where high sedimentation rates occur (eg O Cofaigh & Dowdeswell, 2001; Syvitski, 1996), the sediments found in the lamination are rather fine grained. Therefore we suggest that the laminated sediments are from a later phase of the deglaciation, which is corroborated by the suggestion that the cores only penetrate the upper layer of the deglaciation.

6.4.2. Meltwater plumes

As described in the chapter 1.2 meltwater plumes deposition are usually graded sediments of grain sizes up to fine sand (O Cofaigh & Dowdeswell, 2001). The coarser lamination of unit 2 may be deposited during warmer temperatures of higher meltwater discharge, as stronger meltwater currents can transport heavier material. The abrupt start of the sand in these layers may reflect an intense start of a meltwater plume with high discharge and speed, while the fining upwards can be explained by a decrease in the discharge and weaker currents resulting in deposition of finer sediments.

At times of lower temperatures, or even in the presence of sea ice finer sediments are deposited due to either weaker or no meltwater plumes. Weaker melt water plumes are recognized by finer silt grading to clay.

Grain size variation is hard to detect in the finer sediments such as clay and silt during visual inspections, and test samples where only collected every fifth cm in the lamination. Considering the thickness of the layers, these gradational characteristics could be hard to detect in the cores. The abrupt changes from mud to sand however can explain the pulsating

nature of meltwater plumes of high discharge, and the grading upwards describes the settling of smaller particles.

The muddy layers appear with a soupy consistence, while the coarser layers are denser. This can be explained by deposition rate where higher amounts of water present in sediments with a slower deposition rate.

6.4.3. Ice Rafted Debris

There are two pattern observed in the IRD content in the cores: Randomly distributed peaks of increasing amounts of IRD, corresponding to an increase in sand content. And a larger scale wave-like pattern of increasing and decreasing amounts of IRD.

The fact that the sand content and the IRD content peak at the same time may be explained by icebergs carrying all sediment sizes, as described in chapter 1 and fig 1.7, and that both sand and IRD are deposited by the same transport mechanism.

There will be a higher content of IRD, as warmer temperatures will increase the calving and migration of icebergs. The opposite is happening when the sea ice suppress the iceberg migration, finer sediments already in suspension will deposit, or meltwater plumes with lower discharge will transport finer particles to the seafloor. Figure 6.1 shows how intervals of increased clay content in unit 2 correspond to few or no IRD deposition.

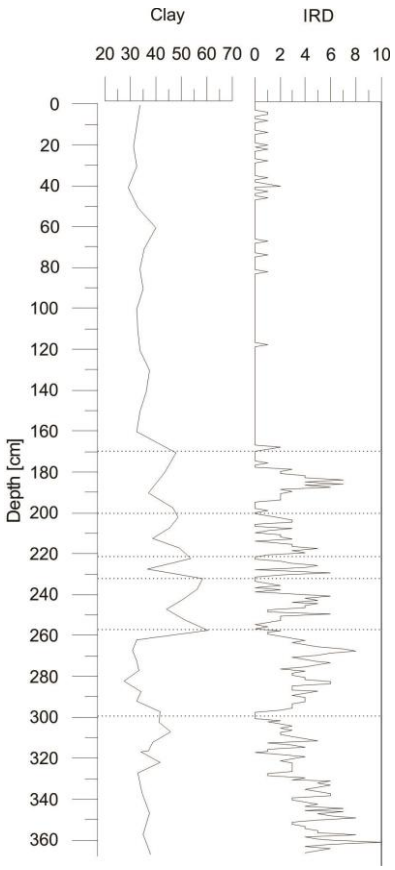

Figure 6.1: Figure illustrating the correlation of increasing clay content and the absence of IRD, indicating sea ice. Core used is HH12-900 GC.

The broken line illustrate where peaks of increased clay content correspond to a decrease in IRD content.

We know that the Barents Sea was covered by sea ice during large periods of the deglaciation (Ivanova et al., 2002). This is suggested to be deposition of fine grained material during periods of sea ice, by either weak meltwater plumes or settling of already discharged matter and suppressed migration of icebergs.

The scalloped pulses of IRD are suggested to indicate warmer periods where the temperatures increase gradually, giving a corresponding gradually increase of IRD which peaks at maximum melting and calving, before decreasing towards a colder period again. The IRD are counted for each cm, while the sand content is measured only every fifth cm in the laminations, which can result in some patterns being overlooked.

The individual peaks of IRD and sand increase are likely to have the same transport mechanism and deposited by icebergs during warmer periods. The increase of clay content corresponding with a decrease in IRD content are suggested to be colder periods where sea ice

might be present and lower meltwater activity let the finer particles settle. The wave pattern of IRD is proposed to be warmer and colder periods on a larger scale.

6.4.4. Sortable silt and relative current speed

The sortable silt fraction follows the grain size distribution, meaning they are likely to have the same transport mechanism.

Throughout unit 2 the relative current speed fluctuates between higher and lower currents, as illustrated in figure 5.6 and 5.10, which indicate abrupt changes in current speed. This might reflect a pulsating meltwater discharge during the deglaciations, where periods of no meltwater or low meltwater discharge will have a weak relative bottom current speed.

Summary Unit 2

The lamination is suggested to be produced by pulsating meltwater plumes, alternating low meltwater discharges were finer sediments have the conditions to settle. The IRD show a scalloped pattern with peak increases corresponding to increasing sand content. In ice marginal locations the sediments are most likely of coarser sediments or at least input of coarser sediments, as well as IRD should be more randomly distributed as more calving and melting takes place at all times (Murdmaa et al., 2006; Ivanova et al., 2002; Elverhøi & Solheim, 1983). Mass waste is common in ice marginal and ice proximal sediments, and since the laminations are suggested not to be a product of mass waste, could indicate an ice distal positioning of the cores. Meltwater plumes are said to be able to transport grain sizes up to fine sand in suspension, and are previously found in proximal sediments (Murdmaa et la., 2006; Ivanovaet al., 2002). Distal environment usually have few IRD (Ivanova et al., 2002) which unit 2 in this study does not have. The lamination of unit 2 is therefore suggested to be deposited ice proximal.

6.5. Unit 1: Holocene

The change in units are abrupt, and easily observed by a distinct change in colour from dark olive coloured sediments to a lighter olive grey/brown, it is reflected in all physical properties, and in grain size as they all go from fluctuating to more stable; indicating a homogenous mass interpreted to be Holocene sediments.

The transition from the deglaciation towards Holocene is dominated by a change in deposition mechanisms. As the climate became warmer a higher biological productivity occurred where the ice sheet was focused on land, as well as ice transport of sediments is reduced (Duplessy et al., 2001; Ivanova et al., 2002; Murdmaa et al., 2006).

Sentralbanken is today a remote area far from sediment sources, which is most likely leading to a low sedimentation rate. From 14 cal ka the ice sheet covering the Barents Sea, was highly focused on land (Hughes et al., 2015; Winsborrow et al., 2010), and the sedimentation during Holocene are largely dependent on bottom currents and reworking of sediments (eg Vorren et al, 1984; Hald & Vorren 1984). The bottom currents in the Sentralbanken area are complex (Murdmaa et al., 2006; McClimans, 1993).

6.5.1. Bottom currents and sediment transportation

Bottom currents of average strength are usually not strong enough to transport sand sized material in suspension over longer distances (Hass, 2002) sand can therefore indicate ice transport or redistributing of sediments due to slides. Even though sand sized material cannot be transported over longer distances, it can be transported as bedload for short distances or down from shallower areas with stronger currents. Bedload is individual grains being transported along the seafloor by either rolling or vertical and horizontal forces lifting it for short distances (Nichols, 2009). Since the dominating grain size are silt (table 5.2) which can be transported with bottom currents, the area where the cores are collected from is suggested to be an accumulation area for sediments.

6.5.2. Sortable silt and relative current speed

The sortable silt in general follows the sand content, as shown in figure 5.5 and 5.9 the correlation between sand and the coarsening silt is high for all cores. However the correlation is higher for core 900 and 901 than for 904 and 905. In the change from unit 2 to unit 1it is clear in all cores which the sortable silt shows a more uniform and stable pattern which can be seen in all core plots, eg fig 5.5. As meltwater plumes will give a highly fluctuating plot

according to different current strengths, bottom currents should show a more smooth nature as they don't change as much. It is evident that there is a change in transport mechanism from unit 2 to unit 1, from looking at these plots.

The speed for all cores show a relative decrease compared to the rest of the unit in the very beginning. All cores except 901 shows a higher current speed towards the top of the unit, and a general pattern where they all are low in the beginning of the Holocene unit, to become stronger towards the top of the unit. In the middle core 900, 904 and 905 show an interval of a relative decrease before increasing towards the top again. A not very different pattern is observed in recent studies by Hass (2002), where cores from the Fram Strait reflect a cooling of climate in mid-Holocene.

The grain size of the sediments in unit 1 are increasing towards the top of the cores, where all cores have a higher content of clay in the very beginning. Early Holocene was dominated by higher currents as the Atlantic Water entered the Barents Sea (Hald & Vorren, 1984). During warmer periods and less ice the currents seem to increase (Hass, 2002), illustrated in figure 6.2.

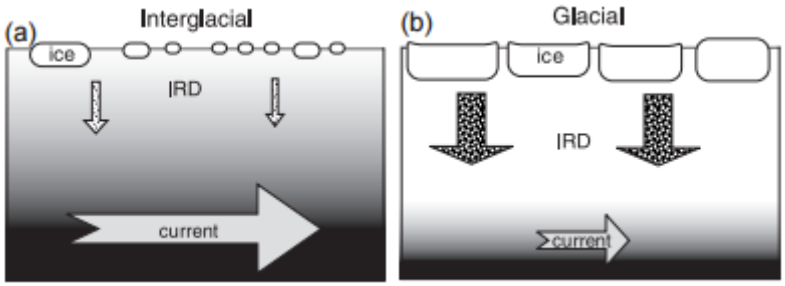

Figure 6.2: Currents increase during warmer periods of less ice, this can be reflected by a drop in IRD. Figure modified by Hass, 2002

Figure 6.2 may explain the correlation between the larger grain sizes and less IRD during warmer periods.

6.5.3. Winnowing

Winnowing is a process that often takes place during times of reduced sedimentation, where bottom currents wash out the finer grained sediments. This is a process where high bottom currents still leads to high sand content, not because the sand are transported by the currents, but because the finer sediments are washed out, leaving the coarser fractions behind (Benn & Evans, 2010). Studies done on cores from banks at deeper depths have recorded a higher

content of sand in the beginning of the Holocene (eg Rüther et al., 2012; Hald & Vorren, 1984) indicating that the finer material has been transported away by winnowing. In the beginning of Holocene higher bottom currents have been as the Atlantic flow entered the Barents Sea (Slubowska-Woldenengen et al., 2008; Hald & Vorren 1984; Vorren, 1984). The cores in this study show the opposite pattern, showing increasing clay content in the very beginning of unit 1 which is best illustrated in 5.6. Since the location of the cores is in the inner part of a trough it is likely that the finer particles has been transported from the banks during a time of higher bottom currents (Vorren, 1984), washing out the finer particle leading to deposition in a more shielded area.

The appearance of a rusty colour in all cores, an unclear yellow-rusty lamination is observed within this interval of increased clay content. In core 901 and 905 this layer covers a short interval and is clear, whereas in the other two cores it is more defuse, covering a larger area. Rusty colours are common in sediment cores as they tend to contain iron which oxidizes in contact with oxygen. For core 901 and 905 where the rusty colour appears in a distinct layer there is also an increase of relative iron content. It is likely that these layers has developed due to a hiatus in the deglaciation (Polyak, 1996) or in this case it can indicate that the ice front has retreated behind the bank top, resulting in an abrupt stop in meltwater and sediment supply.

The transition may show an abrupt change from lamination to a homogenous mass because of the topography where the ice front retreated over a bank. As the glacier front pulls back, the production of a distal source might not be present if the glacier front and source area are located behind the bank.

Throughout the unit there are also intervals of increasing sand content and decreasing clay content in all cores, these are most likely a product of stronger currents at the core site, washing out the finer sediments. These intervals are proposed to be winnowing at the core site, where the finer sediments are washed out.

Holocene also consisted of colder and warmer periods of intrusion of Atlantic Water from the South, but times of extended sea ice was also present after the ice retreat (Slubowska-Woldenengen et al., 2008). The small amounts of IRD throughout unit 1 are therefore suggested to be a product of IRD mostly from sea ice.

6.6. Sediments Provenance

During the deglaciation unit 2 show fluctuations in element chemistry ratios, telling us there is a relative change in elements and therefore source area throughout the unit. The element chemistry of unit 1 is rather uniform, and relative increases in element ratios are not correlated to the other parameters.

In unit 2 iron and calcium show the most prominent changes as well as these elements correspond to the clay content, this is best illustrated in figure 5.4, but also shown in the other core logs. As suggested earlier, the sediments in the cores are most likely dominated by the late glaciation. This indicates a variation of source areas, as the Sentralbankrenna have served as a funnel for flows coming from North, Northeast and Southeast (Bjarnadottir et al., 2014). Changes in element ratio may fluctuate throughout unit 2 due to meltwater flows from all directions.

Approximately where unit 2 goes over to unit 1, there is a change from a fluctuating trend to a more uniform and stable, as well as some of the plots reveals a change in dominating element which is shown in figure 5.8. As mentioned earlier is the Central Barents Sea a remote area, far from inland sources. A more stable ratio plots throughout unit 1 indicate a more stable direction of flow and more stable source area during these times.

As unit 1 is suggested to consist of mostly current transported and reworked sediments. The plots are showing a slight correlation between clay content and element ratios, indicating that grainsize could have an influence on the elements, but this is not evident enough throughout unit 1. The increase of clay and element ratio is consistent with a potential winnowing event, suggesting most of these sediments are transported from the top of the bank (Vorren, 1984). The plots seem to fluctuate more towards the top and the bottom of unit 1, which can be explained with higher currents transporting more sediment from different places into the core sites, while weaker currents don’t have the ability to transport the same amount for further distances.

The Belemnite was extinct in Cretaceous. Belemnites are found in sedimentary rock layers mostly from Jurassic and Cretaceous, and rarely Triassic in the Svalbard region (Doyle et al., 1988). The belemnite found in the core is suggested to be from post-Triassic origin, in figure 6.3, exposed areas of these sediments are marked in blue.

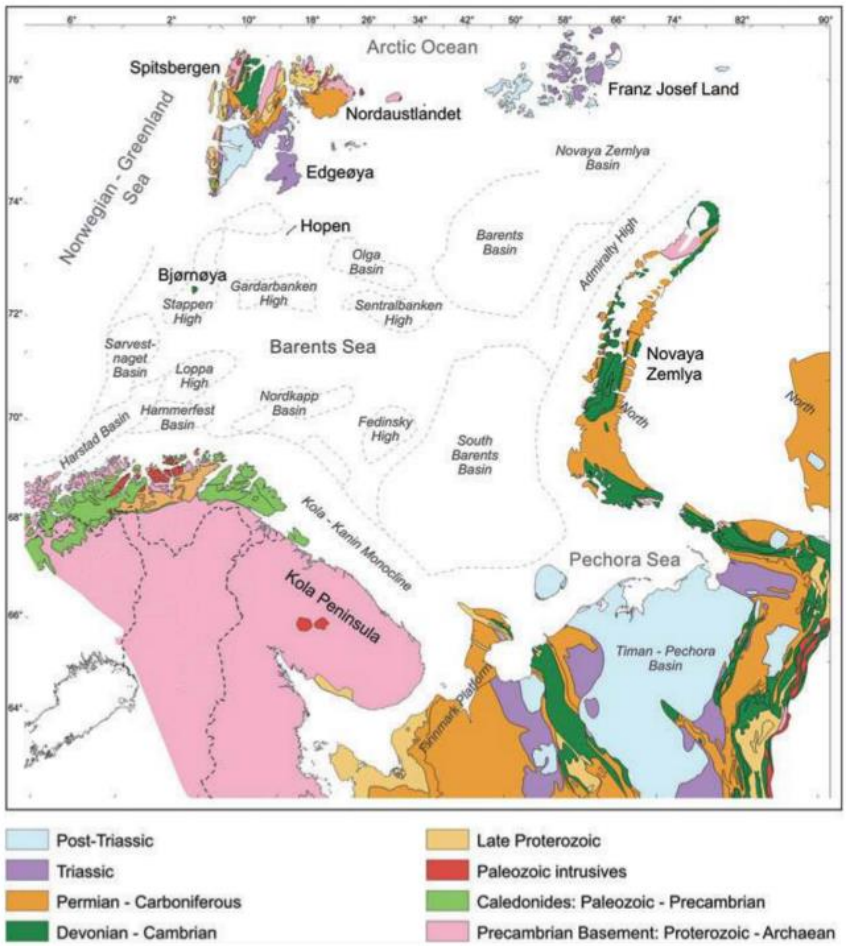

Figure 6.3: Map showing the exposion of rocks in land areas surrounding the Barents Sea. Map retrieved from Worsley, 2008, information compiled by Mørk (1999)

Large parts of Franz Josef Land and in parts of the Pechora Basin both have post-Triassic sedimentary rocks exposed. According to travel path and ice flow (eg Bjarnadottir et al., 2014) this belemnite is suggested to come from Franz Josef Land, which can indicate that sediments from the deeper parts of the core has an origin in the northern Barents Sea. This is consistent with the high amount of kaolinite found in the Central Barents Sea, which is usually reworked from the northern or even the Central Barents Sea (Vogt & Knies, 2009).

Bjarnadottir et al. (2014) has estimated that the later phase of the declaciation was coming from the Northern directions, while the earlier stages were dominated by a Southeastern flow. This can support the suggestion of the cores only penetrating the upper part of the deglacial sediments, and that the lamination is from a later part of the deglaciation.

7. Conclusions

Based on the four cores and marine geophysical datasets the late deglacial and Holocene sedimentary environments of Sentralbankrenna, Central Barents Sea has been reconstructed. The four cores were located within shallow basins along channel features identified by Bjarnadottir (2014; 2012) as tunnel valleys.

- **Seafloor channels** were identified on the multibeam swath bathymetry. Two of them showed an undulating long profile, and all five were connecting with seafloor channels previously identified by Bjarnadottir (2014; 2012). These channels were interpreted to be meltwater channels, transport pathways for **subglacial meltwater** under deglaciation of this area.
- The topography from the chirp profiles reveals that the sediments in the **two basins** interpreted by Bjarnadottir et al (2012), where the cores in this study are collected, are thick as well as no ploughing marks is observed, indicating an area **shielded from disturbances.**
- Chirp profiles reveals two sediments layers: One coarse layer from early deglaciation and one acoustically transparent layer of more homogenous matter. The cores penetrate the first layer, indicating a **later stage of the deglaciation**.

- The laminated sediments of **unit 2** are suggested to represent the **deglaciation**.
- Gradational sand layers of unit 2 are thought to be strong **meltwater plumes** of high meltwater discharge. The alternating layers of few IRD's correlating to muddy layers and an increase in clay content are suggested to be periods of lower meltwater discharge and sea ice cover suppressing ice berg migration and IRD release.
- Due to core penetration of only the uppermost layer, and no sign of mass flow, the sediments of unit 2 are suggested to be from a later phase of the deglaciation. The IRD content is on the other hand high and the **laminated** sediments are therefore suggested to have been deposited in **ice proximal** conditions.
- The IRD content throughout unit 2 shows a scalloped pattern, as well as individual peaks. The individual peaks correlate to an increase in sand content, and are proposed to be **pulses of ice transported material**. The larger scale scalloped pattern is suggested to be longer warmer periods where **IRD increase with temperatures**, before decreasing again as the temperatures drop.

- The **foraminifera** show mixed ages and are suggested to be **reworked** along with sediments from other places in the Barents Sea.
- The belemnite found in the lamination is suggested to have been transported from the **northern parts of the Barents Sea**. This corroborate the suggestion about the lamination being the later phase of the deglaciation, as the melting was more topographically dependent as ice thinned, and meltwater came from a northern direction during the later phase of deglaciation.

- The sediments of **unit 1** are suggested to be dominated by **bottom currents** and **reworked** sediments.
- In the transition between unit 2 and unit 1 a **rusty coloured layer** is suggested to mark a change from high to **low sedimentation rates**, and may reflect a sudden lack of source area and meltwater.
- An **increase in bottom currents** and a coarsening of the sediments towards the top of the cores are suggested to be a product of **winnowing**, where the finer material is washed out. Intervals of higher sand content, are thought to be periodically intense winnowing, while the finer sediments in the beginning of the unit is suggested to be deposition of the finer winnowed sediments.
- **IRD** deposition in unit 1 indicates ice transportation and can either be by periods of **sea ice** or migrating icebergs.

8. References

Andreassen, Karin, Winsborrow, Monica C.M., Bjarnadóttir, Lilja R., & Rüther, Denise C. (2014). Ice stream retreat dynamics inferred from an assemblage of landforms in the northern Barents Sea. *Quaternary Science Reviews, 92*, 246-257.

Benn, D.I., Evans, D.J.A., 2010. Glaciers & glaciation. Second edition. London: Hodder Education.

Bjarnadottir, L., & Andreassen, Karin. (2012). Processes and dynamics during deglaciation of a polar continental shelf. Examples from the marine-based Barents Sea Ice Sheet.

Bjarnadóttir, Lilja R., Winsborrow, Monica C.M., & Andreassen, Karin. (2014). Deglaciation of the central Barents Sea. *Quaternary Science Reviews, 92*, 208-226.

Bamber, J., Vaughan, D., & Joughin, I. (2000). Widespread complex flow in the interior of the Antarctic ice sheet. *Science, 287*(5456), 1248-1250.

Batchelor, C., & Dowdeswell, J. (2015). Ice-sheet grounding zone wedges (GZWs) on high latitude continental margins. *Marine Geology, 363*, 65-92.

Batchelor, C., Dowdeswell, J., & Hogan, K. (2011). Late Quaternary ice flow and sediment delivery through Hinlopen Trough, northern Svalbard margin; submarine landforms and depositional fan. *Marine Geology, 284*(1), 13-27.

Beckman Coulter. (2011). Retrieved 16.11.15, from «Instructions for use; LS 13320 Laser Diffraction Particle Size Analyser": https://www.beckmancoulter.com/wsrportal/techdocs?docname=B05577AB.pdf

Bennett, M. (2003). Ice streams as the arteries of an ice sheet: Their mechanics, stability and significance. *Earth-Science Reviews, 61*(3-4), 309-339.

Bowman, S. (1990). *Radiocarbon dating.* Berkley and Los Angeles: University of California Press.

Breitzke, M., & Spieβ, V. (1993). An automated full waveform logging system for high-resolution P-wave profiles in marine sediments. *Marine Geophysical Researches, 15*(4), 297-321.

Clark, C., Tulaczyk, S., Stokes, C., & Canals, M. (2003). A groove-ploughing theory for the production of megascale glacial lineations, and implications for ice-stream mechanics. *Journal of Glaciology, 49*(165), 240-256.

Dadey, A. K., Janecek, T., Adam, K. 1992. Dry Bulk Density: its use and determination. Proceedings of the ocean drilling program. *Scientific results*, vol 126, 551

Dallmann, W., Blomeier, D., & Elvevold, S. (2015). *Geoscience atlas of Svalbard* (Vol. No.148, Rapportserie (Norsk polarinstitutt : trykt utg.)). Tromsø: Norsk polarinstitutt.

Damuth, J. (1980). Use of high-frequency (3.5-12 kHz) echograms in the study of near-bottom sedimentation processes in the deep-sea; a review. *Marine Geology,38*(1), 51-75.

Dokken, T., & Hald, M. (1996). Rapid climatic shifts during isotope stages 2-4 in the polar North Atlantic. *Geology (Boulder), 24*(7), 599-602.

Doyle, P., & Kelly, S. (1988). *The Jurassic and Cretaceous belemnites of Kong Karls Land, Svalbard* (Vol. 189, Skrifter (Norsk polarinstitutt)). Oslo.

Dowdeswell, J., Elverhoi, A., & Spielhagen, R. (1998). Glacimarine sedimentary processes and facies on the Polar North Atlantic margins. *Quaternary Science Reviews, 17*(1-3), 243-272.

Duplessy, J., Ivanova, E., Murdmaa, I., Paterne, M., & Labeyrie, L. (2001). Holocene paleoceanography of the northern Barents Sea and variations of the northward heat transport by the Atlantic Ocean. *Boreas, 30*(1), 2-16.

Elmore, D., & Phillips, F. (1987). Accelerator mass spectrometry for measurment of long-lived radioisotopes. *Science, 236*(4801), 543-550.

Elverhøi, & Solheim. (1983). The Barents Sea ice sheet - a sedimentological discussion. *Polar Research, 1*(1), 23-42.

Elvsborg, A. (1979). Late Quaternary sedimentation in a glacial trough on the continental shelf off Troms, northern Norway. *Norsk Geologisk Tidsskrift, 59*(4), 309-325.

Ersdal, G., 2001. An overview of ocean currents with emphasis on currents on the continental shelf. (preliminary version). NPD. Tilgjengelig fra: http://www.gerhard.ersdal.com/Filer/current.pdf (Retrieved: 29.03.2016)

Forman, S., & Polyak, L. (1997). Radiocarbon content of pre-bomb marine mollusks and variations in the 14 C Reservoir age for coastal areas of the Barents and Kara Seas, Russia. *Geophysical Research Letters, 24*(8), 885-888.

Forwick, M. (2013). *How to use XRF core scanner data aquired with the Aavatech XRF core scanner at the Department of Geology, University of Tromsø.* Tromsø: Department of Geology.

Fujifilm. (2014). *Fujifilm Technical Handbook: The Fundamentals of Industrial Radiography.* Tokyo: Fujifilm Corporation.

Gelius L.J., 2007. INF-GEO 3310: Introduction to seismic Processing and imaging. UiO

Retrieved 13.11.15 from: http://www.uio.no/studier/emner/matnat/ifi/INF-

GEO4310/h11/undervisningsmateriale/imaging_course.pdf

Geotek . (2014). Geotek X-ray Core Imaging With CT: MSCL-XCT: Linear Images & 3D reconstructions of sediment and rock cores. Retrieved 25.11.15, from http://www.geotek.co.uk/sites/default/files/Geotek_MSCL-XCT.pdf

GEOTEK Ltd. (2014). "Geotek Ltd manual; Multi-Sensor Core logger". Retrieved 10.11.15, from http://www.geotek.co.uk/sites/default/files/MSCLmanual.pdf

Gilbert, R. (1990). Rafting in glacimarine environments. *Geological Society Special Publication, 53*, 105-120.

Grobe, H., 1987. A simple method for the determination of ice-rafted debris in sediment cores. Polarforschung 57, 123-126.

Hass, Christian H., 2002. A method to reduce the influence of icerafted debris on a grain record from northern Fram Strait, Arctic Ocean. Polar Research 21(2), 299-306.

Hjelstuen, B., Haflidason, H., Sejrup, H., & Lysa, A. (2009). Sedimentary processes and depositional environments in glaciated fjord systems; evidence from Nordfjord, Norway. *Marine Geology, 258*(1), 88-99.

Hughes, A. L. C., Gyllencreutz, R., Lohne, Ø. S., Mangerud, J., Svendsen, J. I. 2016 (January): The last Eurasian ice sheets – a chronological database and time-slice reconstruction, DATED-1.Boreas, Vol 45, pp. 1–45. 10.1111/bor.12142. ISSN 0300-9483.

Ivanova, E., Murdmaa, I., Duplessy, J., Paterne, M., & Ganssen, Gerald. (2002). Late Weichselian to Holocene paleoenvironments in the Barents Sea. *Global and Planetary Change, 34*(3), 209-218.

Junttila, J., Aagaard-Sorensen, S., Husum, K., & Hald, M. (2010). Late glacial-Holocene clay minerals elucidating glacial history in the SW Barents Sea. *Marine Geology, 276*(1), 71-85.

Kaparulina, E., Junttila, J., Lunkka, J.P., Strand, K., 2015. SW Barents Sea sediment composition in response to Late Glacial-Holocene ice sheet retreat and provenance changes. Geophysical Research Abstracts Vol. 17, EGU2015, EGU General Assembly 2015

Kongsberg Maritime. (2003). EM 300: 30 kHz multibeam echo sounder for depths reaching 5000 meters. Horten: Kongsberg Maritime AS

Laberg, J., Andreassen, K., & Vorren, T. (2012). Late Cenozoic erosion of the high-latitude southwestern Barents Sea shelf revisited. *Geological Society of America Bulletin, 124*(1), 77-88.

Landvik, Jon Y., Bondevik, Stein, Elverhøi, Anders, Fjeldskaar, Willy, Mangerud, Jan, Salvigsen, Otto, Siegert, Martin J., Svendsen, John-Inge, and Vorren, Tore O. (1998). The last glacial maximum of Svalbard and the Barents Sea: Ice sheet extend and configuration. *Quaternary Science Reviews, 17*(1), 43-75.

Lionel Carter. (2012). "Charting the Sea Floor", Te Ara- The Enclopedia of New Zealand. Retrieved 30.11.15., Updated 13.07.12 from http://www.teara.govt.nz/en/charting-the-sea-floor/sources

Loeng, H. (1991). FEATURES OF THE PHYSICAL OCEANOGRAPHIC CONDITIONS OF THE BARENTS SEA. *Polar Research, 10*(1), 5-18.

Lowe, J.J & Walker M.J.C. (1997). Reconstructing Quaternary Environments. 2nd edition. New York: Routledge

Mangerud, J. (1972). Radiocarbon dating of marine shells, including a discussion of apparent age of Recent shells from Norway. *Boreas, 1*, 143-172

Mccave, I., Manighetti, B., & Robinson, S. (1995). Sortable silt and fine sediment size composition slicing – Parameters for paleocurren speed and paleoceanography. *Paleoceanography,10*(3), 593-610.

McClimans, Thomas A., & Nilsen, Jan H. (1993). Laboratory simulation of the ocean currents in the Barents sea. *Dynamics of Atmospheres and Oceans,19*(1), 3-25.

Murdmaa, Ivanova, Duplessy, Levitan, Khusid, Bourtman, . . . Serova. (2006). Facies system of the eastern Barents Sea since the last glaciation to present.*Marine Geology, 230*(3), 275-303.

Munsell, R. (1973). Soil colour chart. *Macbeth division of kollmorgen corporation, New York*, 19 pp.

Nichols, G. (2009). *Sedimentology and stratigraphy* (2nd ed.). Chichester: Wiley-Blackwell.

O Cofaigh, C. (1996). Tunnel Valleys genesis. Progress in Physical Geography (20), no.1, p. 1-19

O Cofaigh, C., & Dowdeswell, J. (2001). Laminated sediments in glacimarine environments: Diagnostic criteria for their interpretation. *Quaternary Science Reviews, 20*(13), 1411-1436.

Ottesen, D., & Dowdeswell, J. (2009). An inter-ice-stream glaciated margin; submarine landforms and a geomorphic model based on marine-geophysical data from Svalbard. *Geological Society of America Bulletin, 121*(11), 1647-1665.

Patton, H., Andreassen, K., Bjarnadottir, L., Dowdeswell, J., Winsborrow, M., Noormets, R., . Hubbard, A. (2015). Geophysical constraints on the dynamics and retreat of the Barents Sea ice sheet as a paleobenchmark for models of marine ice sheet deglaciation. *Reviews Of Geophysics, 53*(4), 1051-1098.

Polyak, L., Mikhailov, V., Andrews, J.T., & Et al, J.T. (1996). Post-glacial environments of the southeastern Barents Sea: Foraminiferal evidence. *Late Quaternary Palaeoceanography of the North Atlantic Margins,* 323-337.

Quinn, R., Bull, J., & Dix, J. (1998). Optimal Processing of Marine High-Resolution Seismic Reflection (Chirp) Data. *Marine Geophysical Researches,20*(1), 13-20.

Richter, T., Van der Gaast, S., Koster, B., Vaars, A., Gieles, R., De Stigter, H., . . . Rothwell, R. Guy. (2006).The Avaatech XRF core scanner; technical description and applications to NE Atlantic sediments. *Geological Society Special Publications, 267*, 39-50.

Rignot, E., Jacobs, S., 2002. Rapid Bottom melting widespread near Antarctic ice sheet grounding lines. Science 296(5575), 2020-2023.

Rüther, D., & Andreassen, Karin. (2012). Palaeoenvironment of the Barents Sea during the last deglaciation and Holocene : Processes and timing.

Rüther, Denise Christina, Mattingsdal, Rune, Andreassen, Karin, Forwick, Matthias, & Husum, Katrine. (2011). Seismic architecture and sedimentology of a major grounding zone system deposited by the Bjørnøyrenna Ice Stream during Late Weichselian deglaciation. *Quaternary Science Reviews, 30*(19), 2776-2792.

Salvigsen, O. (1981). Radiocarbon Dated Raised Beaches in Kong Karls Land, Svalbard, and Their Consequences for the Glacial History of the Barents Sea Area.*Geografiska Annaler. Series A, Physical Geography, 63*(3/4), 283-291.

Schock, S., LeBlanc, L., & Mayer, L. (1989). Chirp subbottom profiler for quantitative sediment analysis. *Geophysics, 54*(4), 445-450.

Schultheiss, J. P., Mienert. J., Shipboard Scientific Party. (1986). Whole-Core P-Wave Velocity and Gamma Rays Attenuation Logs From Leg 108 (Sites 657 through 668). Retrieved 12.12.15 from: http://www-odp.tamu.edu/publications/108_ir/volume/CHAPTERS/ir108_16.pdf

Skagseth, &., Furevik, T., Ingvaldsen, R., Loeng, H., Mork, K., Orvik, K., & Ozhigin, V. (2007). Transports and propagation of anomalies in the Norwegian and Barents Seas.

Slubowska-Woldengen, M., Koc, N., Rasmussen, T., Klitgaard-Kristensen, D., Hald, M., & Jennings, A. (2008). Time-slice reconstructions of ocean circulation changes on the continental shelf in the Nordic and Barents Seas during the last 16,000 cal yr B.P. *Quaternary Science Reviews, 27*(15), 1476-1492.

Stewart, M., Lonergan, L., Hampson, G., & Stewart, G. (2012). 3D seismic analysis of buried tunnel valleys in the Central North Sea: Tunnel valley fill sedimentary architecture. *Geological Society Special Publication, 368*(1), 173-184.

Syvitski, J., Powell, Ross D., & Elverhoi, Anders. (1989). On the deposition of sediment within glacier-influenced fjords; oceanographic controls. *Marine Geology,85*(2), 301-329.

Syvitski, J., Andrews, J., Dowdeswell, J., Solheim, A., Riis, F., Elverhoi, A., . . . Cloetingh, S. (1996). Sediment deposition in an iceberg-dominated glacimarine environment, East Greenland; basin fill implications. *Global and Planetary Change, 12*(1), 251-270.

Swithinbank, C.W.M. (1954) Ice Streams. *Polar record 7*, 185-186.

Tjallingii, R., Röhl, U., Kölling, M., & Bickert, T. (2007). Influence of the water content on X-ray fluorescence core-scanning measurements in soft marine sediments. *Geochemistry, Geophysics, Geosystems, 8*(2), N/a.

Vorren, T., Hald, M., & Lebesbye, E. (1988). Late Cenozoic environments in the Barents Sea. *Paleoceanography, 3*(5), 601-612.

Vorren, T., Lebesbye, E., Andreassen, K., Larsen, K., Powell, Ross D., & Elverhoi, Anders. (1989). Glacigenic sediments on a passive continental margin as exemplified by the Barents Sea. *Marine Geology, 85*(2), 251-272.

Vorren, T., Hald, M., Thomsen, E., Bornhold, B. D., & Guilcher, A. (1984). Quaternary sediments and environments on the continental shelf off northern Norway. *Marine Geology, 57*(1), 229-257.

Vogt, C., & Knies, J. (2008). Sediment dynamics in the Eurasian Arctic Ocean during the last deglaciation; the clay mineral group smectite perspective. *Marine Geology, 250*(3), 211-222.

Vogt, C., & Knies, J. (2009). Sediment pathways in the western Barents Sea inferred from clay mineral assemblages in surface sediments. *Norsk Geologisk Tidsskrift, 89*(1-2), 41-55.

Wahsner, M., Mueller, C., Stein, R., Ivanov, G., Levitan, M., Shelekhova, E., . . . Thiede, Joern. (1999). Clay-mineral distribution in surface sediments of the Eurasian Arctic Ocean and continental margin as indicator for source areas and transport pathways; a synthesis. *Boreas*, *28*(1), 215-233.

Wentworth, C. K.. (1922). A Scale of Grade and Class Terms for Clastic Sediments. *The Journal of Geology*, *30*(5), 377–392. Retrieved from http://www.jstor.org/stable/30063207

Winsborrow, M., Andreassen, K., Corner, G., & Laberg, J. (2010). Deglaciation of a marine-based ice sheet; late Weichselian palaeo-ice dynamics and retreat in the southern Barents Sea reconstructed from onshore and offshore glacial geomorphology. *Quaternary Science Reviews*, *29*(3), 424-442.

Worsley, D. (2008), The post-Caledonian development of Svalbard and the western Barents Sea. Polar Research, 27: 298–317. doi: 10.1111/j.1751-8369.2008.00085.x